Methods to Predict the Clinical Output Levels of Acoustic Implants

Von der Fakultät für Maschinenbau
der Gottfried Wilhelm Leibniz Universität Hannover
zur Erlangung des akademischen Grades
Doktor-Ingenieur
genehmigte Dissertation
von

Dipl.-Ing. Martin Großöhmichen, M. Sc.

2019

1. Referent: Prof. Dr.-Ing. Peter Wriggers,
2. Referent: Prof. Dr. phil. nat. Hannes Maier

Tag der Promotion: 10.12.2018

Für meine Familie

Zusammenfassung

Für schwerhörige Patienten, bei denen eine Versorgung mit einem konventionellen Hörgerät oder einem Cochlea-Implantat nicht in Frage kommt, haben sich in den vergangenen Jahren aktive Mittelohrimplantate (AMEIs) und Direct Acoustic Cochlear Implantate (DACIs) als erfolgreiche Therapien bewährt. Um die Versorgungsergebnisse mit solchen Implantaten zu verbessern und um neue Therapiemöglichkeiten zu entwickeln, ist eine Methode notwendig, mit der die Effizienz und die erzielbaren Ausgangspegel der Implantate präklinisch bestimmt werden können. ASTM Standard F2504–05 beschreibt eine Methode, um den Ausgangspegel eines AMEI im menschlichen Felsenbeinpräparat durch laservibrometrische Messungen der Schwingungsantwort des Stapes zu bestimmen. Dieser Standard ist jedoch nur für Stimulation der Gehörknöchelchen vorgesehen und erfordert einen mobilen und sichtbaren Stapes. Somit liegen gängige Anwendungen wie die AMEI Rundfensterstimulation und die mechanische Innenohrstimulation mit einem DACI außerhalb des Anwendungsbereichs von ASTM F2504–05 und vorherige Untersuchungen weisen darauf hin, dass die Stapesvibration bei solchen Stimulationen keine zuverlässige Referenz für den Stimulationspegel ist. Daher wurde in der vorliegenden Arbeit zunächst untersucht, ob ASTM F2504–05 so angepasst werden kann, dass Ausgangspegel von mechanischen Rundfenster- und Perilymphstimulationen im Felsenbeinversuch bestimmt werden können. Hierfür wurden diese und weitere Stimulationsmodi mit einem DACI Aktuaktor im humanen Felsenbein durchgeführt und die Vibrationsantworten sowohl des Stapes als auch des runden Fensters wurden laservibrometrisch erfasst und als Referenz verwendet. Die Ergebnisse zeigen, dass eine Anpassung des ASTM Standards möglich ist. Jedoch sollten die so vorhergesagten Pegel aufgrund starker Variabilität nur für erste Abschätzungen verwendet werden, insbesondere bei Frequenzen $\geq 1\,\text{kHz}$. Daher wurde in der vorliegenden Arbeit eine alternative Methode entwickelt, um im Felsenbeinversuch die Ausgangspegel von AMEIs und DACIs vorherzusagen. Diese verwendet die intracochleäre Schalldruckdifferenz (ICPD) zwischen den beiden Innenohrgängen *scala vestibuli* und *scala tympani* als Referenz, da diese im Tierversuch mit auditorisch evozierten Potentialen korreliert und als Eingangssignal des Innenohres betrachtet wird, die die cochleäre Wanderwelle auslöst und zwar unabhängig von der Stimulationsart. Um die Voraussetzung für eine allgemein zugängliche Methode zu schaffen, wurde zunächst getestet, ob kommerziell verfügbare Drucksensoren geeignet sind, um im humanen Felsenbein ICPDs zu messen. Für zwei verschiedene Messsysteme konnte gezeigt werden, dass dies während akustischen Stimulationen mit ausreichendem Signal-Rausch-Verhältnis möglich ist. Daraufhin wurde untersucht, ob Ausgangspegel eines AMEI im humanen Felsenbeinpräparat mittels ICPD bestimmt werden können. Hierzu wurde ein AMEI am Incus angekoppelt und während der Stimulation wurden sowohl die hervorgerufene Stapesvibration als auch die ICPDs gemessen. Die Ausgangspegel wurden dann anhand beider Referenzen berechnet. Zur Validierung wurden die auf diese Weise bestimmten Pegel direkt mit klinischen Ergebnissen verglichen. Obwohl ASTM F2504–05 bereits 2005 veröffentlicht wurde und inzwischen sehr etabliert ist, wurde so ein Vergleich, der die Genauigkeit der Vorhersage demonstriert, zuvor nie durchgeführt. Die hier gewonnenen Ergebnisse zeigen, dass Ausgangspegel, die für ein AMEI nach ASTM F2504–05 mittels Stapesvibrationen bestimmt werden, innerhalb $9\,\text{dB}$ mit den klinischen Daten übereinstimmen. Die ICPD Messungen lieferten sogar noch genauere Werte, die nahezu identisch mit

den tatsächlichen Ausgangspegeln im Patienten waren. Die vorliegende Arbeit demonstriert somit erstmalig, dass sowohl Stapes Vibrationen als auch ICPDs verwendet werden können, um die Ausgangspegel eines AMEI verlässlich in humanen Felsenbeinpräparaten vorherzusagen. Da die Vibrationsmessung nach ASTM F2504–05 schneller und mit weniger Aufwand durchführbar ist, ist diese bei Stimulationen der Gehörknöchelchen zu präferieren. Die ICPD Messung hingegen ist vorzuziehen, wenn noch präzisere Vorhersagen notwendig sind und wenn Stimulationen untersucht werden, die außerhalb des Anwendungsbereichs von ASTM F2504–05 liegen.

Schlagwörter: Intracochleäre Schalldruckmessung, Aktives Mittelohrimplantat, Direct Acoustic Cochlear Implant

Abstract

Over the last years, Active Middle Ear Implants (AMEIs) and Direct Acoustic Cochlear Implants (DACIs) have become well established as a therapy for hearing impaired patients who are not suited for a provision of a hearing aid or of a cochlear implant. To improve the outcome of such devices and to develop new therapies a method is needed that allows to determine the efficiency and the clinical output level of the implant before clinical data are available. ASTM standard F2504–05 describes a procedure to quantify the output levels of AMEIs as equivalent sound pressure levels from stapes vibration measurements in human cadaveric temporal bones (TBs). However, this standard is intended only for stimulations at the ossicular chain and requires a mobile and visible stapes. Common applications such as the round window (RW) stimulation and the mechanical inner ear stimulation with a DACI are thus outside the scope of ASTM standard F2504–05 and earlier studies indicate that stapes vibration is no reliable reference for the outcome of those stimulations. Therefore, in the present thesis it was first tested whether ASTM standard F2504–05 can be modified to quantify the output level of RW stimulations and mechanical inner ear stimulations. For this purpose these and further stimulation modes were performed with a DACI actuator in human cadaveric TBs and the output levels were quantified based on vibration measurements at the stapes and at the RW. The results show that such an adaption of the ASTM standard is possible but the determined output levels showed a pronounced variation and should be used only for rough estimates, especially at frequencies > 1 kHz. Therefore in the present thesis an alternative method was developed to quantify output levels of AMEIs and DACIs in cadaver studies. This method uses the intracochlear sound pressure difference (ICPD) between the inner ear compartments *scala vestibuli* and *scala tympani* as a reference, because this measure has been shown to correlate with auditory evoked potentials in animals and it is considered as the input to the inner ear independent from the mode of stimulation. In order to create the basis for a commonly accessible method it was first tested whether ICPDs are measurable in human TBs with off-the-shelf pressure sensors. The results demonstrate that two pressure measurement systems are usable to measure ICPDs during acoustic stimulation with sufficient SNR and sensitivity. Next, it was investigated whether ICPD can be used to quantify output levels of an AMEI in human cadaveric TBs. For this purpose an AMEI Incus stimulation was performed in TBs and the output levels were quantified as equivalent sound pressure levels from both stapes vibration measurement and ICPD measurement. To validate the results the experimentally obtained levels were directly compared to clinical data. Although ASTM standard F2504–05 has been published already in 2005 and is commonly used today, such a comparison demonstrating that the output levels predicted from cadaver studies actually match the real outputs in patients, had never been performed before. It was found that output levels estimated from stapes vibrations according to ASTM standard F2504–05 and clinical data match within 9 dB but ICPD as reference provided even more accurate results being almost identical to clinical data. So the results of this thesis demonstrate for the first time that both ICPD and stapes motion can be used as a valid measure to predict the clinical output level of AMEIs in cadaver studies. Based on the here presented findings vibration measurement as the faster and easier to conduct method is preferable to assess mechanical stimulations at the ossicular chain, whereas ICPD measurement is preferable if even more accurate results are needed and to assess stimulations outside the scope of ASTM standard

F2504–05.

Contents

List of Symbols

A_{SFP} Area of the stapes footplate
E electrical input signal driving the actuator
H_{ES} equivalent sound pressure transfer function
H_{EV} electro-vibrational transfer function
H_{SVU} acousto-vibrational transfer function
H_{TV} middle ear transfer function
L equivalent sound pressure level
N number of samples
T_{D} sound pressure transformation value
Z_{BM} acoustic impedance across the basilar membrane
Z_{F} acoustic impedance during forward stimulation
Z_{ME} acoustic impedance of the middle ear
Z_{RW} acoustic impedance of the round window
Z acoustic impedance
Δf_{BC} frequency shift added by the bragg cell
Δf_{D} frequency shift due to the Doppler effect
Δp_{A} intracochlear sound pressure difference in the aided condition
Δp_{U} intracochlear sound pressure difference in the unaided condition
Δp intracochlear sound pressure difference
Δ difference between two values
Φ angle between laser beam and direction of motion
λ wavelength
φ phase (angle)
d_{A} displacement in the aided condition
d_{U} displacement in the unaided condition
d distance or displacement
f frequency
p_{S} sound field sound pressure
p_{T} ear canal sound pressure at tympanic membrane

p_{ST}	intracochlear sound pressure in scala tympani
p_{SV}	intracochlear sound pressure in scala vestibuli
p	pressure or statistical p-value (lowest level of significance where the null hypothesis is rejected)
s	signal amplitude
u_{BM}	volume velocity across the basilar membrane
u_{RW}	round window volume velocity
u_{stap}	stapes volume velocity
u	volume velocity
v_A	velocity in the aided condition
v_U	velocity in the unaided condition
v	velocity
z	complex number

List of Abbreviations

AMEI	active middle ear implant
BC	bone conduction
BCD	bone conduction device
BTE	behind-the-ear
CHL	conduction hearing loss
CI	cochlear implant
CIC	completely-in-the-canal
DACI	direct acoustic cochlear implant
FFT	Fast Fourier Transformation
FMT	Floating Mass Transducer™
ICPD	intracochlear pressure difference
IMEHD	implantable middle ear hearing device
ITE	in-the-ear
LDV	laser Doppler vibrometer
PORP	partial ossicular replacement prosthesis
RW	round window
SFP	stapes footplate
SNHL	sensorineural hearing loss
SNR	signal-to-noise ratio
SPL	sound pressure level
ST	scala tympani
SV	scala vestibuli
TB	temporal bone
THD	total harmonic distortion
TLA	transducer loading assistant
TORP	total ossicular replacement prosthesis

Chapter 1

Introduction

1.1 Anatomy and Physiology of the Human Ear

The human ear can be divided into three parts: the outer ear, the middle ear and the inner ear (Figure 1.1). The outer ear consisting of the *pinna* and the outer ear canal collects sound waves and directs them to the tympanic membrane[1] [LENARZ & BOENNINGHAUS, 2012]. Due to its anatomy the outer ear acts as an acoustic resonator and amplifies sound pressure levels by up to 20 dB, depending on the angle of incidence and on the frequency of the sound [SHAW, 1974]. Incoming sound waves set the tympanic membrane to vibration that is transmitted by three small bones (the *ossicles*[2]) to the oval window, an opening of the inner ear. The ossicles, named *malleus*, *incus* and *stapes*, are connected by joints and located in the middle ear. The middle ear acts as an acoustic impedance transformer from the low-impedance air at the tympanic membrane to the high-impedance fluid in the inner ear. This is realized by two mechanisms. First, the area of the oval window of approx. $3.2\,\mathrm{mm}^2$ is much smaller than the effective area of the tympanic membrane of approx. $55\,\mathrm{mm}^2$ [VON BÉKÉSY, 1960]. The ratio of this two areas results in an increase in pressure of approx. 25 dB. Second, due to different operative lengths of malleus and incus, the lever ratio of the ossicles is approx. $1.3 : 1$ [VON BÉKÉSY, 1960]. Theoretically, both effects together amplify the pressure by approx. 27 dB. However, *in vivo*, several factors such as friction, complex vibration modes of the tympanic membrane and the inertia of the ossicles lead to a frequency dependent middle ear gain [PICKLES, 2013]. According to KUROKAWA & GOODE [1995] this amplification has a maximum of 23 dB around 1 kHz, is 0 dB at ≥ 7 kHz and decreases by -8.6 dB / octave in between. Without the impedance matching mechanism of the middle ear, about 98 % of the sound energy would be reflected during the transmission into the inner ear fluid [SCHMIDT ET AL., 2011]. The inner ear consists of two parts, the vestibular system being responsible for the sense of balance and the cochlea being responsible for sound detection and processing. The spiral-shaped cochlea has 2.5 turns and contains two fluid-filled canals called scala vestibuli (SV) and scala tympani (ST) (Figure 1.2) [SCHMIDT ET AL., 2011]. The SV and ST are separated by the *cochlear partition* that includes the basilar membrane, the organ of Corti, the Reissner's membrane and the scala media [GULYA

---

[1]Also known as eardrum.
[2]Also known as ossicular chain.
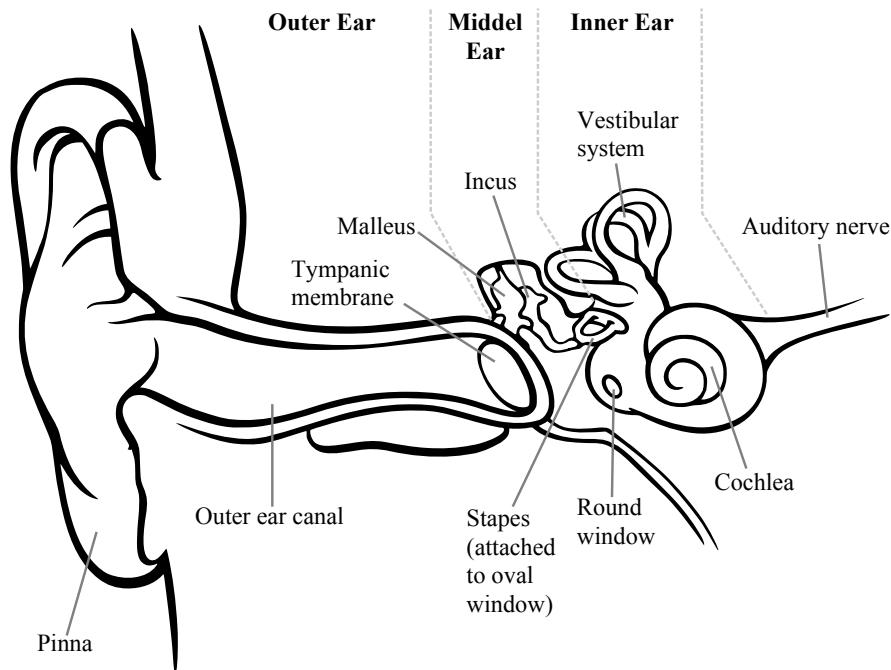
Figure 1.1. Schematic illustration of the human ear. Adapted and modified from CHITTKA & BROCK-MANN [2005] (CC BY 4.0).

ET AL., 2010]. At the *apex* of the cochlea SV and ST are connected by an opening called *helicotrema* (Figure 1.3) and so they are filled with the same fluid called *perilymph*, whereas scala media contains another kind of fluid called *endolymph*.

When the stapes footplate (SFP) pushes during sound perception into the oval window, a pressure wave is produced and the perilymph is displaced in two different ways (Figure 1.3) [SHERWOOD, 2012]: (1) The pressure wave displaces the perilymph from the oval window up the SV through the *helicotrema* and down the ST to the round window (RW). The RW membrane bulges outward and so the intracochlear pressure increase is compensated. Because the perilymph is almost incompressible, the volume displacement at the RW and oval window is equal and has a phase shift of approx. 180° [STENFELT ET AL., 2004a]. (2) Due to the compliance of the basilar membrane, the pressure wave takes additionally a shortcut from the SV to the ST causing a deflection of the basilar membrane. This deflection travels from the base of the cochlea where the oval window is located to the helicotrema and is known as the *traveling wave* [PICKLES, 2013]. From the base to the helicotrema, the basilar membrane becomes wider and more flexible and therefore each region of the basilar membrane vibrates maximally at a specific stimulation frequency [PICKLES, 2013; SHERWOOD, 2012]. A high-frequency tone produces a peak of deflection at the base and a low-frequency tone at the helicotrema [SHERWOOD, 2012]. Only the second pathway causing the deflection of the basilar membrane results in sound perception [SHERWOOD, 2012]. When the basilar membrane oscillates, the outer and inner hair cells in the organ of Corti (Figure 1.2) are bent back and forth and mechanically gated cation channels are activated. The outer hair cells amplify the deflection as they change their length when stimulated and the inner hair cells transform the movement to electrical signals activating the auditory nerve [PICKLES, 2013].
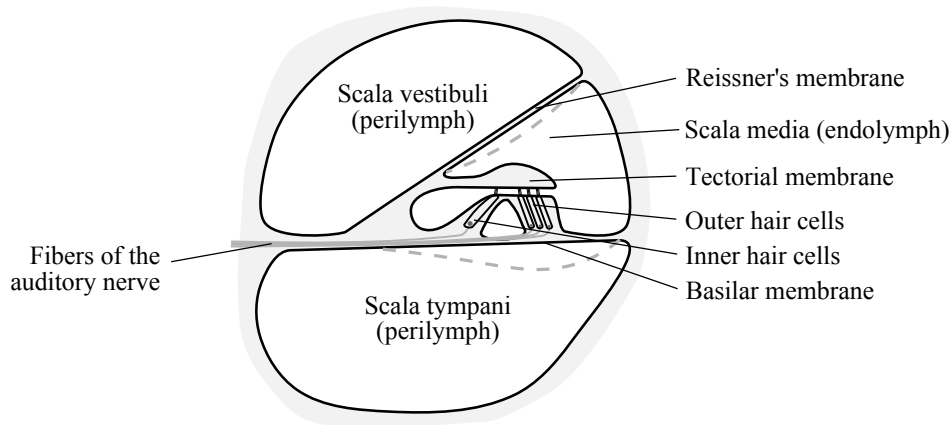
Figure 1.2. Schematic illustration of the cross section through one turn of the human cochlea. The dashed lines illustrate the deflection during sound perception.
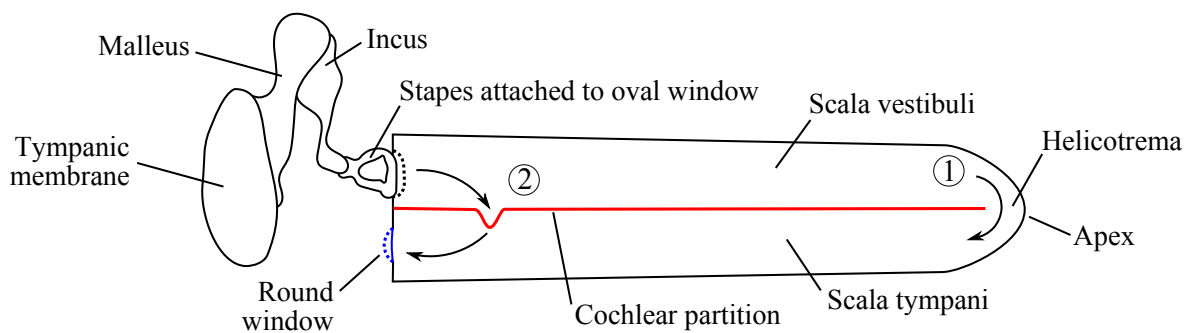
Figure 1.3. Schematic illustration of the human middle ear and cochlea. The cochlea is depicted uncoiled for a better illustration. From the oval window the sound induced intracochlear fluid movement takes two pathways: ① Through scala vestibuli, around the helicotrema, and through scala tympani to the round window. ② From scala vestibuli directly to scala tympani through the cochlear partition. The dashed lines illustrate the displacements during sound perception.

1.2 Hearing Losses

Hearing losses may be caused by various factors. Depending on the location of the cause, a distinction is made between conduction hearing loss (CHL) and sensorineural hearing loss (SNHL) [LENARZ & BOENNINGHAUS, 2012]. In CHL the transmission of sound in the outer or in the middle ear is impaired [KOMPIS, 2013]. Common causes for a CHL are e.g. an *atresia*[3] of the outer ear canal, an *otosclerosis*[4], a perforation of the tympanic membrane or a chronic *otitis media*[5] [KOMPIS, 2013]. A SNHL occurs when the transformation of sound into an electrical signal by the hair cells (cochlear hearing loss) or the transmission in the auditory nerve or in the central auditory pathway (retrocochlear hearing loss) is impaired [KOMPIS, 2013; LENARZ & BOENNINGHAUS, 2012]. Retrocochlear hearing losses are rare and therefore an SNHL is usually understood as a cochlear hearing loss [KOMPIS, 2013]. Common causes for an SNHL are e.g. an acoustic trauma, meningitis, sudden hearing loss and *presbyacusis*[6] [KOMPIS, 2013]. A combination of both types of hearing loss is called mixed hearing loss [LENARZ & BOENNINGHAUS, 2012]. Hearing losses are evaluated not only by their origin but also by their severity measured as the difference to normal hearing in dB HL (0 dB HL = normal hearing) [LENARZ & BOENNINGHAUS, 2012]. According to the WORLD HEALTH ORGANIZATION [2016] the severity is ranked as slight or mild (26–40 dB HL), moderate (41–60 dB HL), severe (61–80 dB HL) and profound (>81 dB HL).

1.3 Therapies of Hearing Losses

Depending on the cause and severity of a hearing loss, various therapies are possible today. These range from middle ear surgery and conventional hearing aids to the implantation of a cochlear implant (CI), active middle ear implant (AMEI), direct acoustic cochlear implant (DACI) or bone conduction device (BCD). AMEIs, DACIs and BCDs are usually summarized under the term acoustic (hearing) implants. As this thesis is focused on the output level characterization of AMEIs and DACIs, only theses kinds of devices are described in detail. However, for the sake of completeness all common therapies of hearing losses are briefly presented.

1.3.1 Middle Ear Surgery

A CHL that is caused by a disrupted or impaired ossicular chain can be treated by a reconstruction with a passive middle ear implant PURIA ET AL. [2013]. There are two different types of such implants, the partial ossicular replacement prosthesis (PORP) and the total ossicular replacement prosthesis (TORP). A PORP replaces the malleus and incus if the stapes is still intact, whereas a TORP is used for a reconstruction of the entire chain [BEUTNER & HÜTTENBRINK, 2009]. In the case of *otosclerosis*, the entire stapes is removed (*stapedectomy*) or the suprastructure of the stapes is removed and the SFP is perforated (*stapedotomy*).

---

[3]"Congenital absence of a normal opening [...]." [STEDMAN, 2005]
[4]Pathological formation of bone causing a fixation of the stapes. [STEDMAN, 2005]
[5]"Inflammation of the middle ear." [STEDMAN, 2005]
[6]Age-related hearing loss. [STEDMAN, 2005]

A piston prosthesis is then attached to the incus and coupled to the perilymph [LENARZ & BOENNINGHAUS, 2012].

1.3.2 Conventional Hearing Aids

Conventional hearing aids are compact sound-amplifying devices that consist basically of one or more microphone(s), an amplifier, a signal processor, a loudspeaker and a battery [POPELKA ET AL., 2016]. Acoustic signals are collected, amplified and processed for an optimal treatment of the individual hearing loss and finally applied to the tympanic membrane. Conventional hearing aids can be built as a completely-in-the-canal (CIC) device, as an in-the-ear (ITE) device or as a behind-the-ear (BTE) device [POPELKA ET AL., 2016]. In ITE and CIC devices all components are housed in a single case that fits entirely in the outer ear canal (CIC) or within the outer ear canal and the bowl of the pinna (ITE). As the name implies, BTE devices are worn behind the pinna and its acoustic output signal is delivered via a tube into an earmold inside the outer ear canal or a loudspeaker in an earmold is electrically driven. The typical indication of conventional hearing aids is a SNHL of approx. 30 to 80 dB HL between 0.5 and 4 kHz and today they are the most common devices for the treatment of hearing losses [KOMPIS, 2013].

1.3.3 Cochlear Implants

CIs bypass the outer ear, the middle ear and the (damaged) hair cells to stimulate the auditory nerve directly with electrical impulses [KOMPIS, 2013]. Basically such an implant consists of two parts, (1) an external BTE unit containing one or more microphone(s), a signal processor, an induction coil transmitter and batteries and (2) an implanted part comprising a receiver/stimulator and an electrode array. The BTE unit collects sound that is analyzed, processed and transmitted transcutaneously as a coded signal to the receiver [KOMPIS, 2013]. The stimulator converts the received signal to electric impulses that stimulate the auditory nerve by an array of usually 12 to 22 electrical contacts inserted in the cochlea [KOMPIS, 2013]. A crucial requirement for the implantation of a CI is an intact auditory nerve and an intact auditory pathway [DEUTSCHE GESELLSCHAFT FÜR HALS-NASEN-OHREN-HEILKUNDE, 2012]. Indications for a CI are an unilateral or bilateral profound cochlear SNHL or a residual hearing that is not enough for speech understanding with a conventional hearing aid [LENARZ & BOENNINGHAUS, 2012].

1.3.4 Active Middle Ear Implants

AMEIs, also known as implantable middle ear hearing devices (IMEHDs), convert external sound to vibration that stimulates the ossicular chain or the RW mechanically [KUHN, 2012]. Today, five AMEIs are approved for use in Europe and/or in the United States of America and commercially available [PIRLICH ET AL., 2017; TISCH, 2017]: the semi-implantable systems MET® (Cochlear™ Ltd.), Vibrant Soundbridge® (Vibrant MED-EL Hearing Technology GmbH) and MAXUM (Ototronix LLC) and the fully implantable systems Carina® (Cochlear™ Ltd.) and Esteem® (Envoy Medical). All semi-implantable devices comprise an

external part that is worn at the skull (MET and Vibrant Soundbridge) or in the outer ear canal (MAXUM) and an implanted part. The external part containing basically one or more microphone(s), a sound processor, an amplifier and a power supply (battery/-ies), converts perceived sound to an electrical signal. The external part of the MAXUM device converts this signal to electromagnetic energy that drives a magnet attached to the ossicles. The MET & Vibrant Soundbridge transmit the electrical signal transcutaneously by an induction system to the implanted part where the signal is then converted to vibration by an electromagnetic transducer. In case of the Vibrant Soundbridge the entire transducer, called Floating Mass Transducer™ (FMT), vibrates and stimulates the structure where it is attached (e.g. the ossicular chain, the oval window or the RW). The transducer of the MET system, called T2 transducer, is mounted in the skull bone and a vibrating rod stimulates the incus, the RW, or the stapes. The fully implantable Carina system is the successor of the MET system [BITTENCOURT ET AL., 2014] and has therefore the same principle of stimulation and mostly the same components, such as the T2 transducer. However, in contrast to the MET system all components including the microphone, the audio processor and the power supply are implanted and the induction system is only needed for charging. The fully implantable Esteem system consist mainly of an audio processor and two piezoelectric transducers, coupled to the incus (sensor) and stapes (driver). If the tympanic membrane is stimulated by sound, the sensor detects the evoked vibrations and converts them to an electrical signal [BITTENCOURT ET AL., 2014]. This signal is amplified and transmitted to the driver stimulating the stapes by vibration. To prevent acoustic feedback, the stapes and the incus have to be disarticulated and a segment of the incus has to be removed [KUHN, 2012]. While a stimulation of the ossicular chain or of the oval window mimics the natural pathway of sound (*forward stimulation*), an excitation of the RW stimulates the ear in reverse direction compared to the physiological sound transmission (*reverse stimulation*). However, the feasibility and clinical applicability of mechanical RW stimulation with an AMEI has been already demonstrated in several studies [e.g. COLLETTI ET AL., 2006; ZWARTENKOT ET AL., 2016].

Depending on the system, AMEIs are indicated for patients with CHL, mixed hearing loss and (bilateral) moderate to severe SNHL [BITTENCOURT ET AL., 2014; KUHN, 2012]. Furthermore they are an alternative for patients who have no sufficient benefit from conventional hearing aids or contraindications to conventional hearing aids such as otitis externa[7], acoustic feedback and occlusion effects [KUHN, 2012].

1.3.5 Direct Acoustic Cochlear Implants[8]

The objective of a DACI is to bypass the physiological sound transmission pathway through the outer and middle ear and to stimulate the perilymph fluid directly by vibration. In the past, this approach, also known as *direct acoustic cochlear stimulation*, has also been tested with different AMEIs (MET, Vibrant Soundbridge) in cadaver studies and patients [DEVÈZE ET AL., 2010; SCHWAB ET AL., 2012]. However, today, the only available DACI is the semi-implantable Codacs™ system (Cochlear™ Ltd., Australia) (Figure 1.4). Similar to semi-implantable AMEIs the Codacs system consists of an external part and an implant.

---

[7]Inflammation of the outer ear canal. [STEDMAN, 2005]
[8]Parts of this section have been published in GROSSÖHMICHEN ET AL. [2015]
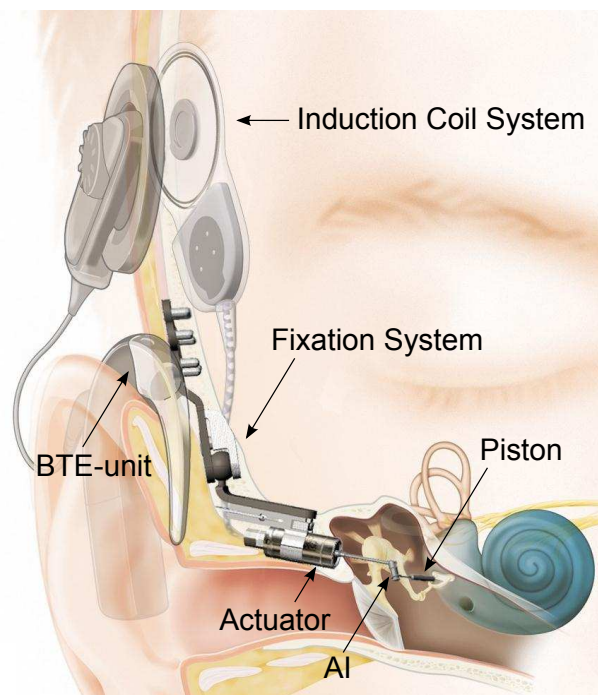
Figure 1.4. Illustration of the implanted Codacs system. Taken from GROSSÖHMICHEN ET AL. [2015] (CC BY 4.0).

The external part, a BTE unit containing two microphones and a sound processor, converts collected acoustic signals to an electrical signal that is transmitted to the implant transcutaneously by an induction coil system. An electromagnetic transducer (Codacs actuator) held by a skull bone mounted fixation system converts the electrical signal to vibration. The vibration is transmitted to the perilymph by a piston prosthesis crimped to the angled tip of the actuator rod, called artificial incus, and inserted into the inner ear through a SFP fenestration (*stapedotomy*). The intended use of the Codacs system is the treatment of severe to profound mixed hearing losses caused by otosclerosis [HÄUSLER ET AL., 2008]. Its clinical applicability as well as that of a similar device have been demonstrated in several studies [e.g. BUSCH ET AL., 2013; LENARZ ET AL., 2014, 2013].

1.3.6 Bone Conduction Devices

BCDs convert perceived sound to vibration that is transmitted via the skull bone to the cochlea, bypassing the outer and middle ear [REINFELDT ET AL., 2015]. According to REINFELDT ET AL. [2015] today's BCDs can be divided into two groups: (1) direct-drive-systems such as the Baha® (Cochlear Bone Anchored Solutions AB), the Ponto™ (Oticon Medical) and the Bonebridge™ (Vibrant MED-EL Hearing Technology GmbH) and (2) skin-drive-systems such as the Baha Attract (Cochlear Bone Anchored Solutions AB) and the Sophono™ (Medtronic). Direct-drive-systems transmit the vibration directly to the bone, either through an implanted screw where the vibrating transducer is attached (Baha & Ponto) or by an implantation of the vibrating transducer in the skull bone (Bonebridge). Skin-drive-systems transmit the vibration from an external transducer through the intact skin to an

implanted magnet. The common indications of BCDs are conductive and mixed hearing loss and single-sided deafness (impaired hearing in only one ear) [REINFELDT ET AL., 2015].

1.4   Predicting Output Levels of AMEIs and DACIs: State of the Art

For many reasons it is necessary to determine the system output of AMEIs and DACIs before clinical data are available. These include the improvement of existing devices, feasibility studies on new stimulation modes, assessment of new devices and the definition of an indication range for an implant. Already 150 years ago HELMHOLTZ has used human cadaveric ears to study the mechanics of human hearing [HELMHOLTZ, 1868] and in 1928 VON BÉKÉSY observed the traveling wave of the basilar membrane for the first time when he performed experiments in human cadaver ears [OLSON ET AL., 2012]. In the recent past, several studies [e.g. CHIEN ET AL., 2009; GOODE ET AL., 1993; ROSOWSKI ET AL., 1990] demonstrated that the sound transmission through the human middle ear is comparable in cadaveric and live ears. Thus, the human cadaveric ear has become the by far most accepted model to study the mechanics of human hearing [e.g. AIBARA ET AL., 2001; HATO ET AL., 2003] and to investigate mechanical stimulations with an acoustic implant [e.g. CHATZIMICHALIS ET AL., 2012; MAIER ET AL., 2013; PENNINGS ET AL., 2010]. For this reason the present thesis is focused on methods to determine output levels of AMEIs and DACIs in human cadaveric ears and rarely used methods such as animal studies [e.g. JAVEL ET AL., 2003; KOKA ET AL., 2010; LUPO ET AL., 2009], experiments in artificial ear models [STIEGER ET AL., 2007] and computer simulations [e.g. BÖHNKE ET AL., 2013; BORNITZ ET AL., 2010; LIU ET AL., 2014] are not discussed. Such cadaver experiments are usually performed in so-called temporal bone (TB)[9] preparations extracted from the human head [e.g. CHATZIMICHALIS ET AL., 2012; MAIER ET AL., 2013; PENNINGS ET AL., 2010; ROSOWSKI ET AL., 2007]

   To assess the performance of AMEIs and DACIs in TBs various approaches are conceivable. One of them is the measurement of the stapes vibration amplitude because this quantity is considered as the mechanical input to the inner ear (see section 1.1). To predict the clinical system output of AMEIs from stapes vibration measurements ASTM standard F2504–05 [ASTM, 2005] defines a procedure which is intended for applications where the ossicles are stimulated. Inside the cochlea, the stapes motion produces a sound pressure difference between SV and ST which causes a deflection of the basilar membrane. Therefore, both values the intracochlear pressure difference (ICPD) and the vibration amplitude of the basilar membrane could also be used as a measure of AMEI or DACI stimulation levels. The state of the art of all these approaches is described in the following sections 1.4.1–1.4.4 and finally the limitations of all relevant methods are discussed in section 1.4.5.

---

[9]An irregular bone containing the external, middle, and inner ear [STEDMAN, 2005].

1.4.1 Measuring the Vibration of the Stapes

Today, stapes vibration measurement is certainly the most popular method to assess AMEI stimulations in cadaveric ears, even in cases where the RW is stimulated and the stapes motion is not the mechanical input to the inner ear. Measured vibration responses are often directly compared to determine the difference in stimulation efficiency between similar stimulation modes, e.g. RW stimulation with and without interposed materials [PENNINGS ET AL., 2010].

At 1 kHz, an acoustic sine-wave signal of 94 dB SPL produces stapes displacement magnitudes of approx. 10–40 nm [ASTM, 2005]. To measure these small magnitudes of vibration in cadaver ears various techniques have been used in the past with varying degrees of success, e.g. stroboscopic light illumination, capacitive probe technology and the Mössbauer method [NUTTALL & FRIDBERGER, 2012]. However, current best practice for this purpose is laser Doppler vibrometry because this technique is contactless and has a high sensitivity, accuracy, linearity and bandwidth [CASTELLINI ET AL., 2009; NUTTALL & FRIDBERGER, 2012; ZAHNERT, 2003]. The working principle of an laser Doppler vibrometer (LDV) is based on the detection of the Doppler effect. The beam of a laser (usually HeNe) is split into a measurement beam and a reference beam and the former is focused on the reflective surface of a vibrating object (Figure 1.5). Due to the Doppler effect the frequency f of the reflected laser beam has a frequency shift of

$$\Delta f_{\mathrm{D}} = \frac{2v}{\lambda} \,, \tag{1.1}$$

where v is the object's velocity along the axis of the beam and λ is the known wavelength of the laser (e.g. $\lambda_{HeNe} = 632.8$ nm) [CASTELLINI ET AL., 2009]. This Doppler frequency shift is detected on a photodetector as an interference of the reflected beam with the reference beam (Figure 1.5). The velocity of the object's vibration is derived from the frequency shift and converted into an analog voltage signal that is directly proportional to the velocity of the object [POLYTEC, 2003]. To distinguish the object's motion direction along the laser axis, an acousto-optic modulator (Bragg cell, Figure 1.5) adds a fixed frequency shift Δf_{BC} (usually 40 MHz) to the reference beam [POLYTEC, 2003]. If the total frequency shift

$$\Delta f_{\mathrm{tot}} = \Delta f_{\mathrm{D}} + \Delta f_{\mathrm{BC}} \tag{1.2}$$

detected by the photodetector is smaller than Δf_{BC}, the object moves towards the LDV, and if $\Delta f_{\mathrm{tot}} > \Delta f_{\mathrm{BC}}$ the object moves away from the LDV [CASTELLINI ET AL., 2009; POLYTEC, 2003]. It is also possible to measure the displacement of the vibrating target with an LDV. For this purpose not the Doppler frequency shift is demodulated, but the number of fringes caused by destructive and constructive interferences is counted by an digital counter [CASTELLINI ET AL., 2009; POLYTEC, 2003]. According to the linear relationship

$$\Delta \varphi = \frac{4\pi d}{\lambda} \,, \tag{1.3}$$

each fringe, i.e. phase shift $\Delta \varphi = 2\pi$, corresponds to a displacement d of $\lambda/2$ (e.g. 316.4 nm for HeNe laser) [JOHANSMANN ET AL., 2005].
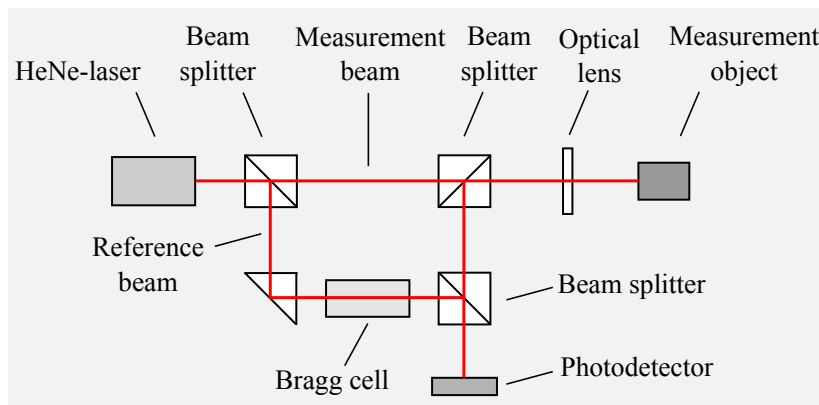
Figure 1.5. Illustration of the components of a laser Doppler vibrometer.

In the field of auditory research, three different types of commercially available LDVs [POLYTEC, 2003] are commonly used (Figure 1.6): single-point LDVs, scanning LDVs and single-point 3D LDVs. A single-point LDV measures the velocity component along the axis of the measurement laser beam at one single point of the measurement object. A major advantage of these devices is that the sensor head can be integrated in a surgical microscope allowing a precise positioning of the laser beam and a fast measurement procedure. The single-point LDV is the by far most commonly used LDV type to measure vibrations responses in TB experiments. A scanning LDV combines a single-point LDV with a computer-controlled scanning system. Motorized mirrors direct the laser beam automatically point-by-point over the object's surface (Figure 1.6), allowing quick multi-point measurements and a visualization of the vibrating surface [POLYTEC, 2003]. In TB experiments scanning LDVs are used to investigate the complex vibrations modes of the tympanic membrane, the stapes and the RW membrane [BORNITZ ET AL., 1999; CHATZIMICHALIS ET AL., 2012; KWACZ ET AL., 2011; SIM ET AL., 2010]. A 3D-LDV measures three angled (12°) vibration velocity components at one point of the measurement object with three laser beams simultaneously and converts them to three 3 orthogonal velocity components (Figure 1.6) [POLYTEC, 2005]. In hearing research, this technology is used to reconstruct the complex three-dimensional motion of the ossicles [LAUXMANN, 2012].

1.4.2 ASTM Standard F2504-05[10]

In order to standardize the assessment of AMEIs, the standards organization *ASTM International* published the "Standard Practice for Describing System Output of Implantable Middle Ear Hearing Devices" F2504–05 [ASTM, 2005]. It contains both a procedure to quantify the output levels of an AMEI stimulating the ossicular chain in a human cadaveric TB as equivalent sound pressure levels [eq. dB SPL] and selection criteria for adequate TBs. Today, this standard is commonly used [e.g. DEVÈZE ET AL., 2013; MLYNSKI ET AL., 2015a; ROSOWSKI ET AL., 2007].

---

[10]Parts of this section have been published in GROSSÖHMICHEN ET AL. [2015]
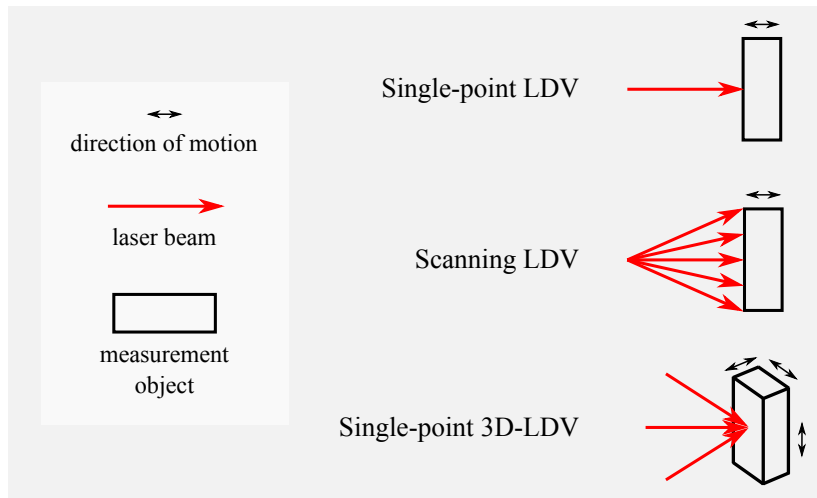
Figure 1.6. Illustration of the measuring principle of different kinds of laser Doppler vibrometers commonly used in auditory research.

AMEI Output Level Quantification

The output quantification is based on a comparison of stapes velocities measured with an LDV in human cadaveric TBs in response to sound and to AMEI stimulation (Figure 1.7). First, a sound field sound pressure p_S [Pa] is applied to the ear canal of the unaided TB. While the ear canal sound pressure p_T [Pa] is recorded 2–3 mm in front of the tympanic membrane by a probe microphone, the vibration response of the stapes (velocity v_U) is recorded by the LDV. The velocity can be measured either at the head, the posterior crus or the footplate of the stapes, with the latter option being preferred. The angle of incident of the LDV laser beam shall be $\leq 60°$ to the SFP normal. From this measurement the frequency-specific middle ear transfer function H_{TV} is determined as

$$H_{TV} = \frac{v_U}{p_T} \, . \tag{1.4}$$

After the AMEI transducer is implanted, the velocity of the stapes v_A during transducer stimulation is measured similarly and the electro-vibrational transfer function H_{EV} is then computed as

$$H_{EV} = \frac{v_A}{E} \, , \tag{1.5}$$

with E being the electrical input to the transducer (voltage or current). Using values of sound pressure transformation from tables I–III in SHAW & VAILLANCOURT [1985], the recorded ear canal sound pressure p_T can be transformed into sound field pressure p_S and the acousto-vibrational transfer function H_{SVU} can be determined as

$$H_{SVU} = \frac{v_U}{p_S} \, . \tag{1.6}$$

Having H_{SVU} and H_{EV}, the equivalent sound pressure transfer function H_{ES} can then be computed as

$$H_{ES} = \frac{H_{EV}}{H_{SVU}} \, . \tag{1.7}$$
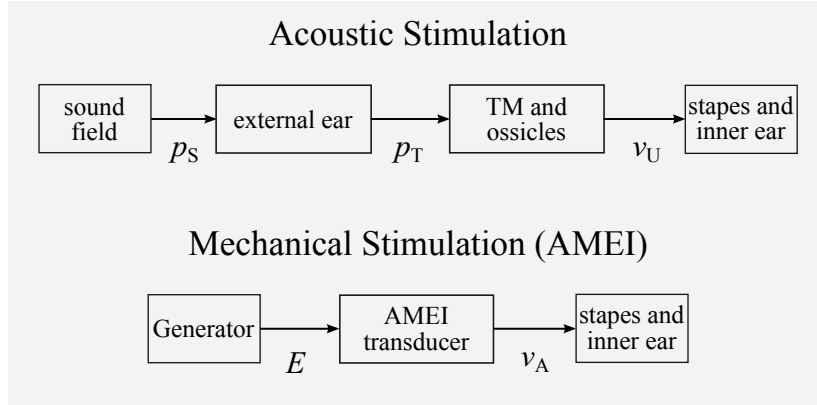
Figure 1.7. Illustration of the signal flow in the middle ear during acoustic and mechanical stimulation according to ASTM [2005]. During acoustic stimulation sound field sound pressure p_S [Pa] is transformed by the external ear to ear canal sound pressure p_T [Pa] at the tympanic membrane. The tympanic membrane and the ossicles transform p_T to stapes velocity v_U, considered as the mechanical input to the inner ear. During mechanical stimulation the electrically driven (input voltage E) AMEI transducer generates stapes velocity v_A.

Finally, the maximum equivalent sound field pressure level $L_{E\max}$ [eq dB SPL$_{FF}$] produced by the AMEI can be calculated by

$$L_{E\max} = 20 \log_{10} \left(\frac{H_{ES} \cdot E_{\max}}{2 \cdot 10^{-5} \mathrm{Pa}} \right) = 20 \log_{10} \left(\frac{\frac{v_A}{E} \cdot \frac{p_S}{v_U} \cdot E_{\max}}{2 \cdot 10^{-5} \mathrm{Pa}} \right) , \qquad (1.8)$$

with $E_{\max}$ being the device-specific maximum electrical input to the AMEI transducer.

Differing from the original ASTM procedure, AMEI output levels predicted in cadaver studies are usually [e.g DEVÈZE ET AL., 2013; ROSOWSKI ET AL., 2007; TRINGALI ET AL., 2011] determined as equivalent *ear canal* sound pressure level [eq. dB SPL$_{TM}$] and not as equivalent *sound field* sound pressure level [eq. dB SPL$_{FF}$]. In that case, sound pressure p_T recorded at the tympanic membrane is not transformed into sound field pressure p_S and thus $L_{E\max}$ is calculated as equivalent *ear canal* sound pressure level [eq. dB SPL$_{TM}$] by

$$L_{E\max} = 20 \log_{10} \left(\frac{\frac{H_{EV}}{H_{TV}} \cdot E_{\max}}{2 \cdot 10^{-5} \mathrm{Pa}} \right) = 20 \log_{10} \left(\frac{\frac{v_A}{E} \cdot \frac{p_T}{v_U} \cdot E_{\max}}{2 \cdot 10^{-5} \mathrm{Pa}} \right) . \qquad (1.9)$$

In this thesis, sound pressure level (SPL) [dB SPL] without index stands for the ear canal sound pressure level at the tympanic membrane [dB SPL$_{TM}$], unless otherwise indicated. From the equations it is recognizable that the procedure of output level quantification according to ASTM F2504–05 requires a linear change in transducer vibration output amplitude with electrical transducer input at values $\leq E_{\max}$ and a linearity of the middle ear transfer function H_{TV} in human cadaveric TBs below $L_{E\max}$. The former is device-specific, but can easily be confirmed in a bench test and the latter has been demonstrated for ear canal sound pressure levels (SPLs) of up to 124 dB SPL at 0.4–6 kHz by GOODE ET AL. [1994] and of up to 130 dB SPL at 0.1–4 kHz by VOSS ET AL. [2000].

| Frequency [kHz] | Stapes Velocity | |
	Upper Limit [mm/s/Pa]	Lower Limit [mm/s/Pa]
0.125	0.048	0.004
0.25	0.074	0.012
0.5	0.180	0.029
1	0.250	0.062
2	0.138	0.037
3	0.094	0.020
4	0.060	0.014
6	0.047	0.007

Table 1.1. Acceptance range of stapes velocity responses to sound given by ASTM [2005] for TB selection.

Qualification Criteria for TB Selection

In the beginning of the experiment before AMEI implantation the morphological integrity of all relevant structures of the TB shall be confirmed by visual inspection. If this is the case, it has to be checked that the frequency-specific middle ear transfer function H_{TV} (stapes velocity produced by an ear canal sound pressure of 94 dB SPL, equation (1.4)) of the TB lies at 0.25–4 kHz within a given acceptance range (Table 1.1). However, this range was found to be too strict and a 20 % widened range was recommended [ROSOWSKI ET AL., 2007] that is commonly used as reference [e.g. DEVÈZE ET AL., 2010, 2013; MAIER ET AL., 2013; MLYNSKI ET AL., 2015b; TRINGALI ET AL., 2011]. The acoustic stimulation for the TB selection shall be performed with ear canal SPLs in the range of 80 to 100 dB SPL.

1.4.3 Intracochlear Sound Pressure Measurement[11]

As described in section 1.1, the motion of the SFP produces in the cochlea a difference in sound pressure between SV and ST initiating the traveling wave of the basilar membrane. This so called ICPD

$$\Delta p = p_{\text{SV}} - p_{\text{ST}} \tag{1.10}$$

measured at the cochlear base has been shown to correlate with auditory evoked potentials in animals [DANCER & FRANKE, 1980] and is considered as the "input signal to the cochlea"[NAKAJIMA ET AL., 2009]. Measuring ICPD is therefore a potential method to quantify the output level of an AMEI or DACI in human cadaveric ears. For this approach a technique is needed which measures sound pressures in SV and ST simultaneously. Early attempts to measure intracochlear sound pressure in guinea pigs [BURGEAT ET AL., 1963, 1964] provided only limited results but indicated the general feasibility of such measurements. Ten years later, the first systematic measurements and quantifications of intracochlear sound pressure have been reported in NEDZELNITSKY [1974] and were followed by similar

---

[11]Parts of this section have been published in GROSSÖHMICHEN ET AL. [2017]

studies [DANCER & FRANKE, 1980; FRANKE & DANCER, 1982; LYNCH ET AL., 1982; NEDZELNITSKY, 1980]. In these works a "probe hydrophone" consisting of a probe tube (250–350 µm outer diameter) connected to a piezoresistive transducer was used to measure intracochlear sound pressures *in vivo* in guinea pigs and cats. The probe was filled with silicone fluid and its open end was inserted into the perilymph through a hole that has been drilled into the cochlea (*cochleostomy*). DANCER & FRANKE [1980] and NEDZELNITSKY [1980] demonstrated that the sound-evoked sound pressure difference between SV (P_{SV}) and ST (P_{ST}) measured *in vivo* at the cochlear base in guinea pigs and cats corresponds to the cochlear microphonics[12]. These results supported the assumption that intracochlear sound pressure difference at the cochlear base is the input signal to the cochlear partition that causes its deflection and that it correlates with cochlear excitation [DANCER & FRANKE, 1980].

Measurements of intracochlear sound pressure in human cadaveric TBs have been reported for the very first time one decade later by LODWIG ET AL. [1993]. In this and a later study from the same laboratory [HÜTTENBRINK & HUDDE, 1994] sound pressures have been recorded in the SV with a self-made "probe hydrophone" which worked on a similar principle as the devices that have been used before in the animal studies by DANCER & FRANKE; LYNCH ET AL. and NEDZELNITSKY. PURIA ET AL. [1997] modified this technique and measured sound pressures more directly with a hydropressure transducer without a probe tube inserted into the cochlear vestibule of human cadaveric TBs.

A completely different approach was taken by OLSON [1998] who developed a miniature optical pressure sensor for intracochlear sound pressure measurement based on the principle of an optic lever. This sensor consists of a glass capillary of 167 µm outer diameter closed at one side with a pressure sensitive and light-reflecting gold coated membrane. Using an optical fiber coupler with 50:50 splitting ratio the other side of the capillary is connected to an LED and to a photodiode sensor. Light coming from the LED is reflected by the gold coated membrane at the tip and returns to the photodiode sensor. A variation in external pressure at the sensor tip deflects the membrane and changes the amount of the returning light detected by the photodiode sensor. In OLSON [1998] intracochlear sound pressures were measured simultaneously in SV and ST in gerbils using two of these sensors. With two of these sensors NAKAJIMA ET AL. [2009] measured for the first time intracochlear sound pressures simultaneously in SV and ST in human cadaveric TBs and determined the ICPD across the basilar membrane. Their results demonstrated that intracochlear sound pressure levels in both scalae increase linear with the SPL input at the tympanic membrane (p_T) and so they concluded that ICPD measured at the cochlea base can be used as a measure for the input signal to the cochlea. Furthermore they stated that ICPD is a superior measure for the cochlear input than p_{SV} alone. In following studies [NAKAJIMA ET AL., 2010; PISANO ET AL., 2012; STIEGER ET AL., 2013] ICPDs have been successfully measured during forward (acoustic) and reverse (mechanical) stimulations in human cadaveric TBs using the sensor developed by OLSON. Later, the "Olson sensor" has been stepwise miniaturized to an outer diameter of 126 µm and then of 81 µm [OLSON & NAKAJIMA, 2015]

---

[12]Measurable potentials generated by the hair cells in response to acoustic stimulation [LENARZ & BOENNINGHAUS, 2012].

1.4.4 Measuring the Vibration of the Basilar Membrane

Various techniques have already been used to detect the motion of the basilar membrane during acoustic and mechanical stimulations in TBs and animals. These include LDV measurements through a cochleostomy [CHEN ET AL., 2014; NUTTALL ET AL., 1991], optical coherence tomography (OCT) [CHEN ET AL., 2011], volumetric optical coherence tomography (VOCT) [LEE ET AL., 2015] and ultrasound (US) [TORBATIAN ET AL., 2012]. However, compared with stapes vibration measurement and ICPD measurement these approaches have two major disadvantages. Either the mechanics of the cochlear might be strongly affected because a cochleostomy must remain open during the measurement (LDV, OCT) and glass beads have to be placed on the basilar membrane (LDV) or the equipment is custom-built and hard to replace by off-the-shelf devices (VOCT, US). Therefore basilar membrane vibration measurement was not taken into further consideration in the present thesis.

1.4.5 Limitations of Current Measurement Methods[13]

Comparing measured stapes vibration amplitudes is an adequate method to compare the efficiencies of similar mechanical stimulations directly in the same TB. This approach allows, for example, to compare the efficiencies of AMEI stimulations at the RW with and without interposed material [MLYNSKI ET AL., 2015b], at the ossicles with different coupling elements [DEVÈZE ET AL., 2013] and at the incus before and after filling the middle ear space with saline (simulated middle ear effusion) [LUPO ET AL., 2014]. However, to perform objective comparisons between different studies, different stimulation modes (e.g. reverse vs. forward stimulation) and different implants and, most importantly, to define an indication range for an acoustic implant before clinical results are available, the expected clinical output level of an implant for a given input voltage has to be determined from the cadaver experiment. As described before, ASTM standard F2504–05 is intended exactly for this purpose and so it provides a procedure to quantify the output level of an AMEI as equivalent SPL from stapes velocity measurements. However, although this standard has been published already in 2005 and has become the "gold standard method" for preclinical evaluations of AMEIs, it has never been investigated whether the predicted output levels actually match the real outputs in patients. Furthermore, the ASTM procedure has only a limited applicability. First, the procedure requires a mobile and visible stapes. Second, the ASTM standard is intended only for AMEI stimulations at the ossicles. Of course, one could assume that the standard can easily be used for other acoustic implant stimulations as well, but according to current research stapes velocity is not a good measure of cochlear excitation in these cases. This is due to the fact that ASTM standard F2504–05 is based on a direct comparison between the stapes velocity v_U measured during acoustic stimulation and v_A measured during mechanical stimulation (see equation (1.8)). In other words, it is assumed that the relationship between the measured stapes velocity (considered as the mechanical inner ear input) and the cochlea excitation (sound pressure difference Δp across the basilar membrane) is identical in both acoustic and mechanical stimulation. This is only the case if the induced volume velocity u (i.e. the flow of sound) acts against the identical magnitude of total acoustic impedance

---

[13]Parts of this section have been published in GROSSÖHMICHEN ET AL. [2015, 2016b, 2017]

Z in both acoustic and mechanical stimulation. However, according to current knowledge and model theories this appears to be only the case if the actuator stimulates the ossicular chain and the cochlea is intact. A simple model of the system of the acoustic impedances and volume velocities in forward acoustic stimulation adapted from STIEGER ET AL. [2013] is given in Figure 1.8A. In this case, the vibrating SFP produces at the oval window the volume velocity u_{stap} that faces the total cochlear impedance

$$Z_{\text{F}} = Z_{\text{BM}} + Z_{\text{RW}} , \tag{1.11}$$

with Z_{BM} being the differential impedance across the basilar membrane and Z_{RW} being the impedance of the RW [STIEGER ET AL., 2013]. Measurements performed by STENFELT ET AL. [2004a] demonstrated that in acoustic stimulation the volume velocities at the oval window (u_{stap}) and at the RW (u_{RW}) are almost identical. It can therefore be assumed that

$$u_{\text{stap}} \approx u_{\text{BM}} \approx u_{\text{RW}} , \tag{1.12}$$

meaning that leakage flows through third window paths[14] in SV and ST can be neglected [STIEGER ET AL., 2013]. Thus, in forward stimulation, stapes volume velocity (u_{stap}) can be considered as proportional to the volume velocity (u_{BM}) and to the sound pressure difference ($\Delta p = p_{\text{SV}} - p_{\text{ST}}$) across the basilar membrane [STIEGER ET AL., 2013]. The same applies to the stapes velocity (v_{stap}) because

$$u_{\text{stap}} = v_{\text{stap}} \cdot A_{\text{SFP}} , \tag{1.13}$$

with A_{SFP} being the area of the SFP.

Most AMEIs were initially developed for the treatment of SNHL where the ossicular chain is stimulated [KASIC & FREDRICKSON, 2001; MLYNSKI ET AL., 2015b] and ASTM F2504–05 is intended for this stimulation mode. In this case, volume velocity u_{stap} faces the identical set of acoustic impedances as during acoustic stimulation (Figure 1.8B). This means that the relationship between stapes velocity v_{stap}, u_{BM} and Δp is identical in acoustic stimulation and mechanical forward stimulation making ASTM standard F2504–05 applicable to AMEI stimulations at the ossicular chain.

More recently, the indication of AMEIs was extended to conductive and mixed hearing loss applications where the implant stimulates the inner ear reversely at the RW [COLLETTI ET AL., 2006; MARTIN ET AL., 2009]. In this application the AMEI actuator generates u_{RW} that faces a set of acoustic impedances consisting of Z_{BM} and the impedance of the middle ear Z_{ME} (Figure 1.8C) [STIEGER ET AL., 2013]. STIEGER ET AL. [2013] demonstrated that $Z_{\text{ME}} >> Z_{\text{F}}$ meaning that the total acoustic impedance in reverse RW stimulation is higher than in forward (sound) stimulation. Therefore they assumed that in reverse stimulation u_{BM} is divided into u_{stap} and u_{SVL} (third window leakage flow in SV) (Figure 1.8C). This assumption was confirmed by their finding that stapes velocity v_{stap} normalized to ICPD Δp, was much less in RW stimulation than in acoustic stimulation, most pronounced at frequencies $< 1 \, \text{kHz}$. Considering Δp as the correct measure of cochlear excitation in both forward and

---

[14]"Structures such as neurovascular channels, vestibular aqueduct and cochlear aqueduct" [STIEGER ET AL., 2013].
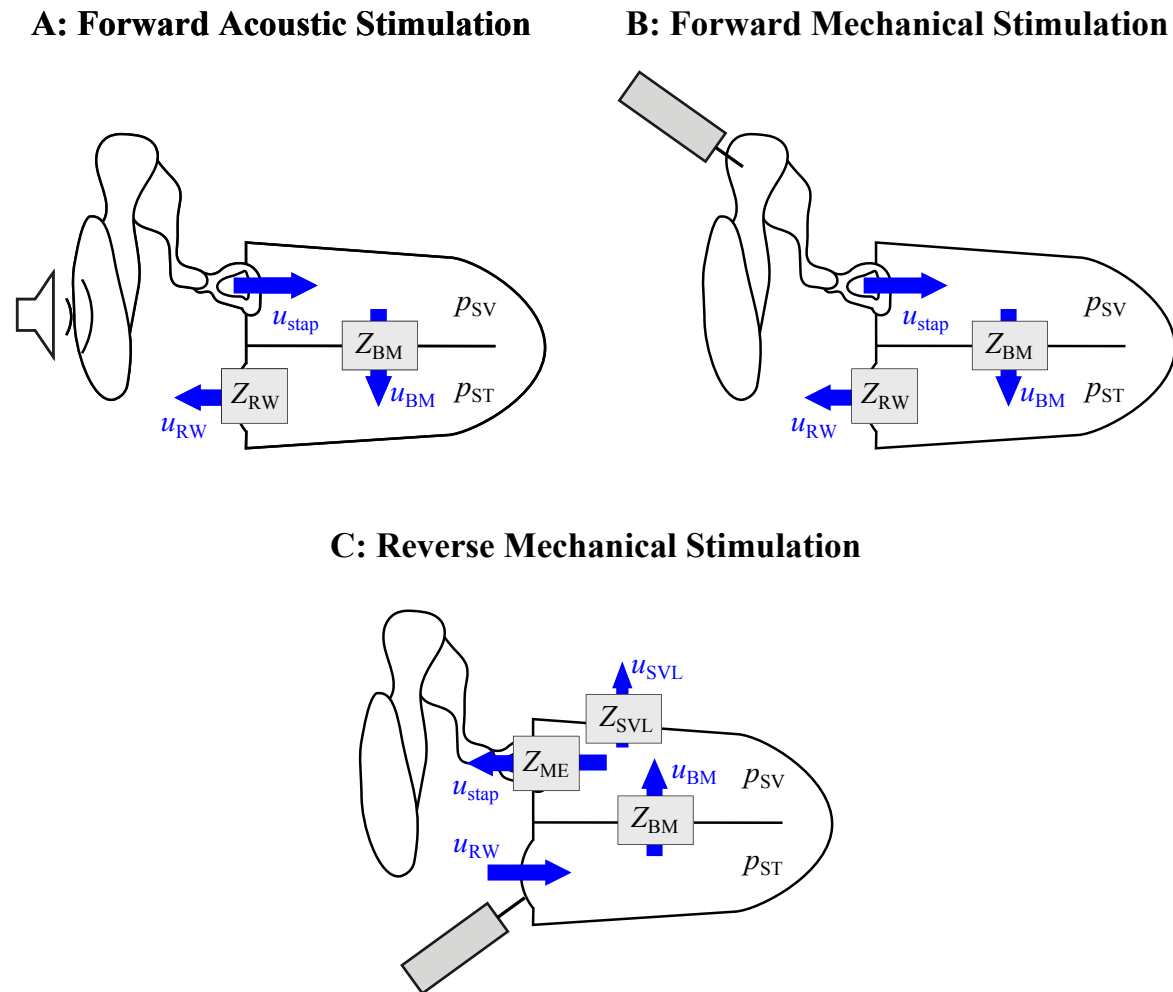
Figure 1.8. Illustration of the system for forward acoustic stimulation (A), forward mechanical stimulation (B) and reverse mechanical stimulation (C). The volume velocities of the stapes (u_{stap}), of the RW (u_{RW}), across the basilar membrane (u_{BM}) and through a third window path (u_{SVL}) are illustrated with arrows. Acoustic impedances of the middle ear (Z_{ME}), of the basilar membrane (Z_{BM}), of the RW (Z_{RW}) and of the third window path (Z_{SVL}) are represented by boxes.

reverse stimulation, this means that the real AMEI stimulation output is underestimated if stapes vibration is used as a reference, especially below 1 kHz.

In AMEI stimulations where the stapes is obscured by e.g. a coupling element or tissue, the stapes is not accessible for the LDV measurement and in direct perilymph stimulation with a DACI the SFP is perforated and bypassed, making stapes vibration measurement meaningless. Therefore stapes vibration measurement according to ASTM standard F2504–05 is not applicable in these cases. To assess direct perilymph stimulations in TB experiments, DEVÈZE ET AL. [2010] measured with an single-point LDV RW velocities instead of stapes velocities. However, to estimate the output level of the direct perilymph stimulation they converted the measured RW velocities to "equivalent expected stapes velocities" based on a regression equation determined in the same study, making this approach indirect and most probably less precise. CHATZIMICHALIS ET AL. [2012] quantified output levels of a DACI stimulation from RW volume displacements reconstructed from scanning LDV measurements at 200 targets. However, such scanning measurements are very time-consuming because numerous points have to be scanned and the scanning LDV cannot be integrated in a surgical microscope. In TB experiments time is a very critical factor because the mechanical behavior of a TB preparation changes significantly with time and therefore the experiment should not exceed eight hours [ASTM, 2005]. Furthermore a scanning LDV is much more expensive than a single-point LDV and therefore not easily accessible for many researchers. In general, RW vibration measurement is probably not a good measure of DACI stimulation level because perforating the SFP and opening the cochlea causes strong changes in the motion pattern of the RW vibration response at frequencies above 1.5 kHz [STENFELT ET AL., 2004b].

A good candidate for an alternative method to quantify the output level of AMEIs and DACIs in human cadaveric ears is the measurement of the ICPD because the differential pressure across the basilar membrane is considered as the direct "input signal to the cochlea"[NAKAJIMA ET AL., 2009] and as a measure of the volume velocity across the basilar membrane independent from the mode and direction of stimulation [STIEGER ET AL., 2013]. As described above, ICPDs have already been measured successfully in human cadaveric TBs, but only with a pressure sensor that is custom-made, complex in manufacture and fragile [OLSON, 1998]. ICPD measurement is therefore currently available only for a limited group of researchers and furthermore it has never been used to determine output levels of an AMEI or DACI.

1.5   Research Objectives and Thesis Outline

In summary in can be said that the "gold standard method" ASTM F2504–05 has never been validated and it is doubtful if this procedure is applicable for stimulation modes other than ossicular chain stimulation. ICPD measurement seems to be a promising method for AMEI and DACI output level predictions but currently it is not generally accessible and it has never been used for this purpose. The overall goals of the present thesis were therefore (1) to investigate whether the procedure of ASTM standard F2504–05 can be adapted to mechanical stimulation modes other than ossicle stimulation, (2) to investigate whether ICPDs are measurable in human cadaveric TBs with commercially available equipment, (3) to investi-

gate whether output levels of actuator stimulations can be determined in cadaveric TBs from ICPD measurement and (4) to validate that output levels predicted from TB experiments match the actual outcome in patients. Therefore the present thesis has the following structure: Chapter 2 presents the general materials and methods used for this thesis. Chapter 3 investigates the possibilities and limitations of vibration measurements according to ASTM F2504–05. For this purpose mechanical stimulations at the ossicular chain, at the RW and direct perilymph stimulation are performed in human cadaveric TBs with a DACI actuator. To quantify the output level in all performed stimulation modes, vibration responses of the stapes and RW are measured with an LDV and a procedure adapted from ASTM standard F2504–05 is used. In Chapter 4 two different off-the-shelf pressure sensor systems are tested for ICPD measurement during acoustic stimulation in cadaver ears. Measurements results are assessed by comparisons with results obtained with the "OLSON sensor". In Chapter 5 the output level of an AMEI is quantified in human cadaveric ears using both stapes vibration measurement according to ASTM standard F2504–05 and ICPD measurement. To validate both methods of actuator output prediction, the experimentally determined output levels are directly compared to clinical data. Finally, Chapter 6 summarizes and discusses the results and findings of the present thesis.

Chapter 2

Materials and Methods[1]

This chapter describes materials and methods that were repeatedly used. Materials and methods that are relevant only for specific experiments are described in the individual chapters.

2.1 Temporal Bone Preparation

All TBs used here were obtained from the Institute for Pathology of the Hannover Medical School and from the Department of Legal Medicine of the University Medical Center Hamburg-Eppendorf. The donors were anonymous and no biographical donor data are known. Harvesting and use of the TBs was conducted in accordance with the Helsinki declaration and approved by the ethics committee of the Hannover Medical School (approval No. 1963-2013, 2168-2014 and 3452-2016). All TBs were harvested within 48 h *post mortem*, immediately frozen at approx. -19 °C and thawed at room temperature shortly before preparation. According to ROSOWSKI ET AL. [1990] freezing and thawing has a negligible effect on the acoustic impedance of the middle ear. The required (visual) access to the incus, to the stapes, to the RW and to the promontory was gained by a *mastoidectomy*[2], a *facial recess approach*[3], a removal of the facial nerve and drilling of the bony rim of the RW niche overhang down to approx. 1 mm (Figure 2.1). After this preparation, the TB was refrozen in saline containing approx. 0.005 ‰ thimerosal and thawed shortly before the experiment. If the time between preparation and experiment was less than 15 h, the TB in the saline solution was stored at approx. 4 °C until the experiment. In the beginning of each experiment the integrity and the mobility of all relevant structures (e.g. RW membrane, SFP, ossicular chain) were carefully checked using a surgical microscope (OPMI-1, Zeiss, Germany) and surgical tools. Only those TBs with a middle ear transfer function H_{TV} within the ASTM acceptance range modified by ROSOWSKI ET AL. [2007] (see section 1.4.2) were used for the experiments and contributed data to the analyses. During the experiment the TB was fixed in a laboratory clamp on a magnetic stand (Horex®, Germany) (Figure 2.2) and all mechanically relevant structures (e.g. RW membrane, SFP, ossicular chain) were moistened with saline as

---

[1]Parts of this chapter have been published in GROSSÖHMICHEN ET AL. [2015, 2016b, 2017].

[2]Surgical removal of the cells of the mastoid process (part of the TB) [LENARZ & BOENNINGHAUS, 2012].

[3]"A surgical approach to the middle ear from the mastoid through the recess lateral to the facial nerve canal and medial to the *chorda tympani* nerve" [STEDMAN, 2005].
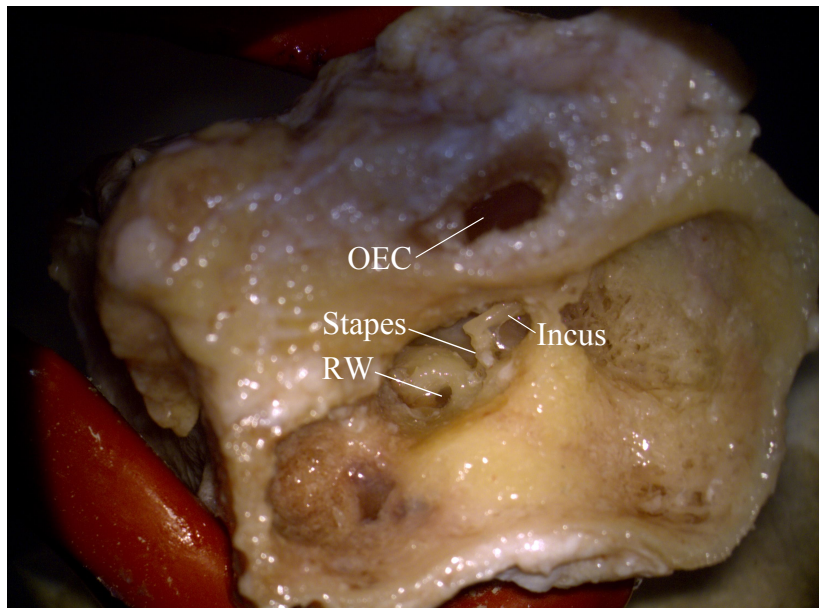
Figure 2.1. Temporal bone (TB) preparation used for this thesis. The middle ear cavity is opened by a mastoidectomy and a facial recess approach. The facial nerve and the RW niche overhang are removed to expose the round window (RW), the stapes and the incus. The outer ear canal (OEC) is left intact for the acoustic stimulation.

recommended by ASTM [2005] to avoid changes in mechanical behavior.

2.2   Sound Application Setup

To allow recordings of the sound pressure level input at the tympanic membrane p_T during acoustic stimulations a custom sound application setup (Figure 2.2) had been designed and manufactured in collaboration with the research workshop of the Hannover Medical School. Basically, the housing of the setup consists of an aluminum cylinder, an off-the-shelf ear speculum (122005, Karl Storz, Germany) and a plastic screw cap (Polyoxymethylene). Once the speculum is cemented (Paladur, Heraeus Kulzer GmbH, Germany) into the outer ear canal, a probe microphone (ER-7C, Etymotic Research Inc., USA) is inserted into the housing through a side opening and a loudspeaker (DT48, beyerdynamic, Germany) is connected by a silicone tube. After positioning the tip of the microphone's probe tube 1–2 mm from the tympanic membrane the housing is closed by the screw cap.

2.3   Actuator Stimulation Setup with Force Measurement

For the stimulation experiments with the Codacs actuator and the T2 actuator custom holding rods had been designed and manufactured in collaboration with the research workshop of the Hannover Medical School. The body of the actuator was glued (Sekundenkleber blitzschnell, UHU GmbH & Co KG, Germany) to the tip of this rod and then the rod was screwed into the load cell of a calibrated single axis force sensor system described below (Figure 2.3). Using
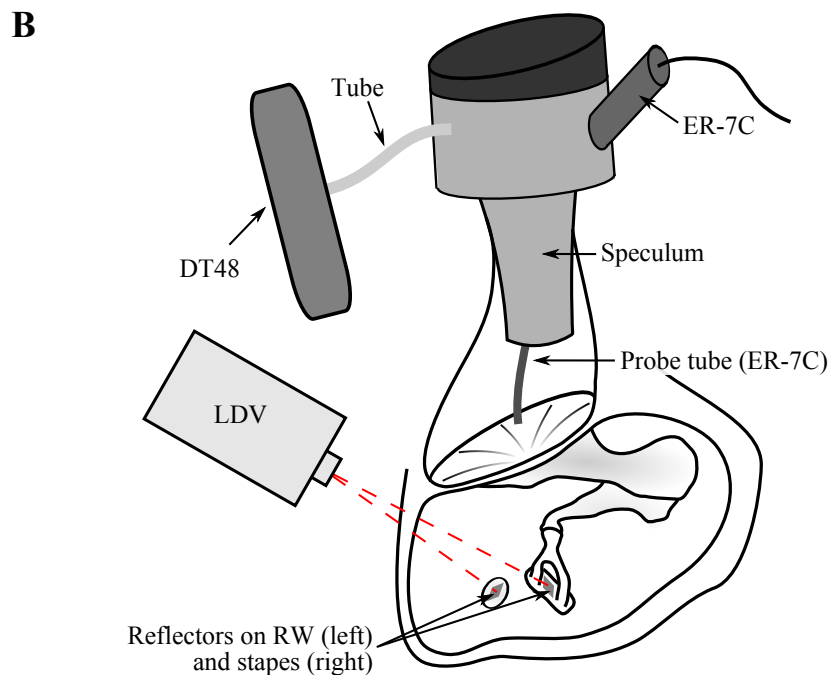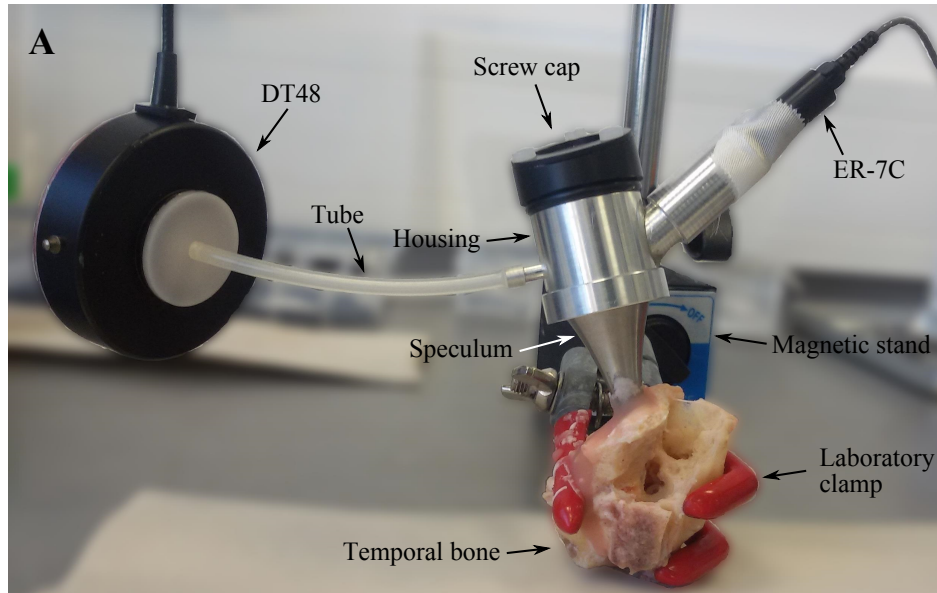
Figure 2.2. Setup used for the vibration measurement during acoustic stimulation in the TB preparation. The temporal bone was fixed in a laboratory clamp attached to a magnetic stand. A sound application setup comprising a speculum, a cylindrical housing, an ER-7C probe microphone, a DT48 loudspeaker and a screw cap was cemented in the outer ear canal. The laser beam of an LDV was directed at a small piece of retroreflective tape on the stapes and on the RW. A: Photo. B: Schematic illustration. Dimensions are not true to scale.
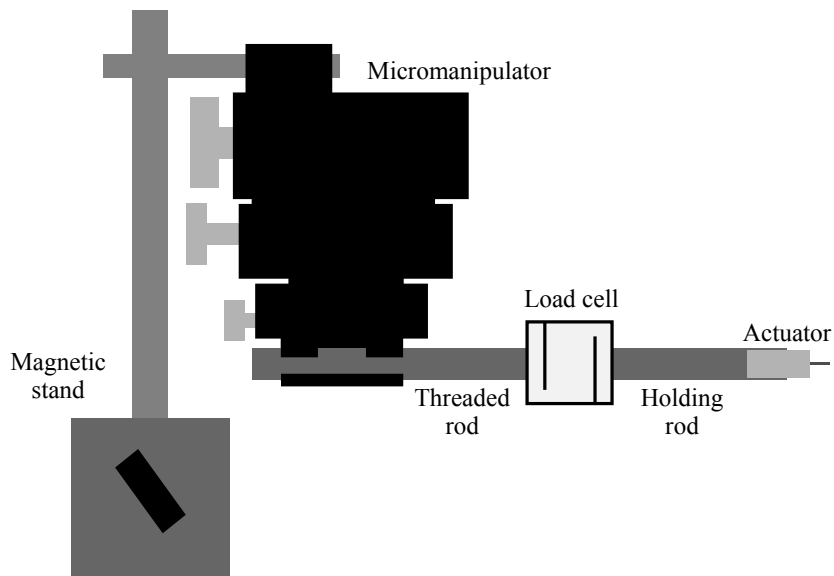
Figure 2.3. Schematic illustration of the setup used for the positioning of the actuator and the measurement of the axial forces. Dimensions are not true to scale.

a threaded rod the load cell was attached to a three-axis micromanipulator (M3301R, World Precision Instruments Germany GmbH, Germany) mounted on a magnetic stand (Horex®, Germany). With this setup the actuator could be positioned in all three spatial directions while monitoring the axial forces applied to the tip of the actuator. The used force sensor system (FUTEK Advanced Sensor Technology, USA) consists of an miniature S-beam load cell (LSB200 & LSB210, 100 g capacity) having a female M3 thread on each force sensitive side and an USB acquisition module (USB200) controlled by the measurement software SensIT V2.1. Measured forces were displayed by the software on a standard computer as numerical values and recorded manually.

2.4   Laser Doppler Vibration Measurement

Vibration measurements were performed with two different commercially available single-point LDV systems. The first system comprises sensor head CLV 700 and controller HLV 1000 and the second comprises sensor head OFV 534 and controller OFV 5000 with velocity decoder VD-09 (all Polytec, Germany). In order to integrate the LDV in a surgical microscope (OPMI-1, Zeiss, Germany), the sensor head was mounted on a micromanipulator (HLV MM 30 and HLV MM 2, Polytec, Germany) that allows a positioning of the laser beam by a joystick. Both LDV systems were operated with a measurement range of 5 mm/s/V. To ensure a sufficient signal-to-noise ratio (SNR), a small piece (< 0.3 mm $\times$ 0.3 mm) of retrore-flective tape (Polytec, Germany) was placed at the measurement site (e.g. SFP, RW, actuator rod) (Figure 2.2). As recommended in ASTM F2504–05 [ASTM, 2005], the visually esti-mated incident angle between the LDV laser beam and the normal of the SFP and RW was

Figure 2.4. Schematic illustration of the functional principle of a Fabry-Pérot Interferometer.

considered during analysis using a cosine correction of

$$v_{\mathrm{cor}} = \frac{v_{\mathrm{meas}}}{\cos\left(\Phi\right)} ,$$ (2.1)

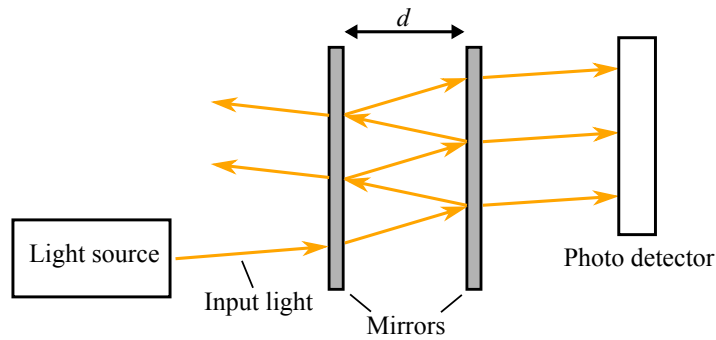with v_{meas} being the measured velocity magnitude, Φ being the difference in angle [rad] and v_{cor} being the corrected velocity magnitude.

2.5 Intracochlear Sound Pressure Measurement

The goal of this thesis was to develop measurement techniques that are generally available and thus all used technologies and devices should be off-the-shelf and not custom made. As there was no off-the-shelf pressure measurement system available that is intended for intra-cochlear sound pressure measurement, researches in literature and the Internet have been performed to identify off-the-shelf devices that are potentially suitable for this purpose. Six systems were found fulfilling the main criterion of a sensor tip diameter of ≤ 0.5 mm (Table 2.1). However, the frequency limit of the systems from Opsens Solutions and RJC Enterprise of 1 kHz was too low because ICPDs have to be measured in the frequency range of 0.1 –8 kHz (better 0.1 –10 kHz). The frequency limit of the systems from SA Instruments and Millar were not specified. Furthermore the Millar pressure catheter has a side mounted sensing element and therefore this sensor would have required a deeper insertion into the cochlea than a front end sensor. From all systems listed in Table 2.1 the pressure measurement systems from FISO and Samba were considered as the most appropriate devices and were therefore purchased for experimental investigations. Both are fiber-optic systems based on the Fabry-Pérot interferometer principle described below.

(1) Samba: This system consists of two pressure fiber-optic transducers (Samba Preclin 420 LP, Samba Sensors AB, Sweden) connected to a two-channel control unit (Samba control unit 202, Samba Sensors AB, Sweden). The pressure transducer has a tip diameter of 420 μm (Figure 2.5), is calibrated by the manufacturer, valid for lifetime with a long term stability of < 0.5 % , is designed for a measurement range of -5 to +35 kPa, and can be reused for several measurements [SAMBA SENSORS AB, 2007, 2011]. The control unit has a maximum sampling rate of 40 kHz and provides a proportional voltage signal at each analog output channel [SAMBA SENSORS AB, 2007]. The theoretical resolution limit of the entire samba

Manufacturer	System	Sensor Diameter	Measuring Principle	Frequency Limit (Control Unit)
Opsens Solutions, Canada	OPP-M25 pressure sensor, ProSens signal conditioner	0.25 mm	Fiber-optic (Fabry-Pérot)	1 kHz
RJC Enterpises, USA	Model 40 pressure sensor, Model 440 measurement system	0.279 mm	Fiber-optic (Fabry-Pérot)	1 kHz
SA Instruments, USA	fiber optic pressure sensor, Model 1025 monitoring system	0.3 mm	Fiber-optic (Fabry-Pérot)	n/a
Millar®, USA	SPR-1000 Mikro-Tip® pressure catheter, different control units	0.333 mm	Wheatstone bridge	n/a
Samba Sensors, Sweden	Samba Preclin 420 pressure transducer, samba 202 control unit	0.42 mm	Fiber-optic (Fabry-Pérot)	40 kHz
FISO, Canada	FOP-M260 pressure transducer, Veloce 50 control unit	0.26 mm (0.31 mm incl. sheathing)	Fiber-optic (Fabry-Pérot)	200 kHz

Table 2.1. List of off-the-shelf miniature pressure sensor systems having a sensor diameter ≤ 0.5 mm. Specifications taken from manufacturer's data sheets, brochures and websites.

system is approx. 1.8 Pa [SAMBA SENSORS AB, 2007]. Under the assumption of a middle ear amplification of 23 dB at ≤ 1 kHz, 0 dB at ≥ 7 kHz and a decrease of -8.6 dB / octave in between [KUROKAWA & GOODE, 1995], the theoretical resolution limit of the samba pressure measurement system is approx. 72 dB SPL input to the tympanic membrane at ≤ 1 kHz and approx. 95 dB SPL at ≥ 7 kHz.

(2) FISO: This system consists of two fiber-optic pressure transducers (FOP-M260, FISO Technologies Inc., Canada) connected to a two-channel control unit (Veloce 50, FISO Technologies Inc., Canada). The pressure sensitive tip of the transducer (outer diameter: 260 μm [FISO, 2015]) is sheathed by a polyimide tubing filled with gel resulting in an total outer diameter of 310 μm. The pressure transducer is designed for a measurement range of $\approx$ -40 to +40 kPa. The control unit has a sampling rate of 200 kHz [FISO, 2012] and provides a proportional voltage signal at each analog output channel. Since the resolution of the control unit is not given in the data sheet, the theoretical resolution limit of the system in terms of input to the tympanic membrane can not be calculated. Before the experiments, the phases of the pressure transducers were calibrated in air against a 1/4″ reference microphone (Type 4939, Brüel & Kjær, Denmark) and amplitudes against a probe microphone (ER-7C, Etymotic Research Inc., USA).

Both systems are based on the Fabry-Pérot interferometer principle. A Fabry-Pérot interferometer consists basically of two parallel and partially reflective mirrors separated by a distance d with the reflective surfaces facing each other (Figure 2.4) [SILVESTRI & SCHENA, 2011]. A light beam coming from a light source enters the interferometer cavity and is reflected repeatedly between the two mirrors. With each reflexion a small portion of the beam is transmitted through the mirrors and the resulting interference fringes are collected by a photo
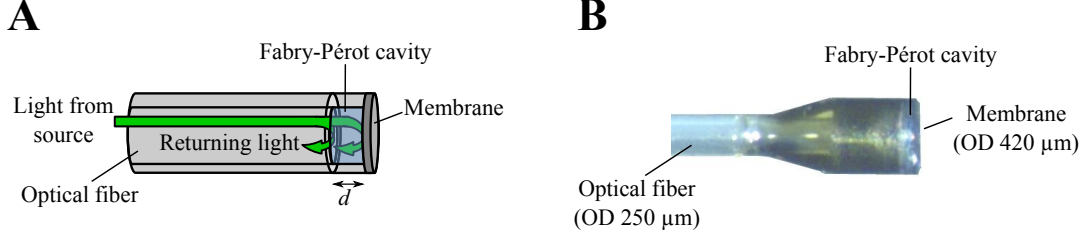
Figure 2.5. Constuction of a fiber-optic pressure measurement transducer based on Fabry-Pérot interferometry. A: Schematic illustration modified from [POEGGEL ET AL., 2015] (CC BY 4.0). B: Photo of a Samba Preclin 420 LP pressure transducer with dimensions given in SAMBA SENSORS AB [2007].

detector [SILVESTRI & SCHENA, 2011]. If the optical path length of the reflected beams is an integer multiple of the light wavelength, the beams interfere constructively meaning that the intensity of transmission depends on the distance d between the two mirrors [SILVESTRI & SCHENA, 2011]. In fiber-optic pressure measurement transducers based on Fabry-Pérot interferometry, the Fabry-Pérot cavity is typically located at the tip of an optical fiber and a pressure sensitive membrane acts as one of the partially reflective mirrors [SILVESTRI & SCHENA, 2011]. A control unit containing a light source, a photo detector system and signal processing electronics is connected to the fiber. When the tip of the fiber is exposed to a pressure change, the membrane is deflected and the length of the Fabry-Pérot cavity d is changed. The altered light escaping the Fabry-Pérot cavity returns to the control unit where device-specific signal processing electronics computes the Fabry-Pérot cavity length and determines the corresponding pressure. The operating procedure of the Samba system is detailed in SONDERGAARD ET AL. [2002] and the one of the FISO system in PINET [2009].

2.6 Intracochlear Sound Pressure Difference Calculation

To calculate the ICPD (Δp) that induces the deflection of the basilar membrane, not only the amplitude but also the phase of the sound pressures in SV and ST has to be considered. Therefore Δp was calculated as the vector difference between the sound pressures in SV and ST in the frequency domain. First, their real $(\text{Re}(z_{p_{\text{SV}}}), \text{Re}(z_{p_{\text{ST}}}))$ and imaginary parts $(\text{Im}(z_{p_{\text{SV}}}), \text{Im}(z_{p_{\text{ST}}}))$ were calculated by

$$\text{Re}(z_{p_{\text{SV}}}) = |z_{p_{\text{SV}}}| \cos \varphi_{p_{\text{SV}}} \,, \tag{2.2}$$

$$\text{Re}(z_{p_{\text{ST}}}) = |z_{p_{\text{ST}}}| \cos \varphi_{p_{\text{ST}}} \,, \tag{2.3}$$

$$\text{Im}(z_{p_{\text{SV}}}) = |z_{p_{\text{SV}}}| \sin \varphi_{p_{\text{SV}}} \,, \tag{2.4}$$

$$\text{Im}(z_{p_{\text{ST}}}) = |z_{p_{\text{ST}}}| \sin \varphi_{p_{\text{ST}}} \,, \tag{2.5}$$

where $|z_{p_{\text{SV}}}|$ and $|z_{p_{\text{ST}}}|$ are the magnitudes [Pa] and $\varphi_{p_{\text{SV}}}$ and $\varphi_{p_{\text{ST}}}$ the phases [rad] of the sound pressures in SV and ST. These were then used to calculate the real part

$$\text{Re}(z_{\Delta p}) = \text{Re}(z_{p_{\text{SV}}}) - \text{Re}(z_{p_{\text{ST}}}) \tag{2.6}$$

and the imaginary part

$$\text{Im}(z_{\Delta p}) = \text{Im}(z_{p_{\text{SV}}}) - \text{Im}(z_{p_{\text{ST}}}) \tag{2.7}$$

of the complex intracochlear sound pressure difference $z_{\Delta p}$. The magnitude Δp [Pa] and the phase $\varphi_{\Delta p}$ [rad] of the ICPD were then calculated by

$$\Delta p = |z_{\Delta p}| = \sqrt{(\text{Re}(z_{\Delta p}))^2 + (\text{Im}(z_{\Delta p}))^2} \tag{2.8}$$

and

$$\varphi_{\Delta p} = \arg(z_{\Delta p}) = \begin{cases} \arctan\left(\frac{\text{Im}(\Delta p)}{\text{Re}(\Delta p)}\right) & \text{if } \text{Re}(\Delta p) > 0 \\ \arctan\left(\frac{\text{Im}(\Delta p)}{\text{Re}(\Delta p)}\right) + \pi & \text{if } \text{Re}(\Delta p) < 0, \text{Im}(\Delta p) \geq 0 \\ \arctan\left(\frac{\text{Im}(\Delta p)}{\text{Re}(\Delta p)}\right) - \pi & \text{if } \text{Re}(\Delta p) < 0, \text{Im}(\Delta p) < 0 \\ \frac{\pi}{2} & \text{if } \text{Re}(\Delta p) = 0, \text{Im}(\Delta p) > 0 \\ -\frac{\pi}{2} & \text{if } \text{Re}(\Delta p) = 0, \text{Im}(\Delta p) < 0 \end{cases} \tag{2.9}$$

and finally $\varphi_{\Delta p}$ was converted from radians to degree.

2.7 Signal Generation and Acquisition

Two different systems were used to generate and acquire electrical signals: (1) A commercial data acquisition software (VibSoft 4.8.1, Polytec, Germany) controlling a 16-bit, 4 channel data acquisition system (PC-D and VIB-E-400, Polytec, Germany) and (2) a custom data acquisition software self-programmed in LabVIEW™ 2015 (National Instruments™, Germany) controlling two 24 bit, 4-channel data acquisition modules (2 x NI USB-4431, National Instruments™, Germany). With both systems, the electric input signals to the loudspeaker and to the actuators were generated at 25.6 kHz sample rate and buffered by a power amplifier (SA1, Tucker-Davis Technologies, USA). Electric output signals from the probe microphone, LDV or pressure measurement system were acquired as averaged complex spectra using 800 Fast Fourier Transformation (FFT) lines between 0 and 10 kHz with 12.5 Hz resolution. At each stimulation frequency f_{stim}, the $\text{SNR}(f_{\text{stim}})$ [dB] of the acquired signal amplitude $s(f_{\text{stim}})$ [dB re 1 V] was calculated using the average of the signal amplitudes [dB re 1 V] at the three adjacent FFT lines below ($s_{-1} = s(f_{\text{stim}} - 12.5\text{Hz}), s_{-2} = s(f_{\text{stim}} - 25\text{Hz}), s_{-3} = s(f_{\text{stim}} - 37.5\text{Hz})$) and above ($s_{+1} = s(f_{\text{stim}} + 12.5\text{Hz}), s_{+2} = s(f_{\text{stim}} + 25\text{Hz}), s_{+3} = s(f_{\text{stim}} + 37.5\text{Hz})$) as noise level estimate:

$$\text{SNR}(f_{\text{stim}}) = s(f_{\text{stim}}) - \frac{s_{+1} + s_{+2} + s_{+3} + s_{-1} + s_{-2} + s_{-3}}{6}. \tag{2.10}$$

During sine wave signal stimulations with the self-developed LabVIEW program the SNR was calculated during measurement and the averaging was stopped automatically when a defined SNR and a minimum number of averages were reached. In all other cases, the measurement was averaged until a limiting maximum number and the SNR was calculated manually during the analysis.

2.8 Statistical Analyses

All statistical analyses in this thesis were performed with the SigmaStat package integrated in SigmaPlot™ 12.5 (Systat Software Inc., USA). For all tests a significance criteria of $p < 0.05$ was used.

Chapter 3

Adapting ASTM Standard F2504–05 to Assess Alternative Stimulations with a DACI Actuator[1]

As described in section 1.4.2, ASTM standard F 2504 – 05 [ASTM, 2005] provides a commonly used procedure to predict output levels of an AMEI actuator from stapes vibration measurement in human TBs. However, this method is intended only for AMEI actuators stimulating the ossicular chain and requires a mobile and visually accessible stapes. As discussed in section 1.4.5, earlier studies suggest that an adaption of the procedure to other common stimulation modes might lead to inaccurate or inconsistent results. Furthermore the clinical output level of an DACI has never been estimated directly from single-point LDV measurements. These issues are addressed by the present chapter where the efficiency of an DACI actuator (Codacs actuator, Cochlear Ltd., Sydney Australia) in different stimulation modalities is investigated experimentally in human cadaveric TBs by single-point LDV measurements. For this purpose it was tested whether the procedure of ASTM standard F2504-05 can be adapted by using RW vibration responses as a reference and if this practice provides consistent results.

3.1   Materials and Methods

Experiments were performed in 25 human cadaveric TBs obtained and prepared as described in section 2.1. For the acoustic stimulation the sound application setup described in section 2.2 was fixated in the outer ear canal and for the actuator stimulation a Codacs actuator was positioned using the setup described in section 2.3. All components were placed on a vibration isolated table (LW3048B, Newport, Germany). During both acoustic stimulation and actuator stimulation the vibration amplitudes of the SFP and of the RW were measured with an LDV. Based on these data the equivalent output levels of the actuator stimulation modes were quantified and compared.

---

[1]Parts of this chapter have been published in GROSSÖHMICHEN ET AL. [2015].
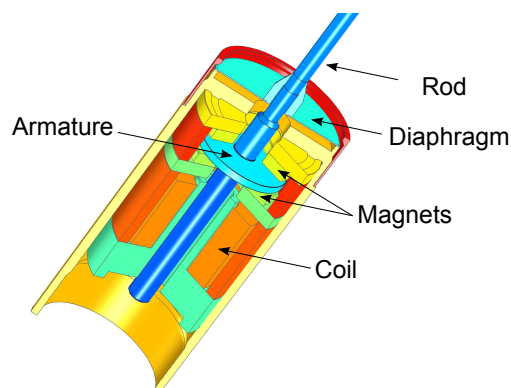
Figure 3.1. Illustration of the Codacs actuator (section view). Taken from GROSSÖHMICHEN ET AL. [2015] (CC BY 4.0).

3.1.1 The Codacs Actuator

The Codacs actuator is the electromagnetic transducer of the Codacs system (Cochlear Ltd., Sydney Australia), intended for the treatment of severe to profound mixed hearing losses caused by otosclerosis (see section 1.3.5). Beside the original use of the Codacs system, further applications involving the stimulation of mobile middle ear structures or the RW are imaginable and would extend the indication range to patients with other pathologies. Therefore the efficiency of the Codacs actuator in stapes head stimulation, SFP stimulation and RW stimulation is investigated here experimentally in human cadaveric TBs and compared to the intended direct perilymph stimulation.

The Codacs actuator is based on the "balanced armature principle" [HÄUSLER ET AL., 2008], meaning that inside the housing a disk-like part is positioned between two permanent ring magnets. This disk is connected to a rod which is enclosed by a titanium diaphragm sealing the housing and acting as a spring. The rigidity of the diaphragm is partially compensated by the force-displacement characteristics of the armature inside the magnetic field resulting in a reduced dynamic stiffness of the ensemble and a frequency characteristic of the actuator similar to that of the human middle ear [BERNHARD ET AL., 2011]. An electromagnetic coil modifies the magnetic flux and vibrates the rod axially. The mobile magnetic armature is exactly centered to result in a symmetric spring constant of the ensemble for perilymph piston stimulation when no static forces are applied to the vibrating rod [BERNHARD ET AL., 2011]. Therefore the Codacs actuator functioning crucially depends on the working point of the balanced armature. On the other hand, stimulation of solid middle ear structures or the RW requires some static force preload for efficient transmission [DEVÈZE ET AL., 2013; MAIER ET AL., 2013; SCHRAVEN ET AL., 2012; TRINGALI ET AL., 2011]. Therefore the performance of the Codacs actuator may be impaired when used in applications as in this study.

RW stimulations were performed with a modified Codacs actuator without artificial incus allowing a perpendicular coupling of the actuator rod to the RW membrane (Figure 3.2A). In all other stimulations the standard Codacs actuator was used having an artificial incus where a prosthesis was attached (Figure 3.2B–D).
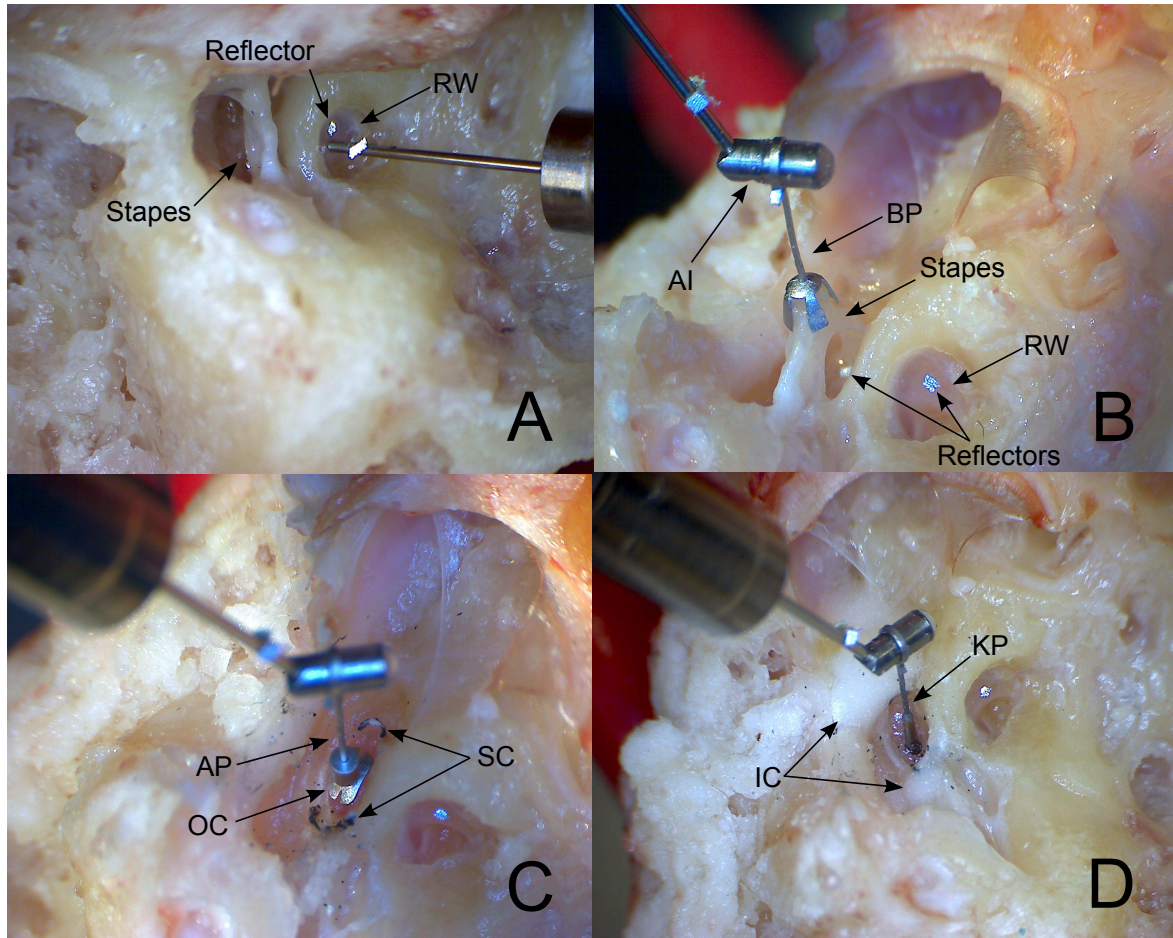
Figure 3.2. Performed stimulation modes: (A) *RW stimulation*: Codacs actuator without artificial incus perpendicular to the RW membrane. (B) *Bell stimulation*: Codacs actuator coupled to the exposed stapes head with a Bell prosthesis. (C) *Omega/Aerial stimulation*: An Aerial prosthesis (AP) is crimped to the artificial incus (AI) and coupled to the Omega connector (OC) lying between the remains of the stapes crura (SC). (D) *K-piston stimulation*: K-Piston (KP) inserted into the inner ear through a SFP fenestration after immobilization of the SFP by ionomer cement (IC). Reflectors are placed on SFP and RW. Taken from GROSSÖHMICHEN ET AL. [2015] (CC BY 4.0).

3.1.2   Vibration Measurement

To measure vibration responses of the SFP and of the RW the single-point LDV system comprising CLV 700 and HLV 1000 (see section 2.4) was integrated in a surgical microscope (OPMI-1, Zeiss, Germany). For the analysis the measured velocity $v(f)$ of the SFP and RW was converted to displacement $d(f)$ by

$$d(f) = \frac{v(f)}{2 \cdot \pi \cdot f} \,, \tag{3.1}$$

with f [Hz] being the stimulation frequency. The visually estimated incident angle of the LDV laser beam was $\leq 60°$ to the SFP and $\leq 45°$ to the RW normal and has been considered during analysis by a cosine correction (equation (2.1)).

3.1.3   Signal Generation and Acquisition

All electrical signals were generated by the commercial data acquisition system (Polytec, Germany) described in section 2.7 using a 25.6 kHz sample rate. Both the DT48 loudspeaker and the Codacs actuator were driven by the same custom written multi-sine signal having equal amplitudes of approx. -25 dB re 1 V_{rms} for the loudspeaker and of approx. -30 dB re 1 V_{rms} for the actuator at 0.125, 0.25, 0.5, 1, 2, 3, 4, 6, 8 and 10 kHz. Electric output signals from probe microphone and LDV were acquired simultaneously as averaged complex spectra using 800 FFT lines between 0 and 10 kHz with 12.5 Hz resolution. At each stimulation frequency the SNR [dB] of the signal from microphone and LDV was calculated according to equation (2.10) and responses with an SNR < 10 dB were excluded from analysis.

3.1.4   Experimental Procedure

Acoustic Stimulation

The tympanic membrane was stimulated acoustically and the velocities of the SFP and of the RW were recorded with the LDV. These measurements served for the selection of adequate TBs and as reference for the calculation of the equivalent SPL. The acoustic input signal at the tympanic membrane was recorded by the probe microphone and the SFP and RW vibration responses were measured with the LDV. Only if the SFP vibration magnitude normalized to the sound pressure input at the tympanic membrane (middle ear transfer function H_{TV}) was at 0.25–4 kHz within the modified acceptance criteria [ROSOWSKI ET AL., 2007] of ASTM standard F2504-05 [ASTM, 2005], the experiment was continued and the following sequence of actuator stimulations was performed.

Actuator Stimulation

1.) *RW stimulation* ($N = 10$): The tip of the actuator rod (diameter 0.4 mm), having no sharp edges, was directed perpendicular to the center of the RW. Using the micromanipulator, the actuator was advanced towards the RW until a axial contact force of approx. 5 mN was measured (Figure 3.2A). This force level was selected based on bench tests described in

section 3.1.6. The actuator was electrically driven and the vibration response of the SFP was measured with the LDV.

2.) *Bell stimulation* (N = 9): To gain direct access to the stapes, the incus, the malleus, the outer ear canal and the tympanic membrane were removed with surgical tools. A titanium Bell prosthesis (length: 3.0 mm, Heinz Kurz GmbH, Germany) was manually crimped to the artificial incus of the actuator (Figure 3.2B). The bell-shaped end of the prosthesis was plugged onto the exposed stapes head. As before, the axial static force was adjusted to approx. 5 mN and lateral forces were minimized by avoiding visible tilting of the stapes. While the actuator was electrically driven, the vibration responses of the SFP and of the RW were measured with the LDV. The measurement was performed at both sites to test their equivalence as reference for actuator output level quantification. This stimulation mode was omitted in experiment TB10.

3.) *Omega/Aerial stimulation* (N = 8): The stapes suprastructure was removed with a surgical diode laser (Iridis, Quantel Medical, France) and a titanium Omega connector (Heinz Kurz GmbH, Germany) was placed on the SFP between the remains of the crura (Figure 3.2C). The loop of a titanium Aerial prosthesis (length: 5.5 mm, Heinz Kurz GmbH Medizintechnik, Germany) was manually crimped to the actuator artificial incus and the cylindrical end of the prosthesis was plugged onto the ball of the omega connector to form a ball joint. The adjustment of the axial coupling force to approx. 5 mN and lateral forces minimization were done as before. During actuator stimulation the RW vibration response was recorded because the stapes crura were removed and the footplate was mostly occluded. This stimulation mode was omitted in experiments TB10 and TB12.

4.) *K-Piston stimulation* (N = 10): Otosclerosis was simulated by immobilizing the SFP with ionomer cement (Denseal Superior, Prevest Denpro GmbH, Germany) and a stapedotomy was performed with the surgical laser. A titanium K-Piston prosthesis (0.4 x 5.0 mm, Heinz Kurz GmbH Medizintechnik, Germany) was manually crimped to the artificial incus of the Codacs actuator before it was inserted into the cochlea through the fenestration of the SFP (diameter approx. 0.5–0.6 mm) (Figure 3.2D). In this condition the axial coupling force was approx. 0 mN, while lateral forces were minimized by centering the piston in the opening perpendicular to the SFP. Since the SFP was immobile, perforated and not directly actuated, the RW velocity was measured during actuator stimulation.

Before each stimulation it was controlled that the vibration signal generated by the Codacs actuator was within the specifications[2] given by the manufacturer. For this purpose the unloaded actuator was driven with a frozen pseudo random white noise input signal (25.6 kHz sample rate, 800 FFT lines) at approx. -50 dB re 1 V_{rms}/FFT line and the vibrational output was measured at the rod with the LDV. The resonance frequency was determined and compared to the specifications.

---

[2]Resonance frequency $\leq$ 2.5 kHz; maximum deviation of measured resonance frequency from device-specific resonance frequency given by the manufacturer: $\pm$ 0.3 kHz (personal communication with Cochlear Ltd.)

3.1.5   Equivalent Sound Pressure Level Determination

To quantify the output levels of AMEI actuators stimulating the ossicles in human cadaveric TBs as eq. SPL the procedure of ASTM standard F2504-05 compares stapes vibration responses to sound and to actuator stimulation (see section 1.4.2). Therefore a mobile and visually accessible stapes is required for this method. Since this was not the case for all stimulation modes performed in the present study, the ASTM procedure had to be adapted to quantify the Codacs actuator output level in all stimulation modes. For this purpose RW vibration measured at a fixed position in response to sound and to actuator stimulation was used as alternative reference in the stimulation modes "Omega/Aerial" and "K-Piston" where no stapes vibration response was measurable. As discussed in section 1.4.5, the RW vibration motion pattern was found variable at frequencies $> 1.5\,\text{kHz}$ [STENFELT ET AL., 2004a,b], but independent of the acoustic stimulation level in the range between 80 and 110 dB SPL [STENFELT ET AL., 2004b]. Moreover ASAI ET AL. [1999] showed that RW displacements amplitudes at the center of the RW increases linear with acoustical stimulation level in the range 50–110 dB SPL. These findings suggest that RW vibration amplitudes measured at a single position cannot be used as indicator of absolute RW volume displacement, but that the constancy of the vibration pattern should allow a relative estimation of stimulation efficiency in forward stimulation from such measurements. Hence, the reflector position on the RW was kept constant throughout each of the experiments at a position approx. halfway between the center and the edge. This specific position was chosen to allow the stimulation of the RW centrally without changing the position of the reflector. In Bell stimulation mode where both the SFP and the RW vibration responses were measurable both sites were used as reference to test the equivalence of both approaches. To determine the actuator output level as eq. SPL from both references the calculation procedure of ASTM F2504–05 (equations (1.4)–(1.9) in section 1.4.2) was adapted as follows. First, the transfer functions $H_{\text{TV,SFP}}$ and $H_{\text{TV,RW}}$ were calculated by

$$H_{\text{TV,SFP}} = \frac{d_{\text{U,SFP}}}{p_{\text{T}}} \quad \text{and} \tag{3.2}$$

$$H_{\text{TV,RW}} = \frac{d_{\text{U,RW}}}{p_{\text{T}}}, \tag{3.3}$$

with $d_{\text{U,SFP}}$ and $d_{\text{U,RW}}$ being the displacement amplitudes [µm] of the SFP and RW during acoustic stimulation and p_{T} [Pa] the sound pressure input measured at the tympanic membrane. Similarly, the electro-vibrational transfer functions $H_{\text{EV,SFP}}$ and $H_{\text{EV,RW}}$ were determined by

$$H_{\text{EV,SFP}} = \frac{d_{\text{A,SFP}}}{E} \quad \text{and} \tag{3.4}$$

$$H_{\text{EV,RW}} = \frac{d_{\text{A,RW}}}{E}, \tag{3.5}$$

with $d_{\text{A,SFP}}$ and $d_{\text{A,RW}}$ being the displacement amplitudes [µm] of the SFP and RW during actuator stimulation and E being the electrical input [V] to the actuator. Having H_{TV} and H_{EV}, the equivalent ear canal sound pressure transfer function H_{ET} was computed using either the SFP motion (equation 3.6) or the RW motion (equation 3.7) as reference:

$$H_{\text{ET,SFP}} = \frac{H_{\text{EV,SFP}}}{H_{\text{TV,SFP}}}, \tag{3.6}$$

$$H_{\text{ET,RW}} = \frac{H_{\text{EV,RW}}}{H_{\text{TV,RW}}} \; . \tag{3.7}$$

Finally, the maximum achievable equivalent ear canal SPL ($L_{E\max}$) [eq. dB SPL$_{\text{TM}}$] generated by the Codacs actuator at hypothetical input voltage $E_{\max} = 1\,\text{V}_{\text{rms}}$ was calculated by

$$L_{E_{\max},\text{SFP}} = 20 \log_{10} \left(\frac{H_{\text{ET,SFP}} \cdot E_{\max}}{2 \cdot 10^{-5}\text{Pa}} \right) \quad \text{and} \tag{3.8}$$

$$L_{E_{\max},\text{RW}} = 20 \log_{10} \left(\frac{H_{\text{ET,RW}} \cdot E_{\max}}{2 \cdot 10^{-5}\text{Pa}} \right) \; . \tag{3.9}$$

3.1.6   Determination of the Optimal Static Force Working Point

To determine the optimal static force, three bench tests were performed with Codacs actuators before the TB experiments. The aim of these tests was to estimate the magnitude and distortion of the mechanical actuator output at different static axial contact forces. Basically, the measurement setup was the same as in the TB experiments. A flexible plastic element was positioned in front of the actuator tip perpendicular to the actuator axis. By moving the actuator forward with the micromanipulator, axial static contact forces up to approx. 100 mN were applied stepwise in increments of 2.5 mN (1$^{\text{st}}$ and 2$^{\text{nd}}$ test) or 5 mN (3$^{\text{rd}}$ test). Similar to the TB experiments, the forces were measured by the single axis force sensor mounted between actuator and micromanipulator. At every force level the actuator was driven with the same white noise input signal used for the actuator testing during the TB experiments. The velocity of the generated vibration output was measured at the actuator rod using the LDV. To determine the total harmonic distortion (THD) a 0.6 and a 1 kHz sine signal of approx. -13 dB re 1 V$_{\text{rms}}$ electrical actuator input was used. From obtained velocity the THD was calculated using all available higher harmonics $\leq$ 10 kHz above noise level. In all three bench tests the actuator resonance frequency (unloaded approx. 2 kHz) increased with increasing force levels (212.5–437.5 Hz/50 mN) whereas the displacement amplitude at plateau range ($<$ approx. 2 kHz) decreased only mildly (approx. -0.04 to -0.06 dB/mN). For all applied forces below the maximum of 100 mN the THD for 0.6 kHz input remained in a narrow range (1.7 % to 2.1 %), in contrast to THD for 1 kHz that amounted up to 7.4 %. The higher THD of 1 kHz was attributed to the coincidence of the 1st harmonic with the actuator resonance frequency at approx. 2 kHz, because it decreased when the resonance frequency was shifted upwards by higher loading (decrease in resonance frequency: 0.7–2.0 % per 0.2 kHz). For the actuator stimulation in the TBs a static axial force load of 5 mN was selected. This value was chosen for five reasons: (1) minimal decrease in output amplitude at low frequencies, (2) low resonance frequency shift ($<$ 0.175 kHz), (3) tight physical contact, (4) sufficient sound transfer efficiency and (5) low force applied to the stimulated structures.
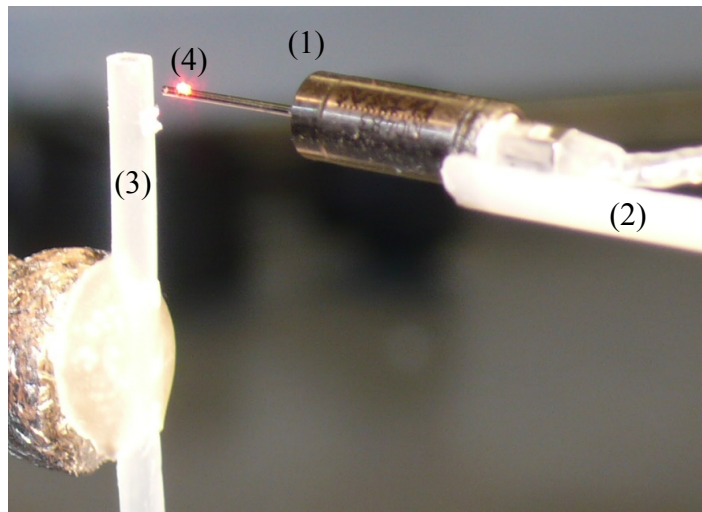
Figure 3.3. Setup to determine the optimum static force working point of the Codacs actuator. A Codacs actuator (1) without artificial incus was glued to a rod (2) mounted to a single axis force sensor (not shown). A flexible plastic element (3) was positioned vertically in front of the actuator. While the actuator was moved forward by a micromanipulator (not shown), resulting forces were measured with a single axis force sensor (not shown). When the actuator was driven electrically, the generated vibration was measured with an LDV directed on a piece of retroreflective tape (4) attached to the actuator rod.

3.2   Results

3.2.1   Stapes Vibration Responses to Sound

The middle ear transfer function $H_{\text{TV,SFP}}$ of 10 out of 25 TBs was in the relevant frequency range of 0.25 to 4 kHz [ASTM, 2005] within the modified acceptance range [ROSOWSKI ET AL., 2007] of ASTM standard F2504-05 (Figure 3.4). Only these TB preparations were used for the actuator stimulation experiments and contributed data to the following analysis.

3.2.2   RW Stimulation

Across all experiments the eq. SPL outputs in RW stimulation were of similar shape. The eq. SPL were between 89.4 and 136.3 eq. dB SPL (Figure 3.5), except in TB25 where the output at frequencies ≤ 2 kHz was distinctly higher (138.0–154.0 eq. dB SPL). The mean eq. SPLs were 108.3–128.2 eq. dB SPL and the average output level at speech relevant frequencies of 0.5, 1, 2, 3, 4 kHz was 117.4 eq. dB SPL at a hypothetical actuator input of 1 V_{rms} .

3.2.3   Stapes Stimulation

The eq. SPL outputs obtained in Bell stimulation (Figure 3.6) and Omega/Aerial stimulation (Figure 3.7) were of similar flat shape and increasing spread at frequencies > 1 kHz. For Bell stimulation, mean outputs were between 127.5 and 141.8 eq. dB SPL and for Omega/Aerial stimulation between 123.6 and 143.9 eq. dB SPL. The average output level at speech relevant
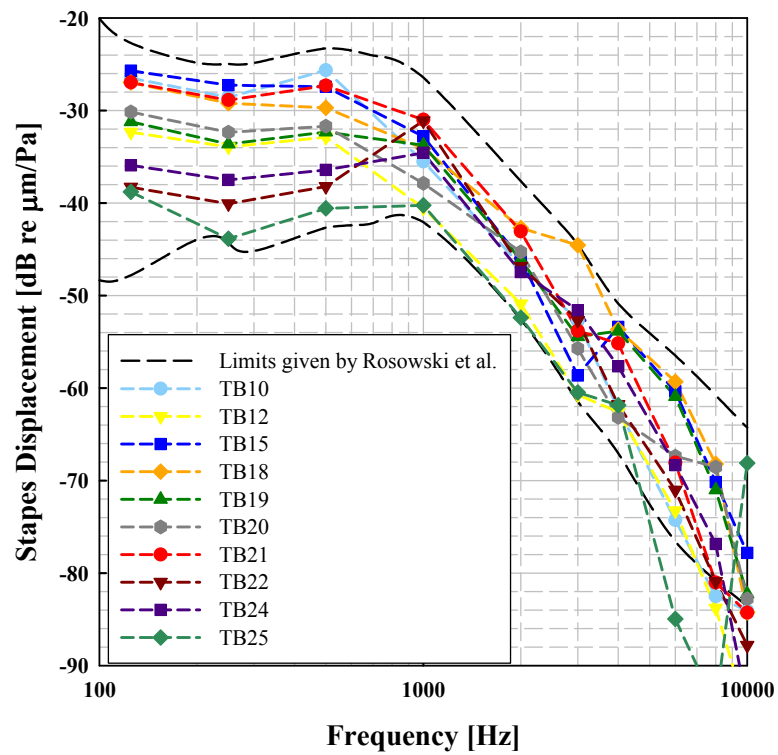
Figure 3.4. SFP displacement responses to sound of TBs used for actuator stimulation (N = 10). The black dashed lines depict the limits given by [ROSOWSKI ET AL., 2007]. Lines connecting symbols are for visual guidance only. Modified from GROSSÖHMICHEN ET AL. [2015] (CC BY 4.0).
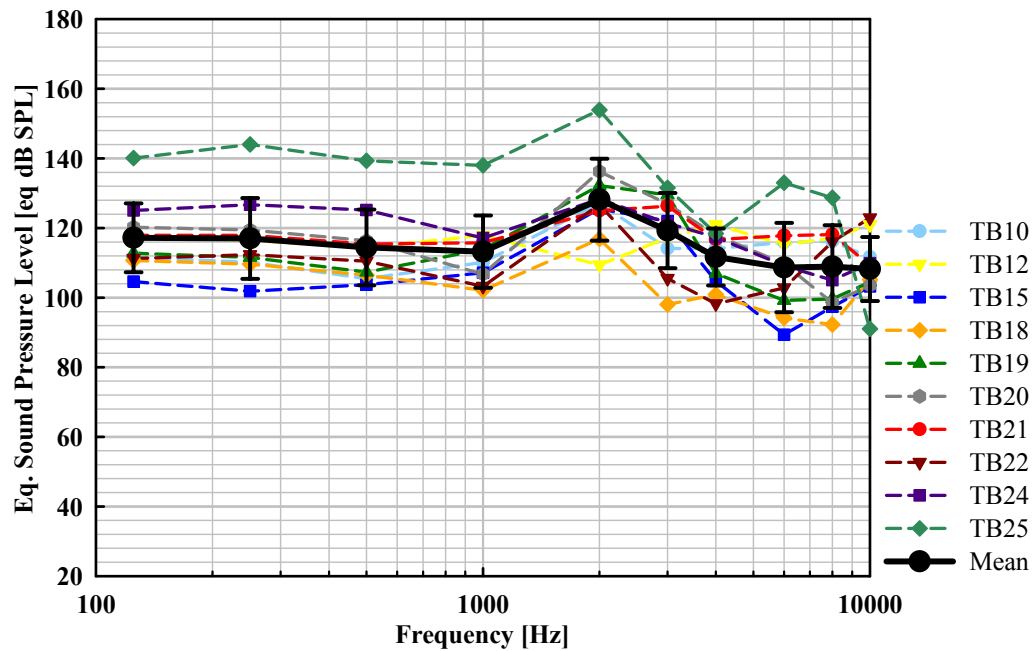
Figure 3.5. Codacs actuator output [eq. dB SPL$_{TM}$] in RW stimulation mode calculated for a hypothetical input voltage of $1\,V_{rms}$ from SFP vibration amplitudes. Colored symbols represent results from individual TBs, black circles means, and error bars standard deviations. Lines connecting symbols are for visual guidance only. Modified from GROSSÖHMICHEN ET AL. [2015] (CC BY 4.0).

Figure 3.6. Codacs actuator output [eq. dB SPL$_{TM}$] in Bell stimulation mode calculated for a hypothetical input voltage of $1\,\mathrm{V_{rms}}$ from RW vibration amplitudes. Colored symbols represent results from individual TBs, black circles means, and error bars standard deviations. Lines connecting symbols are for visual guidance only. Modified from GROSSÖHMICHEN ET AL. [2015] (CC BY 4.0).

frequencies (0.5, 1, 2, 3, 4 kHz) was 133.3 eq. dB SPL with the Bell and 134.2 eq. dB SPL with the Omega/Aerial prosthesis.

3.2.4 K-Piston Stimulation

The equivalent SPL outputs quantified for the Codacs actuator stimulating the inner ear directly with a K-piston were at frequencies $\leq 1\,\mathrm{kHz}$ flat and similar in all TBs (Figure 3.8). At higher frequencies the interindividual variation increased up to 69 dB at 4 kHz. Except in experiments TB19 and TB20, all obtained outputs were > 90 eq. dB SPL. The mean eq. SPL was between 112.8 and 124.5 eq. dB SPL at frequencies $\leq 1\,\mathrm{kHz}$ and between 108.6 and 131.6 eq. dB SPL at frequencies above. The average output at speech relevant frequencies (avg. 0.5, 1, 2, 3, 4 kHz) was 118.3 eq. dB SPL. Measurements at 0.125 kHz in experiments TB12 and TB21 had an SNR $< 10\,\mathrm{dB}$ and were omitted.

3.2.5 Comparison between the Stimulation Modes

In all stimulation modes the average eq. SPL outputs (Figure 3.9, Table 3.1) were of similar shape showing a peak at 2 kHz which corresponds to the typical actuator resonance frequency of ≤ 2.5 kHz (personal communication with Cochlear Ltd.). In the stimulation modes RW, Bell and Omega/Aerial the standard deviations were ≤ 12 dB whereas the standard deviations
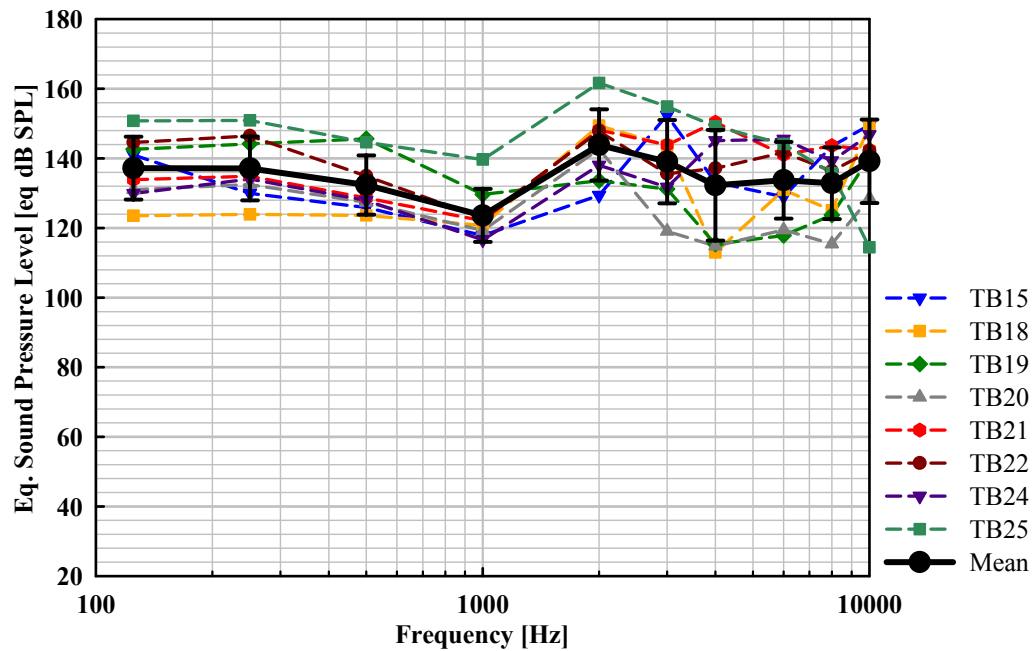
Figure 3.7. Codacs actuator output [eq. dB SPL$_{TM}$] in Omega/Aerial stimulation mode calculated for
a hypothetical input voltage of $1\,V_{rms}$ from RW vibration amplitudes. Colored symbols
represent results from individual TBs, black circles means, and error bars standard deviations.
Lines connecting symbols are for visual guidance only. Modified from GROSSÖHMICHEN
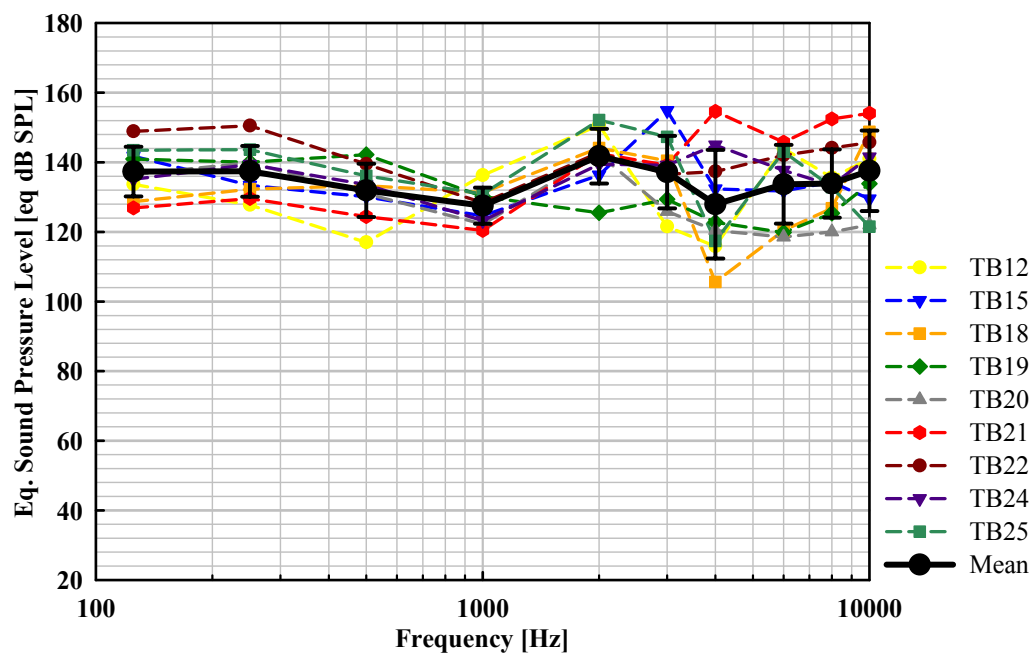ET AL. [2015] (CC BY 4.0).
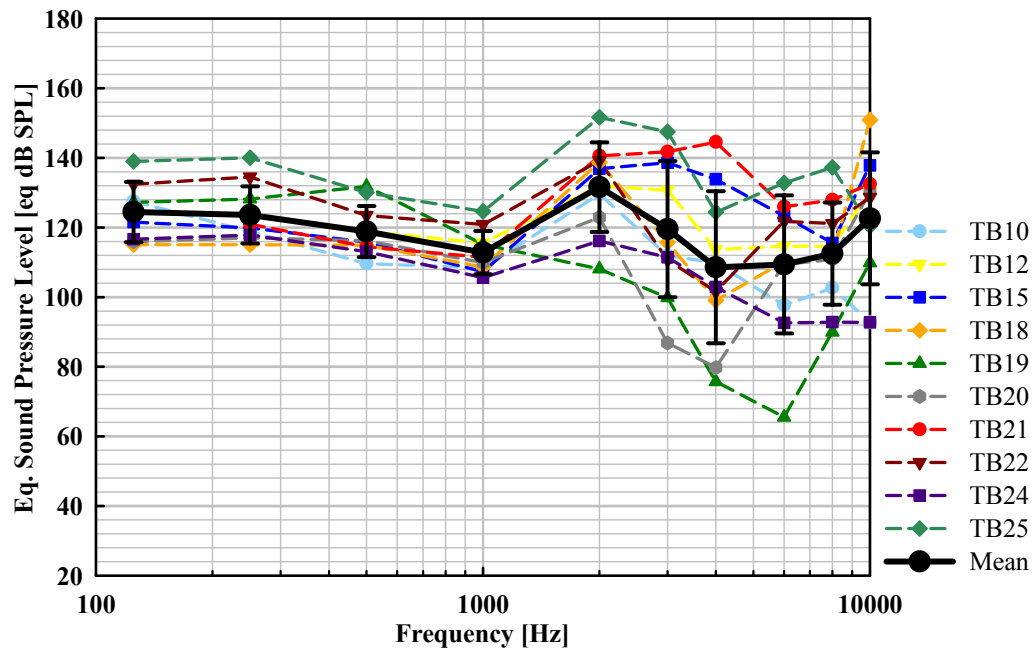
Figure 3.8. Codacs actuator output [eq. dB SPL_TM] in K-Piston stimulation mode calculated for a hypothetical input voltage of $1\,V_{rms}$ from RW vibration amplitudes. Data having SNRs $< 10\,dB$ was omitted (TB12 and TB21 at 0.125 kHz). Colored symbols represent results from individual TBs, black circles means, and error bars standard deviations. Lines connecting symbols are for visual guidance only. Modified from GROSSÖHMICHEN ET AL. [2015] (CC BY 4.0).
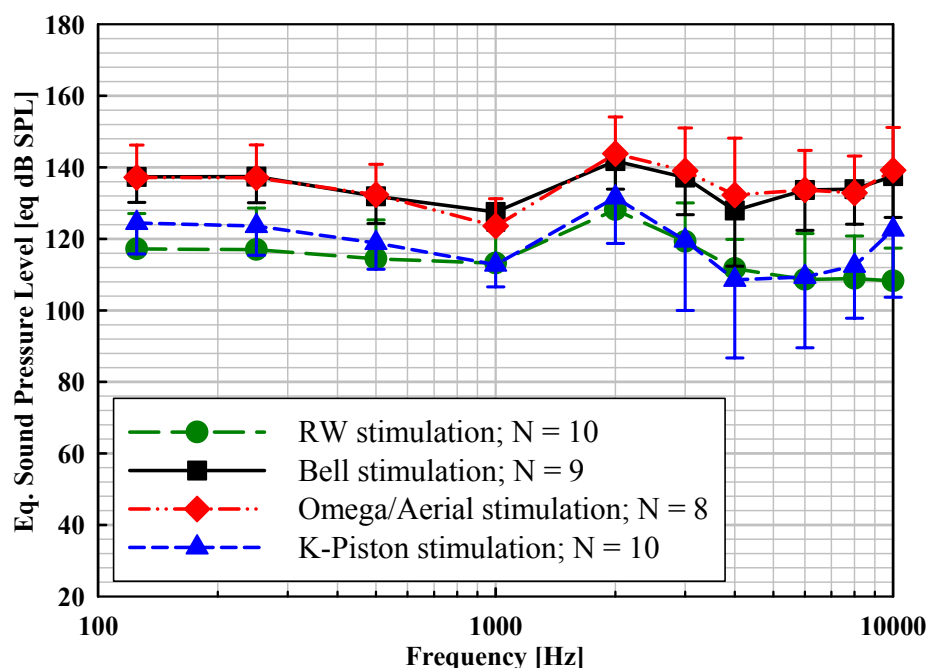
Figure 3.9. Mean values and standard deviations (error bars) of the eq. ear canal SPL [eq. dB SPL]
generated by the Codacs actuator at a hypothetical input voltage of $1\,\mathrm{V_{rms}}$ for the four inves-
tigated stimulation modes. At all frequencies the stimulation efficiency of Bell stimulation
at the stapes head (■) and of Omega/Aerial stimulation at the SFP (♦) was statistically sig-
nificantly higher than K-piston stimulation (▲) and RW stimulation (●). Symbols represent
means and error bars standard deviations. Lines connecting symbols are for visual guidance
only. Modified from GROSSÖHMICHEN ET AL. [2015] (CC BY 4.0).

in the K-Piston stimulation mode was up to 22 dB. Both, Bell stimulation and Omega/Aerial
stimulation provided similar outputs with statistically not significant mean differences of
maximal 3.2 dB (two-tailed paired t-tests, Table 3.2). Compared to K-piston stimulation, the
output of stimulations involving the entire SFP was statistically significant higher (Bell: 10.0
to 23.0 dB; Omega/Aerial: 10.6 to 24.5 dB) (Kolmogorov-Smirnov test; one-tailed paired t-
test, Table 3.2) at most frequencies. Only exceptions were the difference Bell vs. K-Piston
at 6 kHz and Bell vs. Aerial/Omega at 4 kHz.

RW stimulation provided outputs similar to K-piston stimulation with small and sta-
tistically not significant differences of ≤ 7.4 dB (except 14.4 dB at 10 kHz)(Kolmogorov-
Smirnov test; two-tailed paired t-test, Table 3.2). At speech relevant frequencies (0.5–
4 kHz) the average difference between these conditions was ≤ 4.9 dB. In Bell stimulation
and Omega/Aerial stimulation the output was 10.6 to 33.0 dB higher than in RW stimula-
tion, being significant at all frequencies (Kolmogorov-Smirnov test; one-tailed paired t-test,
Table 3.2).

Frequency [kHz]	Bell		Omega/Aerial		RW		K-Piston	
	Mean [eq dB SPL]	SD [dB]	Mean [eq dB SPL]	SD [dB]	Mean [eq dB SPL]	SD [dB]	Mean [eq dB SPL]	SD [dB]
0.125	137.344	7.12	137.20	9.03	117.22	9.90	124.46	8.64
0.25	137.418	7.28	137.14	9.17	117.04	11.60	123.64	8.18
0.5	131.934	7.65	132.36	8.53	114.45	10.86	118.86	7.33
1	127.543	5.19	123.62	7.61	113.24	10.38	112.80	6.21
2	141.79	7.86	143.87	10.23	128.16	11.76	131.61	12.86
3	137.173	10.40	139.06	11.95	119.28	10.78	119.54	19.55
4	127.963	15.61	132.28	15.89	111.68	8.17	108.57	21.86
6	133.7	11.32	133.73	11.01	108.67	12.83	109.42	19.85
8	133.913	9.79	132.87	10.28	108.93	11.87	112.49	14.67
10	137.57	11.56	139.18	12.01	108.25	9.21	122.64	18.95

Table 3.1. Mean equivalent output levels and standard deviations of all stimulation modes tested.

Figure 3.10. Mean values (symbols) and standard deviations (error bars) of the Codacs actuator output levels [eq. dB SPL$_{TM}$] in Bell stimulation mode calculated for a hypothetical input voltage of $1\,V_{rms}$ from RW vibration amplitudes (■) and SFP vibration amplitudes (◆). Lines are for visual guidance only. Modified from GROSSÖHMICHEN ET AL. [2015] (CC BY 4.0).

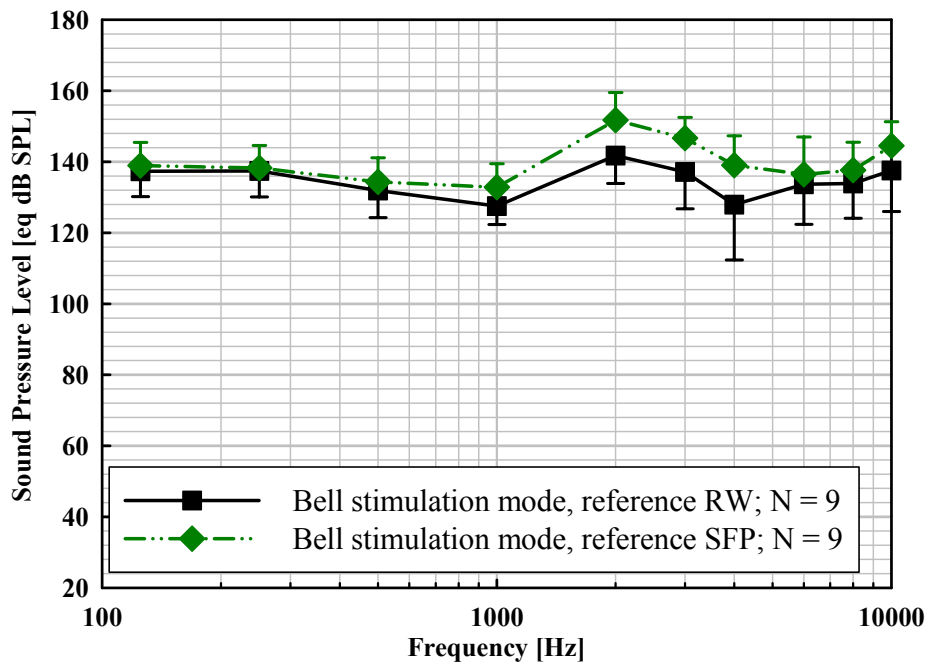### 3.2.6   Comparison of RW and SFP as Output Reference

In Bell stimulation mode both references, SFP displacement and RW displacement, provided comparable mean actuator output levels (Figure 3.10) with differences of 1–5 dB at frequencies ≤ 1 kHz and of 3–7 dB at 6–10 kHz. Between 2 kHz and 4 kHz mean output levels calculated from SFP vibration responses were 10–11 dB higher than the output levels calculated from RW vibration amplitudes. The difference between the mean equivalent SPLs calculated from both references was significant (Kolmogorov-Smirnov, paired t-test) at 1 kHz ($p = 0.008$), 2 kHz ($p = 0.004$) and 3 kHz ($p = 0.026$) and not significant at all other stimulation frequencies.

3.3   Discussion

3.3.1   Using RW Vibration Amplitudes as Reference for Actuator Output Level Determination

To assess the error resulting from single point measurements of RW vibration responses as reference, the mean equivalent SPLs of the Bell stimulations calculated from RW and SFP vibrations were compared (Figure 3.10). The small differences of maximally 5 dB between them at most frequencies are in good accordance with KRINGLEBOTN [1995] who demonstrated a difference of only approx. 3 dB at 0.06–1.5 kHz between the volume displacement of the oval window and of the RW during mechanical SFP stimulation using an acoustic probe at the RW. Likewise, STENFELT ET AL. [2004a] determined a difference in volume displacement between oval window and RW in response to acoustic stimulation of ≤ 3 dB using a 5 point measurement matrix on the SFP and a 27–40 point matrix with 0.2 mm spacing on the RW to determine the integral volume displacement. In contrast, DEVÈZE ET AL. [2010] found that the equivalent SPL output of a T2 MET actuator (Otologics Boulder, USA) in Bell stimulation was between 0.25 kHz and 4.5 kHz 14–23 dB higher when using stapes vibrations as reference compared to RW vibrations. A possible reason for this and for the differences of 10–11 dB at 2–4 kHz in the present study may be the complex nature of stapes motion. Below 1 kHz, the stapes motion is primarily piston-like but above this frequency rocking motion become more dominant with frequency [HATO ET AL., 2003; HUBER ET AL., 2001]. If the stapes motion is recorded with a single-point LDV at sites outside the center of the SFP, at the stapes crus or at the stapes head, these rocking motions could be misinterpreted as piston motion leading to an overestimation of the determined eq. SPL. According to this assumption, this effect would be more pronounced in DEVÈZE ET AL. [2010] because the incidence angle of the LDV was in their experiment 65–80°, whereas in the present study it was $\leq 60°$. In summary, the present results demonstrate that in stapes stimulation the use of RW vibration response as reference provides consistent results comparable to SFP vibration measurement except at 2–4 kHz. However, if RW vibration amplitudes are used to estimate the output level of direct perilymph stimulation it has to be considered that the opening of the cochlea causes significant changes in the RW motion pattern at frequencies above 1.5 kHz [STENFELT ET AL., 2004b] (see section 1.4.5).

Frequency	Bell vs. K-Piston			Omega/Aerial vs. K-Piston			Bell vs. Omega/Aerial			RW vs. K-Piston			RW vs. Omega/Aerial			RW vs. Bell		
	Mean Difference	p-Value	N	Mean Difference	p-Value	N	Mean Difference	p-Value	N	Mean Difference	p-Value	N	Mean Difference	p-Value	N	Mean Difference	p-Value	N
[kHz]	[dB]	[-]	[-]	[dB]	[-]	[-]	[dB]	[-]	[-]	[dB]	[-]	[-]	[dB]	[-]	[-]	[dB]	[-]	[-]
0.125	15.34	0.000168	7	13.65	0.000021500	7	0.61	0.761	8	-7.39	0.103	8	-19.34	0.0012900	8	-19.51	0.00069100	9
0.25	13.26	0.000216	9	12.91	0.000002140	8	1.48	0.515	8	-6.60	0.070	10	-19.17	0.0008250	8	-19.62	0.00059300	9
0.5	12.05	0.000379	9	12.35	0.000000671	8	1.44	0.528	8	-4.94	0.231	10	-16.79	0.0021800	8	-16.49	0.00288000	9
1	14.26	0.000042	9	10.64	0.000068600	8	2.82	0.229	8	0.43	0.880	10	-10.59	0.0027000	8	-13.97	0.00274000	9
2	9.96	0.006900	9	12.07	0.006760000	8	-3.20	0.143	8	-3.45	0.513	10	-13.24	0.0057300	8	-13.52	0.01180000	9
3	16.79	0.008570	9	19.98	0.000753000	8	0.05	0.978	8	-0.26	0.970	10	-18.89	0.0086500	8	-17.32	0.00484000	9
4	19.54	0.012900	9	24.52	0.001930000	8	-2.81	1.00[(]	8	3.11	0.663	10	-22.07	0.0018200	8	-16.55	0.00975000	9
6	22.98	0.001710	9	23.50	0.00800000[(]	8	-1.31	0.505	8	-0.74	0.909	10	-26.79	0.0002710	8	-25.83	0.00006910	9
8	20.33	0.000934	9	19.42	0.005140000	8	0.83	0.724	8	-3.56	0.385	10	-25.88	0.0002390	8	-25.79	0.00003100	9
10	11.61	0.048600	9	13.77	0.045800000	8	-2.04	0.577	8	-14.40	0.063	10	-32.96	0.0000145	8	-29.71	0.00000609	9

Table 3.2. Statistical analysis of differences in eq. output level [eq. dB SPL]. A paired t-test was used except in rare cases where the differences were not normally distributed (Kolmogorov-Smirnov test) and a non-parametric test (Wilcoxon Signed Rank Test) was used.

3.3.2   Stapes Stimulation

When the head (Bell stimulation) or the footplate (Omega/Aerial stimulation) of the stapes is stimulated, the entire oval window acts as the mechanical input to the inner ear. Therefore one can expect that both stimulation modes produce equal outputs. Being statistically indistinguishable, the here determined eq. SPLs of the Bell stimulation and Omega/Aerial stimulation mode confirm this presumption. The obtained output of the Codacs actuator in Bell stimulation mode was higher than the output generated by a T2 MET actuator in a similar stimulation experiment in DEVÈZE ET AL. [2010]. Between 0.25 and 8 kHz the MET provided an output of approx. 113 to 138 eq. dB SPL compared to the Codacs actuator that provided 127.5 to 141.8 eq. dB SPL, at 1 V$_{rms}$ input voltage. However, the results are not strictly comparable, because in DEVÈZE ET AL. [2010] the prosthesis was bent and coupled to the stapes head in another angle and no information about the static coupling force is provided.

3.3.3   RW Stimulation

As discussed in section 1.4.5, ICPD measurements from STIEGER ET AL. [2013] indicated that stapes vibration amplitude as a measure of RW stimulation underestimates the real cochlea excitation because the acoustic input impedance is different compared to the input impedance during acoustic stimulation. Consequently one should consider that the real stimulation output of mechanical RW stimulation is underestimated if the procedure of output level prediction according to ASTM F2504–05 is applied. Nevertheless, here calculated eq. SPLs shall serve as an estimation of the obtained output in reverse stimulation of the cochlea with the Codacs actuator.

Comparison with output levels of the DACS PI (Phonak Acoustic Implants SA, Switzerland) [MAIER ET AL., 2013] and MET T1 actuator (Otologics Boulder, USA) [TRINGALI ET AL., 2010] also estimated from stapes vibrations, shows that the Codacs actuator is similar or more efficient in RW stimulation. In contrast to the DACS PI (spherical prosthesis, ∅0.5 mm, approx. 4 mN) the Codacs actuator output level shows no roll-off at frequencies > 2 kHz (Figure 3.7) in RW stimulation. The output of both actuators were similar at frequencies ≤ 1 kHz (Codacs: 113–117 eq. dB SPL, DACS PI: 110-115 eq. dB SPL), whereas the Codacs actuator output (108–119 eq. dB SPL) was substantially higher than the DACS PI output (90–105 eq. dB SPL) at higher frequencies (> 2 kHz). Compared to RW stimulation with the MET T1 (0.5 mm spherical tip, estimated "several hundred dynes" force load (100 dyne = 1 mN)), averaged output at low- (0.25–1 kHz), mid- (1–3 kHz) and high-frequencies (3–8 kHz) of the Codacs actuator (low: 115, mid: 120 and high: 112 eq. dB SPL) was also substantially higher than of the MET (low: 95, mid: 95 and high 109 eq. dB SPL) [TRINGALI ET AL., 2010].

3.3.4   Perilymph Stimulation

This is the first study quantifying AMEI or DACI actuator output levels as equivalent SPL [eq dB SPL] directly from single-point RW vibration responses measured in human cadaveric TBs. CHATZIMICHALIS ET AL. [2012] determined equivalent SPL of direct perilymph

stimulation also from vibration measurements at the RW, but their reference was the RW volume displacement reconstructed from multi-point measurements using a scanning LDV. Of course, due to the complex RW vibration pattern the volume displacement can be considered as a more accurate measure than the RW displacement at a single point. However, a multi-point measurement is much more time-consuming and a scanning LDV cannot be integrated into a surgical microscope. DEVÈZE ET AL. [2010] measured single-point RW vibration responses with an LDV during direct perilymph stimulation, but to calculate equivalent SPL outputs they first converted the RW velocities to "equivalent expected stapes velocities" based on a conversion factor determined in the same study.

As described before in chapter 1.4.5, estimating the eq. SPL of direct perilymph stimulation from single point RW vibration is subjected to limitations due to the SFP fenestration. STENFELT ET AL. [2004b] found after a stapedotomy and piston prosthesis insertion a moderate change in RW vibration pattern of approx. -3 to -14 dB at 0.1–0.5 kHz and of approx. +/- 5 dB at 0.5–1.5 kHz. At higher frequencies the amplitude and phase of the targets changed strongly (approx. 10 dB to approx. -15 dB) without a trend across targets. These findings suggest that using single-point RW vibration amplitude as reference for output level determination does not provide consistent and accurate results in direct perilymph stimulation, especially at frequencies above 1,5 kHz. This assumption is supported by the present results (Figure 3.8, Table 3.1) showing little variability at frequencies ≤ 1 kHz but a pronounced inter-individual variability at higher frequencies. Variations in the preparations can be excluded as a reason for this variability in SPL, because in all experiments the coupling force was controlled to be 0 mN and the insertion depth of the piston was identical. Therefore the here determined eq. SPL of K-piston stimulation can be used for comparison at frequencies ≤ 1 kHz, but at higher frequencies the results may only serve as an rough estimate.

CHATZIMICHALIS ET AL. [2012] determined an output level of the DACS PI in piston stimulation of approx. 118–126 eq. dB SPL at 0.3 V_{rms} input in the range between 0.125 and 1 kHz. Considering a approx. 4 dB difference, expected theoretically from the different piston diameters used (DACS PI: $\varnothing$ 0.5 mm; Codacs: $\varnothing$ 0.4 mm), the DACS PI is approx. 8–11 dB more efficient. In a similar piston stimulation experiment in DEVÈZE ET AL. [2010] the averaged output of a T2 MET at 1 V_{rms} input was 106, 119 and 101 eq. dB SPL at low- (0.25–1 kHz), mid- (1–3 kHz) and high-frequencies (3–8 kHz). Considering a approx. 4 dB difference, expected theoretically from the different piston diameters used (T2 MET: $\varnothing$ 0.5 mm; Codacs: $\varnothing$ 0.4 mm), the Codacs actuator is approx. 16, 2, 12 dB (low-, mid-, high-frequencies) more efficient.

3.3.5 Comparing the Efficiency in all Tested Stimulation Modes

The Codacs actuator stimulation of the stapes with the Bell prosthesis or Omega/Aerial prosthesis was statistically significant more efficient than the standard K-piston stimulation. At frequencies ≤ 1 kHz both methods provided 10.6–15.3 dB higher outputs (Table 3.2). At higher frequencies, where the output level determined for the K-piston stimulation can only be used as estimation (see section 3.3.4), the output in both stapes stimulation modes was 10.0–24.5 dB higher. These differences are less than the 28 dB difference of volume displacement that are theoretically expected from the ratio of the K-piston area (0.1257 mm^2,

$\varnothing$ 0.4 mm) to the SFP area (3.2 mm^2 [VON BÉKÉSY, 1960]). This suggests that the output
was probably affected by further aspects beside the volume displacement difference resulting
from the area inducing mechanical stimulation. On the other hand, a comparison with the
theoretical difference of volume displacement is possible only to a limited extent since the eq.
SPL calculated for the performed K-piston stimulation may be effected by the disturbance
of the SFP integrity as discussed before.

The RW stimulation output was similar to the K-piston stimulation output with no sta-
tistically significant differences between each other. Compared to the Bell stimulation and
Omega/Aerial stimulation mode, the RW stimulation was statistically significantly less ef-
ficient (10.6–33.0 dB). However, it has to be considered that the eq. SPL output of the RW
stimulation determined from SFP vibrations probably underestimates the real output level as
discussed before .

Based on the here presented results, all four tested stimulation modes are usable with
the Codacs actuator because all of them provided eq. dB SPL being sufficient for hearing
aid applications. However, it has to be considered that the accuracy of eq. SPL determined
from single-point LDV measurements is limited in direct perilymph stimulation and RW
stimulation. To obtain eq. SPL comparable in all stimulation modes and over the entire
frequency range from 0.1 to 10 kHz, an alternative method, such as intracochlear pressure
measurement is needed.

3.3.6 Codacs Actuator Usability with Static Contact Force

In bench experiments the Codacs actuator displacement output in the plateau range below
approx. 2 kHz showed only a mild decrease with increasing static force applied to the ac-
tuator up to the maximum of approx. 100 mN (data not shown). Also the THD remained
at levels below 2.1 % when tested with 0.6 kHz (Figure 3.11A, C, E). Higher THDs using a
stimulus frequency of 1 kHz (Figure 3.11B, D, F) were attributed to the coincidence of the
1st harmonic with the resonance frequency of the actuator and decreased with the applied
force. In earlier performed RW stimulation experiments with an actuator of similar design
(DACS PI, Phonak Acoustic Implants SA, Switzerland) the impact of static preload force on
the output amplitude and resonance frequency was found minor at forces < 37.2 mN [MAIER
ET AL., 2013]. These findings demonstrate that the Codacs actuator originally designed for
stimulations without static force load may also be suitable for applications requiring some
axial forces to the actuator rod. The static preload used in the TB experiments was chosen
not only to achieve minimum output reduction and THD and maximum coupling efficiency,
but also to remain with the SFP vibration in a linear range. Because the SFP has a linear
force-displacement behavior up to approx. 10–15 mN of static load [LAUXMANN ET AL.,
2014], a static preload of 5 mN was taken. Although the Codacs actuator was specifically
designed to be coupled to the perilymph [BERNHARD ET AL., 2011] where no static force
preload is expected, the present results indicate that it can be used in applications applying a
static force preload with sufficiently high output amplitude and low distortion (Figure 3.11).
Whereas the actuator can be used over a wide range of static forces, limitations are more
likely due to force limits by the stimulated structure, for instance saturation of the SFP.

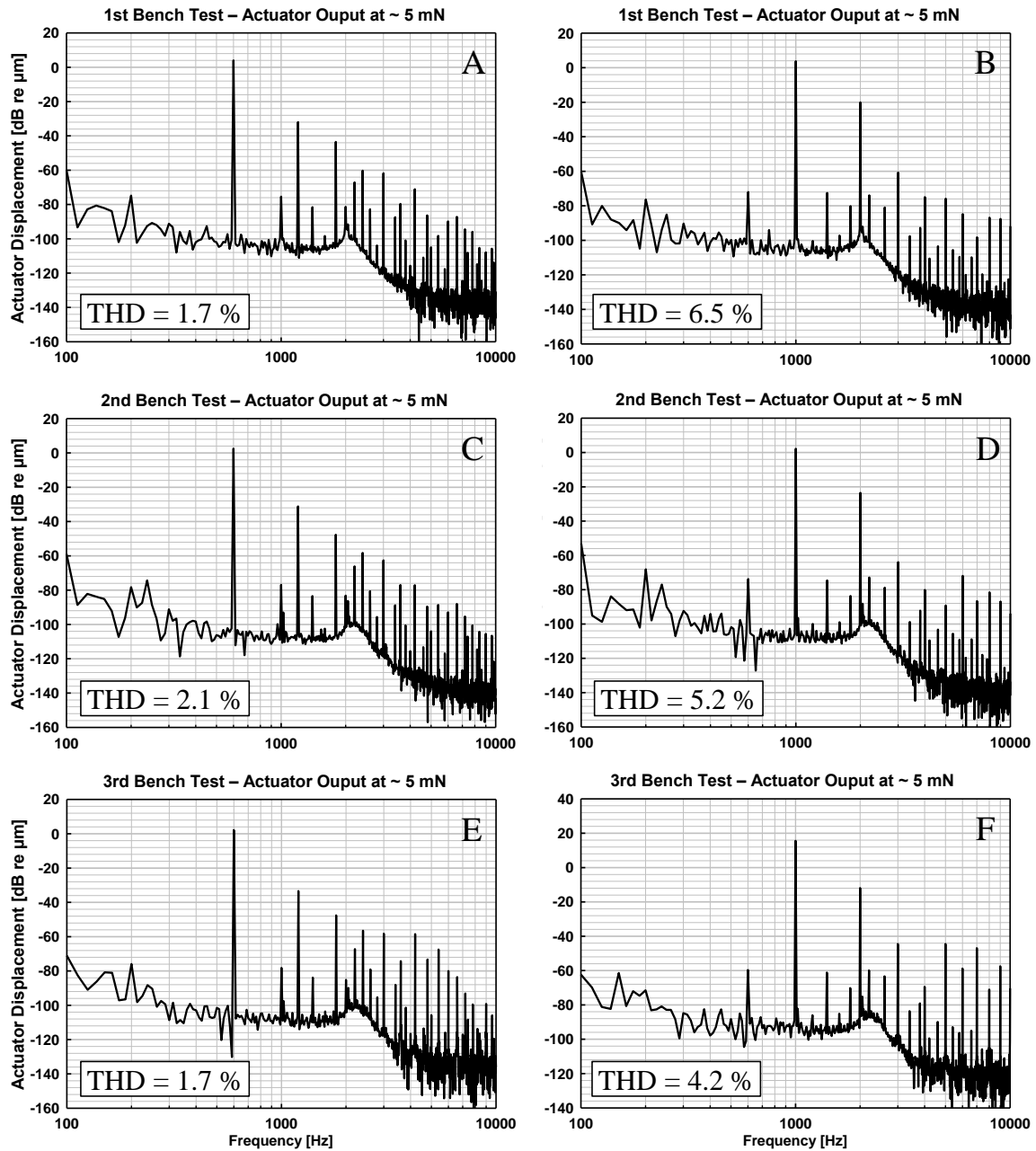**Figure 3.11.** Displacement output of the Codacs actuator driven by an electrical 0.6 kHz & 1 kHz sine wave signal of approx. -13 dB re 1 V$_{rms}$ electrical actuator input in 3 bench tests at a static preload of approx. 5 mN. Estimated THDs are given in each panel. A & B: 1st bench test. C & D: 2nd bench test. E & F: 3rd bench test. Modified from GROSSÖHMICHEN ET AL. [2015] (CC BY 4.0).

3.3.7   Feasibility of Alternative Stimulation Modes with the Codacs Actuator

Although the presented results show that alternative stimulation sites can be successfully addressed with the Codacs actuator it must be emphasized that the experimental conditions were optimized and differ essentially from the clinical situation *in vivo*. The specific experimental configuration was selected to control variables (e.g. static force and geometrical constrictions) that potentially influence the stimulation. For clinical applications this approach has to be adapted to the anatomical constraints. The angle between the actuator axis and the normal of the SFP used in the Bell, Omega/Aerial and K-piston stimulation modes was comparable to *in vivo* applications. In contrast, a coupling of the actuator rod perpendicular to the RW membrane is not feasible *in vivo*. Due to anatomical constraints a shallower angle has to be expected in clinical RW applications which might cause lateral forces to the actuator rod and a decrease in the efficiency of the RW stimulation mode. When a Bell or Aerial prosthesis is crimped to the artificial incus of the Codacs actuator the total length exceeds potentially the space available *in vivo*. Therefore a redesign of the Codacs actuator rod might be necessary for these applications. To achieve *in vivo* force-controlled coupling conditions similar to the present experiments, a mechanism to determine at least the axial component of the loading force has also to be implemented.

3.4   Summary and Conclusion

The procedure of ASTM standard F2504–05 could be successfully adapted to estimate actuator output levels as eq. SPL in direct perilymph stimulation (DACI application) and in SFP stimulation where the stapes is visually not accessible. For this purpose RW vibrations measured at a single point were used as reference instead of stapes vibrations. It could be demonstrated that single-point displacements responses of RW and SFP are both adequate references to determine the eq. SPL output of actuator stimulations at the intact stapes, providing that the measurement target is kept constant during acoustic and mechanical stimulation. The finding that the output level estimated for the DACI stimulations showed pronounced inter-individual variations at frequencies > 1 kHz supported previous findings that an opening of the SFP changes the RW motion pattern significantly. In summary, the here presented results indicate that in applications differing from ossicular chain stimulation, actuator output levels determined from vibration measurements in TBs should only be used for rough estimations, especially at frequencies > 1 kHz. Furthermore it could be demonstrated that the Codacs actuator, originally designed for applications without static axial forces to the rod, is usable under an axial static coupling force of approx. 5 mN. At this force level all investigated alternative stimulation modes (Bell, Omega/Aerial and RW stimulation) provided output levels being sufficient for hearing aid applications and equal or higher than in the standard perilymph stimulation. Stimulation of the stapes using a Bell or Omega/Aerial prosthesis increased the efficiency compared to RW or direct perilymph stimulation with a K-piston.

Chapter 4

Measuring ICPDs in Human Cadaveric Ears with Off-the-shelf Pressure Sensors[1]

The previous chapter confirmed that the output level of mechanical stimulations other than ossicular chain stimulation cannot be precisely determined by single-point vibration measurement. As mentioned in the introduction chapter, measuring the sound pressure difference between SV and ST represent a good candidate for a method to predict the output level of all common AMEI and DACI stimulation modes because the pressure difference correlates with evoked potentials in animals [DANCER & FRANKE, 1980] and is measurable in human cadaveric TBs [NAKAJIMA ET AL., 2009, 2010; PISANO ET AL., 2012; STIEGER ET AL., 2013]. However, the custom-made pressure sensor that has been used in these studies is commercially not available, complex in manufacturing and fragile [OLSON, 1998]. In order to make ICPD measurement generally accessible, the objective of the experiments presented in the present chapter was to investigate whether ICPDs can be measured in human cadaveric ears with off-the-shelf pressure measurement systems.

4.1   Materials and Methods

Intracochlear sound pressures were measured during acoustic stimulation simultaneously in SV (p_{SV}) and ST (p_{SV}) with the two off-the-shelf pressure measurement systems Samba and FISO described in section 2.5. The experiments were performed in two different groups of human cadaveric TBs (Samba: n = 19, FISO: n = 14) obtained and prepared as described in section 2.1.

4.1.1   Experimental Setup

For the acoustic stimulation the sound application setup comprising a DT48 loudspeaker and a ER-7C probe microphone was cemented in the outer ear canal of the TB as described

---

[1]Parts of this chapter have been published in GROSSÖHMICHEN ET AL. [2016b, 2017].
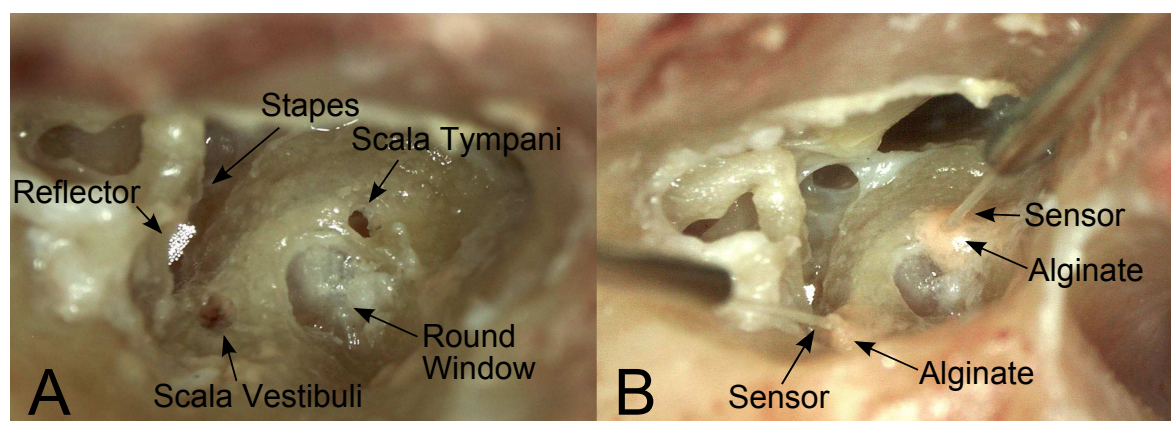
Figure 4.1. Temporal bone preparation for intracochlear sound pressure measurements.   A: Cochleostomies of approx. 0.5 mm diameter in scala vestibuli (SV) and scala tympani (ST) (Picture was taken after the experiment). The reflector was placed on the stapes footplate for LDV measurement. B: Samba Preclin 420 LP transducers placed in SV (left) and ST (right), sealed with Alginate. Taken from GROSSÖHMICHEN ET AL. [2016b] (CC BY 4.0).

in section 2.2. Each pressure measurement transducer was mounted to a custom holder designed and manufactured in collaboration with the research workshop of the Hannover Medical School. Each holder was attached to a 3-axis micromanipulator (Samba: M3301R, FISO: MM3-3, both World Precision Instruments Germany GmbH, Germany) mounted on a magnetic stand (Horex, Germany), allowing the adjustment in all three spatial directions. The entire setup was installed on a vibration isolated table (LW3048B, Newport, USA).

4.1.2   Intracochlear Sound Pressure Measurement

Intracochlear sound pressures in SV and ST were measured simultaneously either with the Samba or the FISO system described in section 2.5. For this purpose the promontory was first thinned where the *cochleostomies*[2] were intended and then an opening of approx. 0.5 mm diameter for the Samba transducers and of approx. 0.4 mm diameter for the FISO transducers was made in SV and ST using a diamond burr and a footplate perforator (Figure 4.1A). When the tip of the transducer was visually estimated 100–300 μm inserted into the scalae (Figure 4.1B), the transducer was sealed with the surrounding bone using three different techniques: (1) In Samba_TB05–07 dental impression material alginate (Alginoplast®, Heraeus Kulzer GmbH) was applied . (2) In Samba_TB16, 18, 19 a disc-shape silicone rubber plug (Silikonkautschuk RTV, Wacker-Chemie GmbH, Germany) was permanently mounted to the optical fiber. (3) In all FISO_TBs transducers were sealed with both a 3 mm piece of silicone tube (Sedat, France) permanently mounted to the optical fiber and alginate (Alginoplast®, Heraeus Kulzer GmbH). During cochleostomy, sensor insertion and sealing, the middle ear cavity was immersed in saline to prevent air from entering the cochlea.

---

[2]A (drilled) opening into the cochlea [CLARK, 2003].

4.1.3 Vibration Measurement

Vibration responses of the stapes were measured in the Samba experiments with the LDV system consisting of the devices OFV 534 and OFV 5000 and in the FISO experiments with the LDV system comprising the devices CLV 700 and HLV 1000, detailed in section 2.4. In both cases the LDV system was integrated in a surgical microscope (OPMI-1, Zeiss, Germany). The laser beam was directed either on the footplate or on the posterior crus of the stapes, depending on the individual visual access. The visually estimated angle of incidence of the laser beam was $\leq 45°$ to the normal of the SFP and was considered during analysis by a cosine correction according to equation (2.1).

4.1.4 Experimental Procedure

In each TB the following procedure was performed:

(1) The TB preparation was checked visually using the surgical microscope. In case of damages of anatomical structures such as a ruptured RW or broken SFP the TB was rejected. This was the case for three out of 19 TBs of the Samba study and for none TB of the FISO study.

(2) The sound application setup was attached to the outer ear canal. The loudspeaker was driven by a custom multi-sine signal, having equal amplitudes of approx. -25 dB re 1 V_{rms} at 0.125, 0.25, 0.5, 1, 2, 3, 4, 6, 8 and 10 kHz. Simultaneously the vibration of the stapes was measured with the LDV and the sound pressure level (SPL) at the tympanic membrane p_T was recorded by the probe microphone. Only if the stapes vibration response was within the modified acceptance range [ROSOWSKI ET AL., 2007] of the ASTM standard F2504-05 [ASTM, 2005], the experiment was continued. Six out of the remaining 16 TBs of the Samba study and ten out of 14 TBs of the FISO study fulfilled this criterion and were used for the experiments.

(3) The pressure transducers were placed in SV and ST and sealed as described in section 4.1.2.

(4) Stapes vibrations were measured again in response to the acoustic multi-sine stimulation. This measurement served to investigate the effect of cochleostomy and sensor insertion on the middle ear transfer function.

(5) The tympanic membrane was stimulated acoustically between 0.1 and 10 kHz with a sequence of 23 pure tones with a frequency resolution of approx. three signals / octave at levels of 105–130 dB SPL (Samba) and 80–120 dB SPL (FISO). During stimulation the sound pressures in SV and ST were measured by the pressure transducers, the SPL at the tympanic membrane by the probe microphone and the vibration of the stapes by the LDV. In the Samba experiments, all measurements were performed simultaneously. In the FISO experiments, intracochlear sound pressures and vibratory responses were measured sequentially for technical limitation of the 2 x 4-Ch data acquisition system.

During the first stimulation the sound pressures p_{SV} and p_{SV} were measured by the pressure transducers and during the second stimulation the vibration of the stapes was measured by the LDV. The acoustic input signal at the tympanic membrane was recorded both times by the probe microphone. Although amplitudes and phases of the acoustic input signal had minor differences during both stimulations (maximum difference: $0.07\,\text{dB}$, $0.54°$), all measurement results were re-normalized to the same input. In the FISO experiments, after all acoustic stimulations were completed, additional stimulations with an AMEI actuator were performed (described in chapter 5).

(6) After completing all measurements the pressure transducers were removed and the correct positioning of the cochleostomies in SV and ST and the integrity of the basilar membrane was confirmed visually by dissection of the TB.

4.1.5 Signal Generation, Acquisition and Analysis

Signals were generated and acquired in the Samba study with the commercial data acquisition system (Polytec, Germany) and in the FISO study with the custom built data acquisition system based on LabVIEW™ as detailed in section 2.7. The signal-spectra obtained during multi-sine stimulation in the steps (2) and (4) of the experiment were averaged 500 times with both data acquisition systems. In the Samba experiments the signal-spectra obtained during sequential stimulation (step (5)) were averaged 1000 times and the SNR was calculated afterwards by equation (2.10). Vibration responses with SNR $< 12\,\text{dB}$ and intracochlear sound pressure responses with SNR $< 7\,\text{dB}$ were then excluded from analysis. In the FISO experiments the LabVIEW™ program stopped the averaging automatically when an SNR of $\geq 12\,\text{dB}$ was reached, but earliest at 30 times and latest at 1000 times. In a great majority of FISO measurements an SNR of 20 to $60\,\text{dB}$ was already reached with 30 averages and averaging more than 30 times was necessary in a few cases only. Responses with SNR $< 12\,\text{dB}$ (after 1000 averages) were not considered for analysis. ICPDs were calculated as described in section 2.6. To compare the measurement data across all TBs and with other studies, p_{SV}, p_{SV} and Δp were normalized to the inputs outer ear canal sound pressure p_T and stapes velocity v_{stap}.

4.2 Results

4.2.1 Stapes Vibration Responses to Sound

Before the insertion of the pressure transducers, six TBs in the Samba study and ten TBs in the FISO study a had middle ear transfer function H_{TV} within the modified acceptance range [ROSOWSKI ET AL., 2007] of ASTM standard F2504-05 [ASTM, 2005] at 0.25–$4\,\text{kHz}$ (Figures 4.2A & 4.3A). The difference between stapes vibration displacement responses to sound before and after insertion of transducers ($\Delta d = d_{\text{post}} - d_{\text{pre}}$) was in the Samba experiments generally within $5\,\text{dB}$ below $3\,\text{kHz}$ and within $7\,\text{dB}$ at higher frequencies (Figure 4.2B). Only at $6\,\text{kHz}$ the difference was higher in Samba_TB06 ($11.6\,\text{dB}$) and Samba_TB19 ($9.4\,\text{dB}$). In the FISO experiments, the difference Δd was maximally $3\,\text{dB}$

at frequencies $\leq 3\,\text{kHz}$ and mostly $\leq 7\,\text{dB}$ at higher frequencies (Figure 4.3B). Only in FISO_TB05 and FISO_TB06 the difference was 9 to 13 dB at 4 kHz (FISO_TB05), 8 kHz (FISO_TB06) and 10 kHz (FISO_TB06).

4.2.2 Sound Pressures in Scala Vestibuli and Scala Tympani

Samba: In all TBs except Samba_TB05, intracochlear sound pressures were measurable between 0.1 and 6.35 kHz with an SNR $> 7\,\text{dB}$ (Figure 4.4 – 4.7). Pressures at 8 kHz were measurable in the experiments Samba_TB18 & Samba_TB19 and at 10 kHz only in experiment Samba_TB18). When normalized to p_T the magnitudes of p_{SV} (Figure 4.4A) were similar in all TBs, whereas the magnitudes of p_{SV} (Figure 4.5A) showed a variability of up to 42 dB with very different frequency characteristics. The magnitudes in Samba_TB19 in particular were below 0.4 kHz up to 27 dB smaller than in all other experiments. The phases of p_{SV} (Figure 4.4B) and p_{SV} (Figure 4.5B) were similar across all TBs showing an increasing lag to p_T with increasing frequency. At frequencies above 4 kHz the phases of p_{SV} decreased significantly, resulting in approx. two cycles shift above 5.5 kHz. The magnitudes of p_{SV} normalized to v_{stap} (Figure 4.6A) were similar in all experiments, only Samba_TB07 showed a prominent peak at 2.525 kHz. In contrast, the magnitudes of p_{SV}/v_{stap} (Figure 4.7A) had no similar frequency characteristics and varied significantly by up to 49 dB at frequencies below 3 kHz. Again, at frequencies $\leq 0.4\,\text{kHz}$ the magnitudes in Samba_TB19 were distinctly smaller compared to all other experiments. At frequencies $\leq 2\,\text{kHz}$ the p_{SV}/v_{stap} and p_{SV}/v_{stap} phases were mainly frequency-independent but at higher frequencies the phases showed a higher variation. In all experiments the normalized magnitude of p_{SV} was higher than the normalized magnitude of p_{SV} at frequencies above 0.4 kHz whereas the pressure magnitudes in both scalae were similar at lower frequencies. Only in Samba_TB07 the magnitudes of p_{SV} and p_{SV} were similar (differences $\leq 2\,\text{dB}$) up to 1.6 kHz and in Samba_TB19 the magnitude of p_{SV} was distinctly higher than p_{SV} at all frequencies.

FISO: In almost all TBs intracochlear sound pressures were measurable in both scalae at all stimulation frequencies with an SNR $> 12\,\text{dB}$, only in FISO_TB04 no pressures were measurable at 10 kHz (Figure 4.8 – 4.10). When normalized to p_T the magnitudes of p_{SV} and p_{SV} (Figure 4.8A & Figure 4.9A) were similar across all experiments with comparable frequency characteristics. Only in FISO_TB09 the magnitude of p_{SV}/p_T was at frequencies below 1 kHz up to 20 dB lower than in all other experiments. The phases of p_{SV} (Figure 4.8B) and p_{SV} (Figure 4.9B) were similar across all TBs showing an increasing lag to p_T with increasing frequency. When normalized to v_{stap} the magnitudes of p_{SV} and p_{SV} were also similar across all experiments (Figure 4.10A & 4.11A). Magnitudes of p_{SV}/p_{SV} had mostly a low frequency dependence whereas p_{SV}/p_{SV} magnitudes showed a prominent dip around 0.6 kHz. Phases of p_{SV}/v_{stap} (Figure 4.10B) were similar in all experiments with values of mostly $\pm 90°$ at frequencies $\leq 3\,\text{kHz}$ and an increased variability above. In all TBs p_{SV}/v_{stap} in magnitude and 180° phase shift. In almost all TBs the phases of p_{SV}/v_{stap} (Figure 4.11B) showed the same frequency characteristic with values around -90° at low frequencies and a 90–180° phase shift around 0.5 kHz.
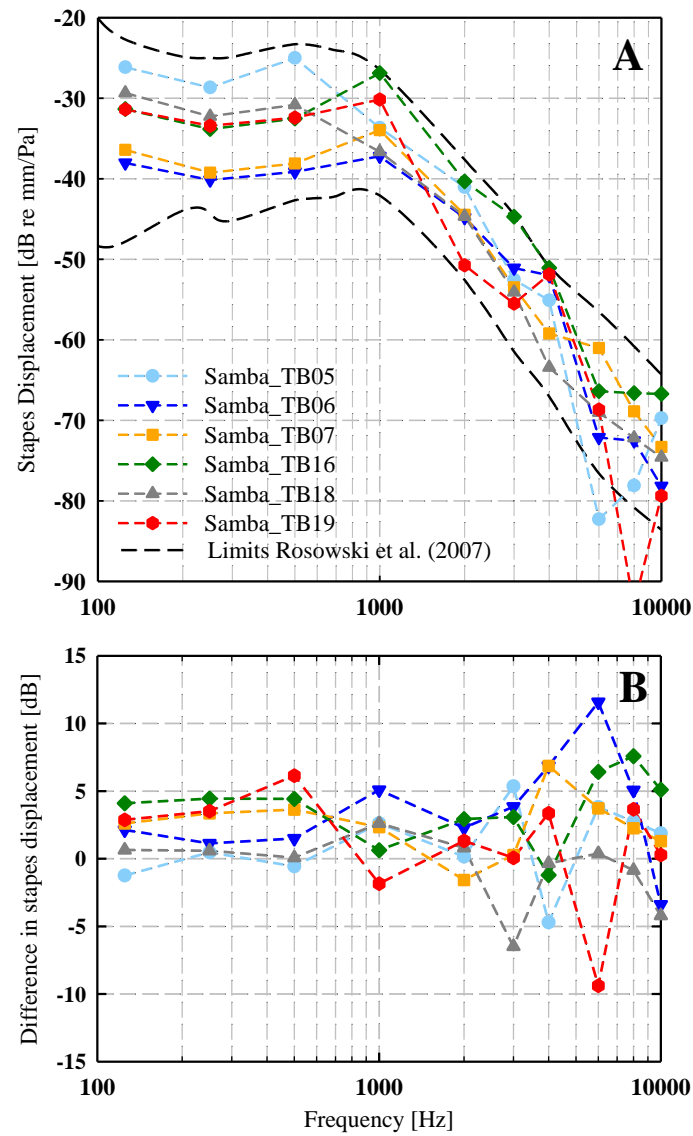
Figure 4.2. Stapes vibration responses to acoustic stimulation in the TB preparations used for Samba experiments. Lines connecting symbols are for visual guidance only. A: Stapes displacement amplitudes before sensor insertion compared to the limits given by ROSOWSKI ET AL. [2007] (black dashed lines). B: Differences in stapes amplitudes before and after insertion of the Samba pressure transducers ($\Delta d = d_{post} - d_{pre}$).
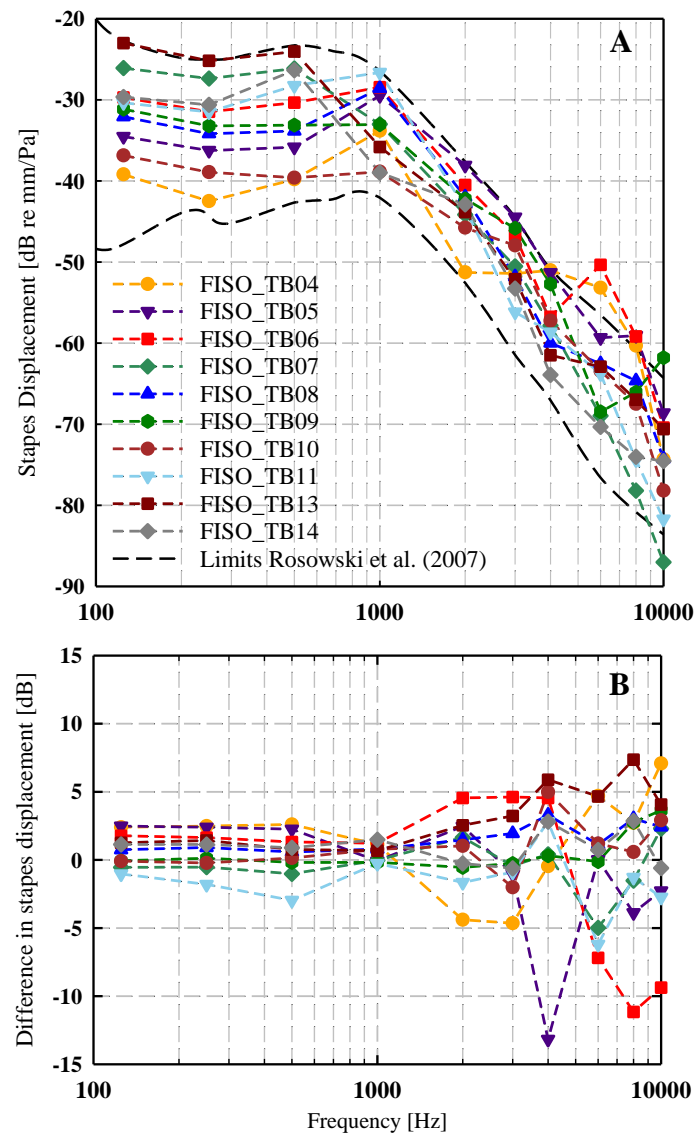
Figure 4.3. Stapes vibration responses to acoustic stimulation in the TB preparations used for FISO experiments. Lines connecting symbols are for visual guidance only. A: Stapes displacement amplitudes before sensor insertion compared to the limits given by ROSOWSKI ET AL. [2007] (black dashed lines). B: Differences in stapes amplitudes before and after insertion of the FISO pressure transducers ($\Delta d = d_{\text{post}} - d_{\text{pre}}$).
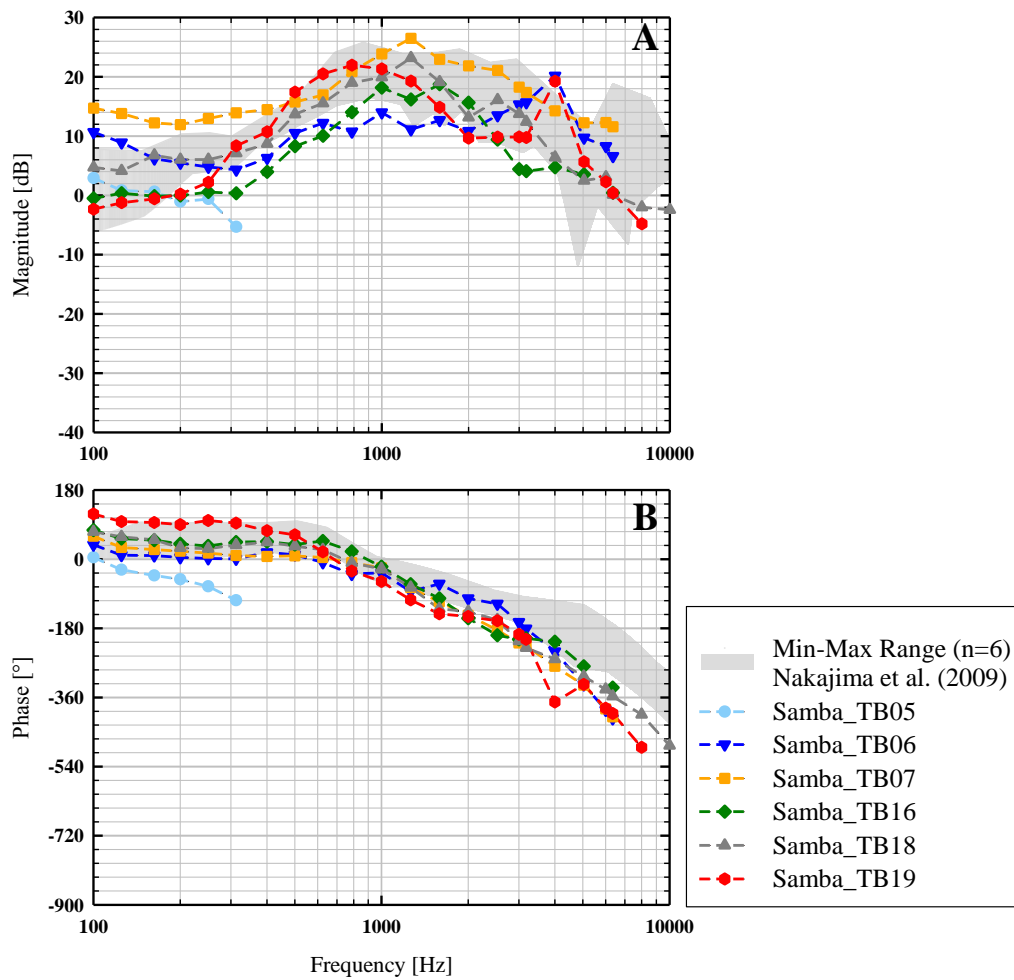
Figure 4.4. Sound pressure p_{SV} (A: magnitudes, B: phases) measured with a Samba pressure sensor in
scala vestibuli, normalized to the ear canal sound pressure p_T. For comparison the range of
results obtained by NAKAJIMA ET AL. [2009] with a custom made pressure sensor is given
as grey shaded area. Data with an SNR $< 7\,$dB were omitted. Lines connecting symbols are
for visual guidance only. Modified from GROSSÖHMICHEN ET AL. [2016b] (CC BY 4.0).

Figure 4.5. Sound pressure p_{ST} (A: magnitudes, B: phases) measured with a Samba sensor in scala tympani, normalized to the ear canal sound pressure p_T. For comparison the range of results obtained by NAKAJIMA ET AL. [2009] with a custom made pressure sensor is given as grey shaded area. Data with an SNR $< 7\,dB$ were omitted. Lines connecting symbols are for visual guidance only. Modified from GROSSÖHMICHEN ET AL. [2016b] (CC BY 4.0).

Figure 4.6. Sound pressure p_{SV} (A: magnitudes, B: phases) measured with a Samba pressure sensor in scala vestibuli, normalized to the stapes velocity v_{stap}. For comparison the range of results obtained by STIEGER ET AL. [2013] with a custom made pressure sensor is given as grey shaded area. Data with an SNR < 7 dB were omitted. Lines connecting symbols are for visual guidance only. Modified from GROSSÖHMICHEN ET AL. [2016b] (CC BY 4.0).
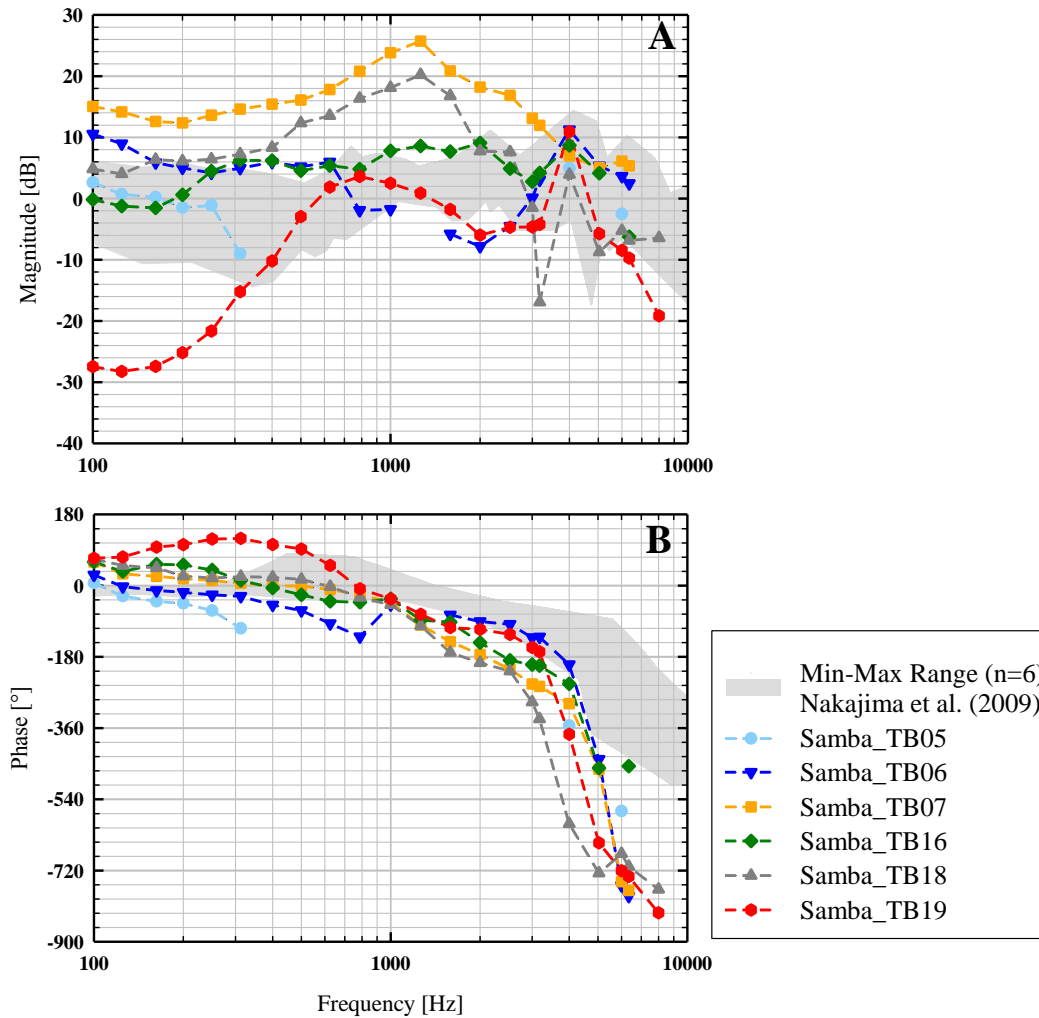
Figure 4.7. Sound pressure p_{ST} (A: magnitudes, B: phases) measured with a Samba pressure sensor in scala tympani, normalized to the stapes velocity v_{stap}. For comparison the range of results obtained by STIEGER ET AL. [2013] with a custom made pressure sensor is given as grey shaded area. Data with an SNR < 7 dB were omitted. Lines connecting symbols are for visual guidance only. Modified from GROSSÖHMICHEN ET AL. [2016b] (CC BY 4.0).
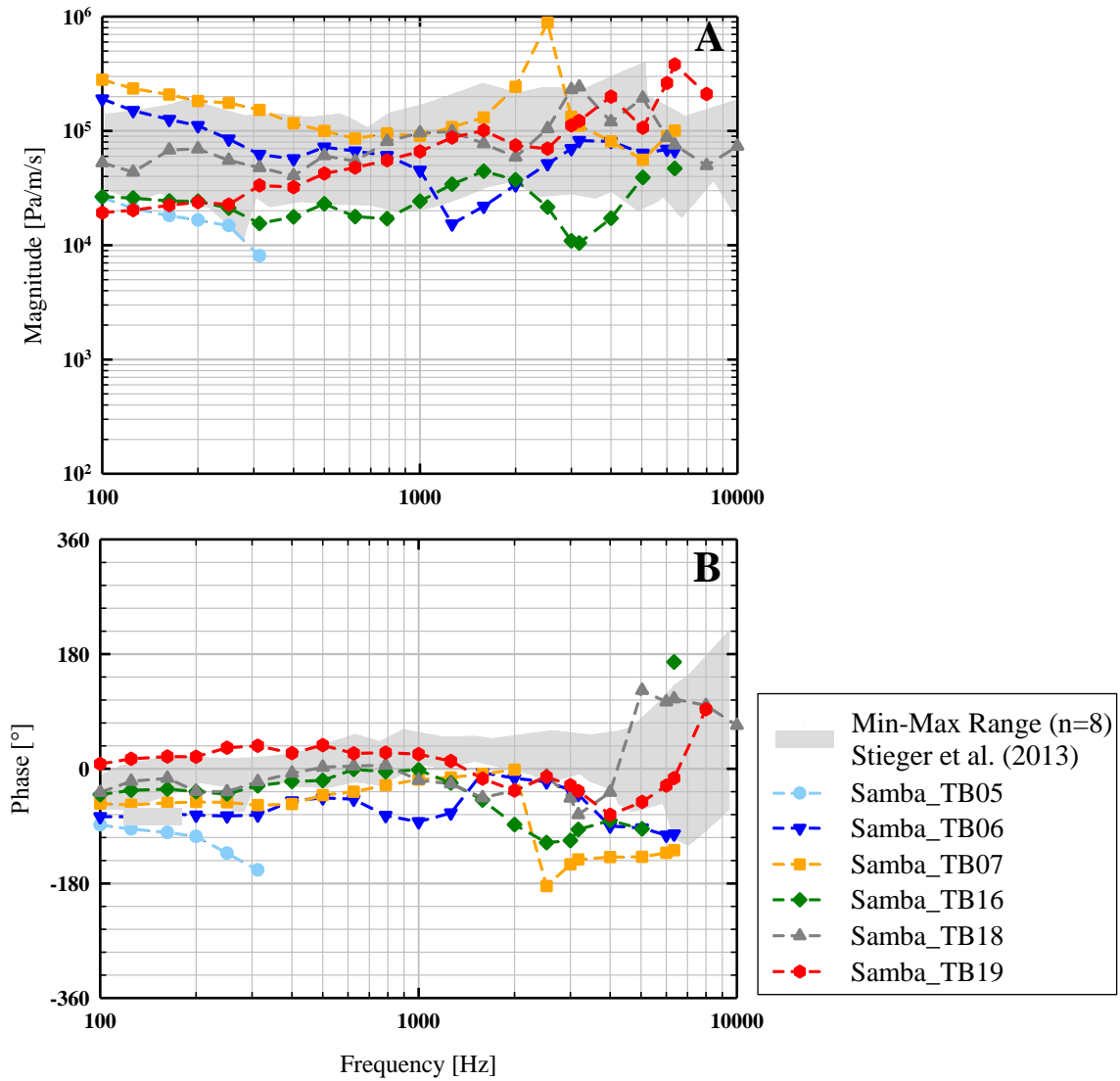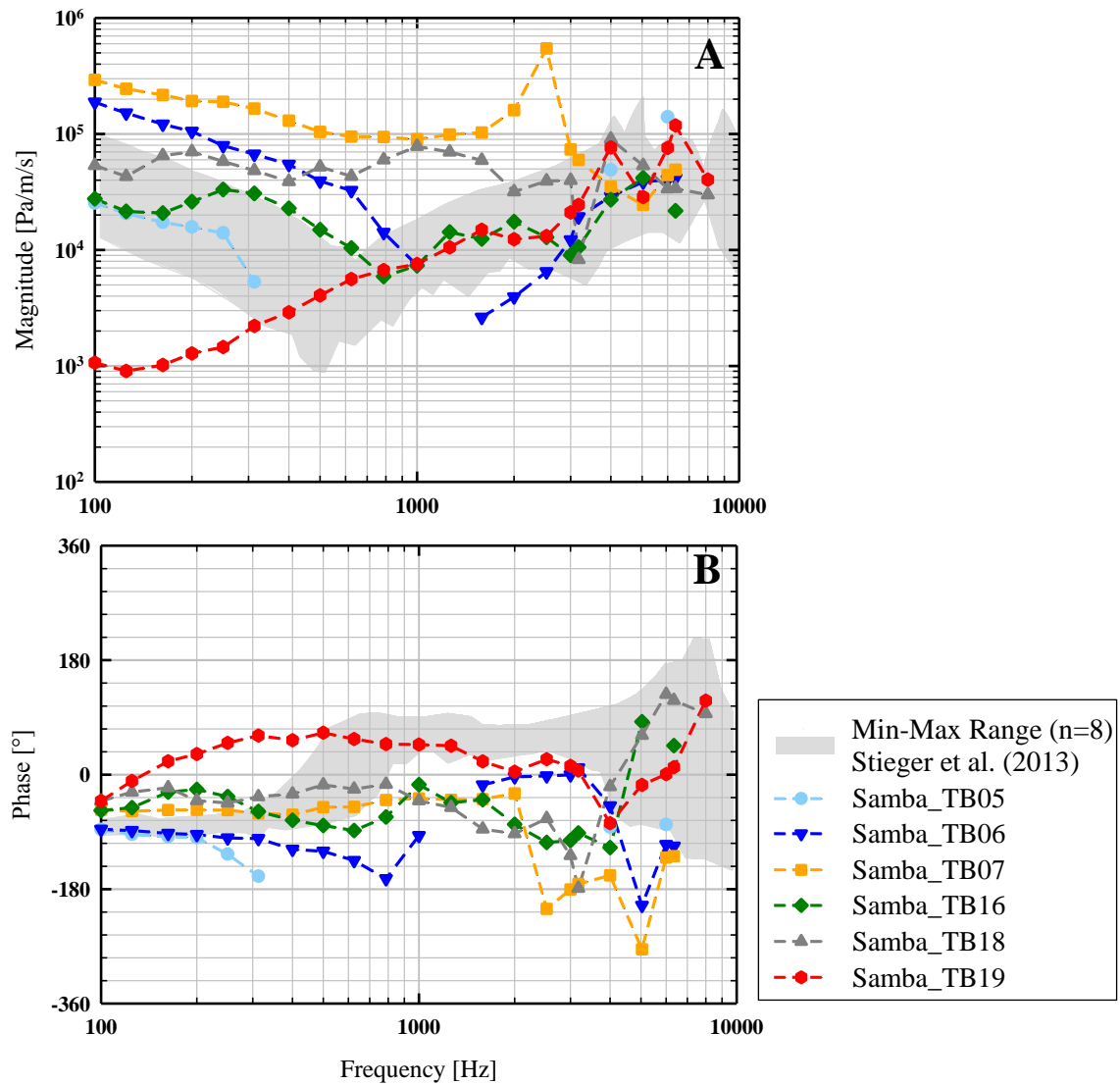
Figure 4.8. Sound pressure p_{SV} (A: magnitudes, B: phases) measured with a FISO pressure sensor in
scala vestibuli, normalized to the ear canal sound pressure p_T. For comparison the range of
results obtained by NAKAJIMA ET AL. [2009] with a custom made pressure sensor is given
as grey shaded area. Data with an SNR $< 7\,$dB were omitted. Lines connecting symbols are
for visual guidance only.

Figure 4.9. Sound pressure p_{ST} (A: magnitudes, B: phases) measured with a FISO sensor in scala tympani, normalized to the ear canal sound pressure p_T. For comparison the range of results obtained by NAKAJIMA ET AL. [2009] with a custom made pressure sensor is given as grey shaded area. Data with an SNR < 7 dB were omitted. Lines connecting symbols are for visual guidance only.
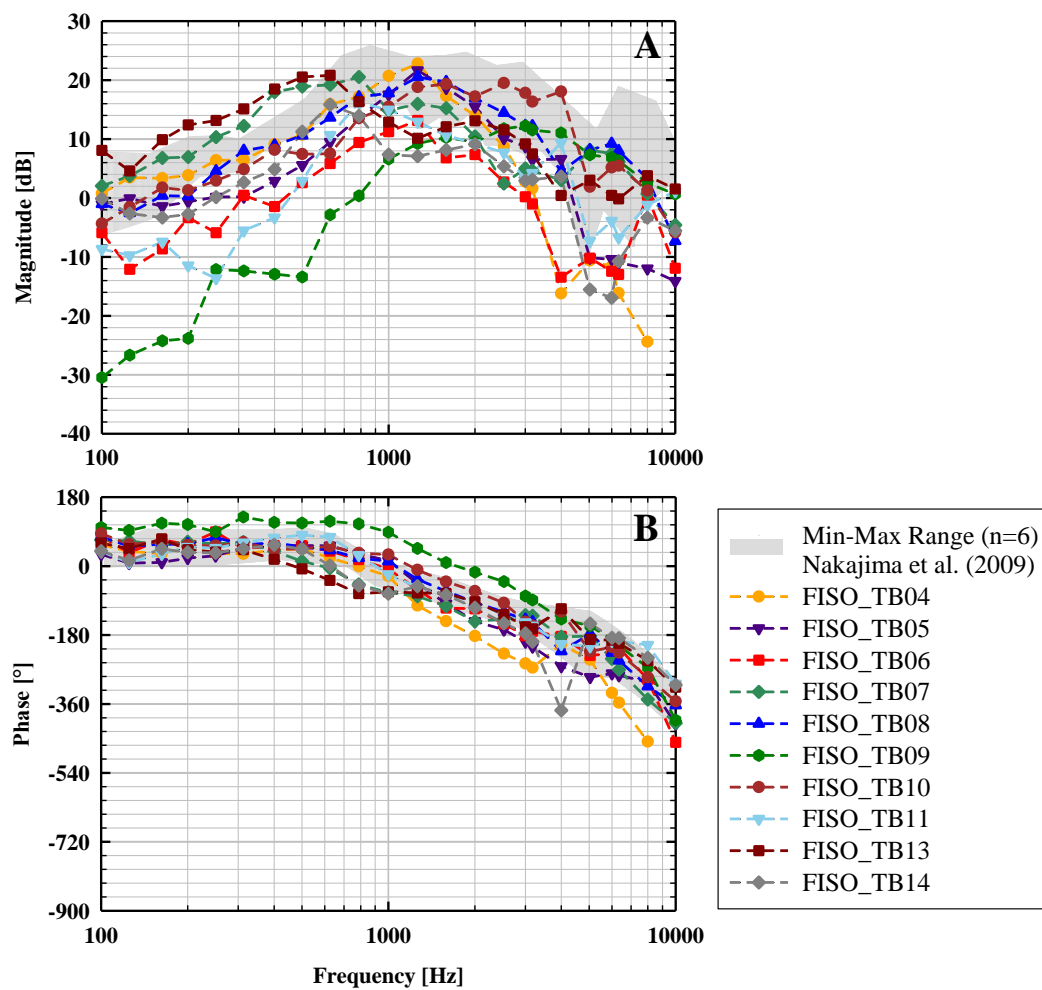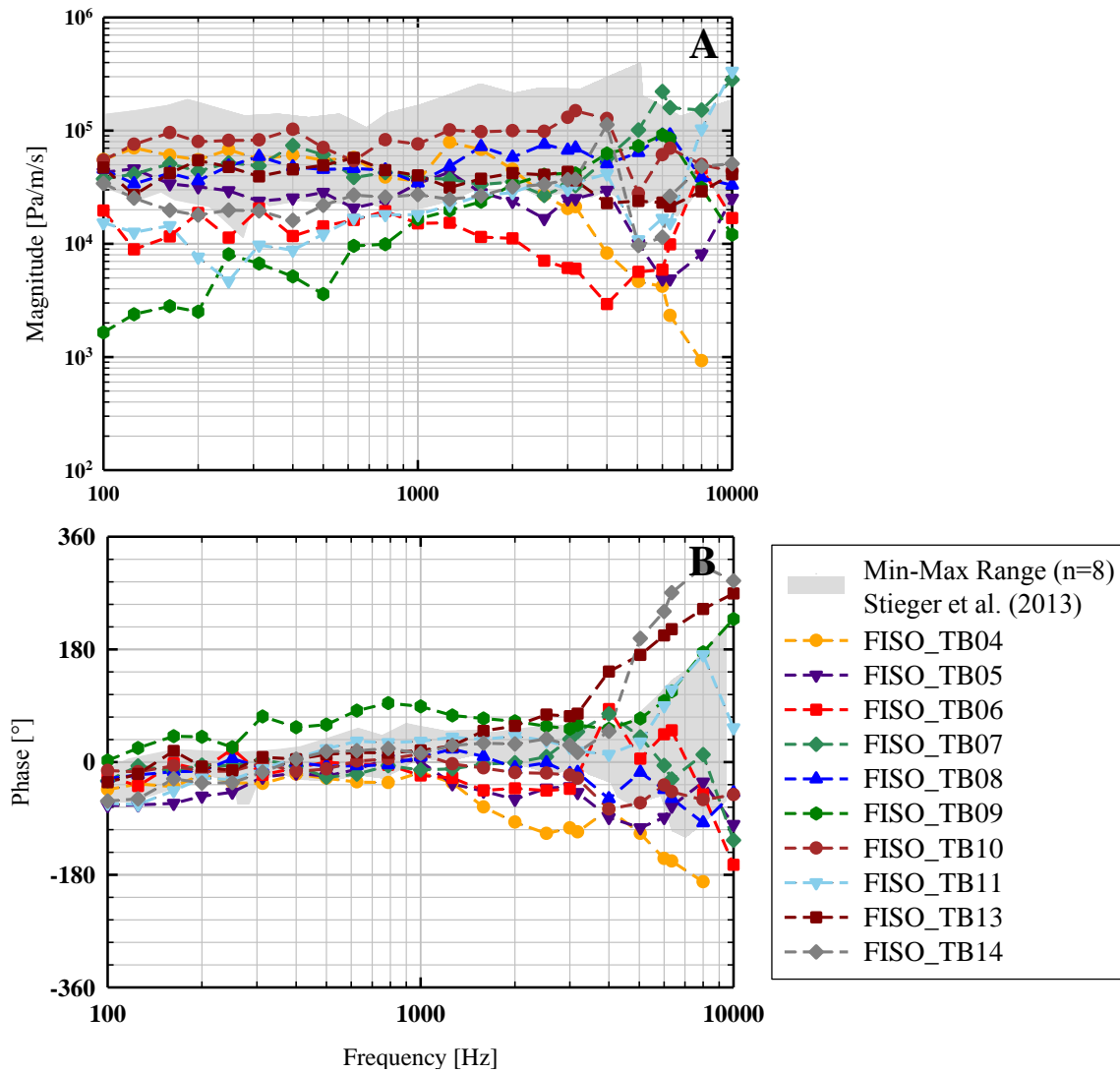
Figure 4.10. Sound pressure p_{SV} (A: magnitudes, B: phases) measured with a FISO pressure sensor in scala vestibuli, normalized to the stapes velocity v_{stap}. For comparison the range of results obtained by STIEGER ET AL. [2013] with a custom made pressure sensor is given as grey shaded area. Data with an SNR $< 7\,$dB were omitted. Lines connecting symbols are for visual guidance only.
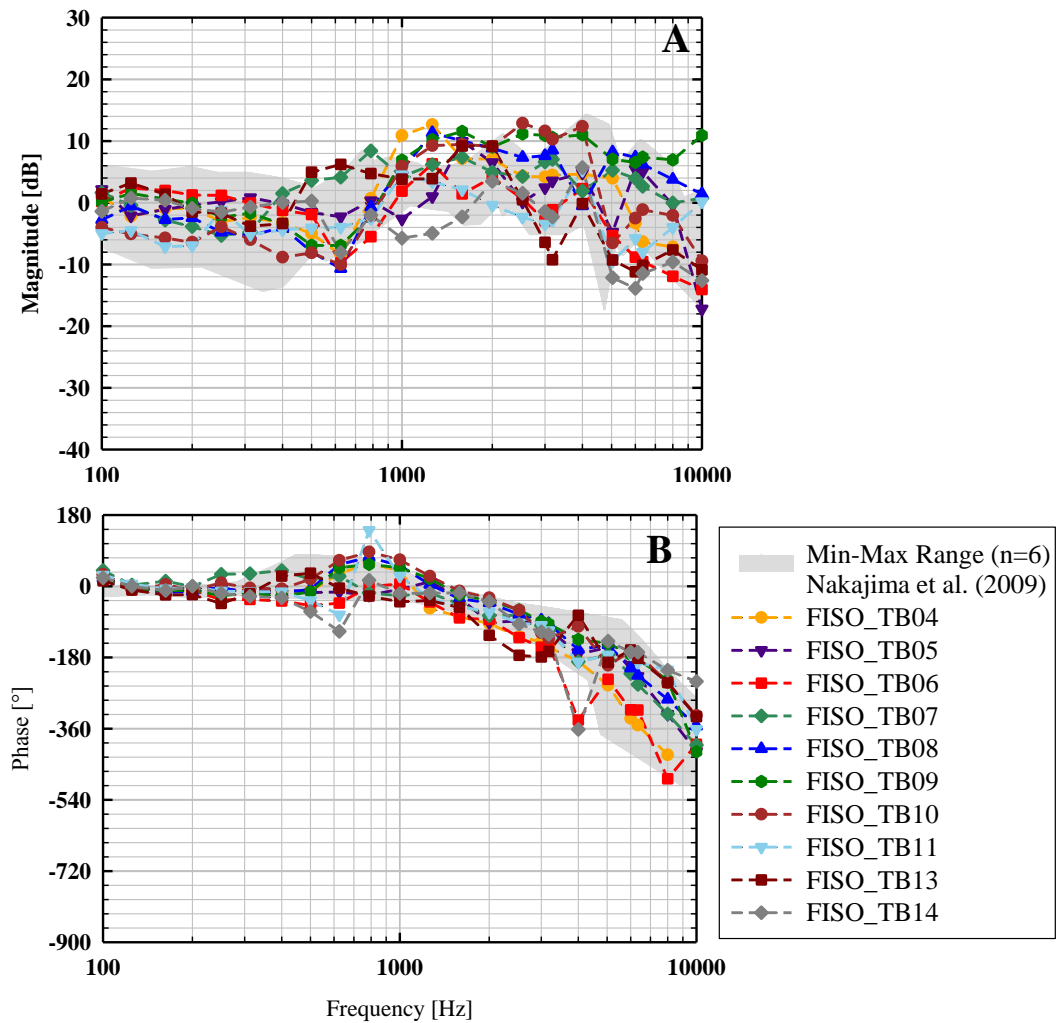
Figure 4.11. Sound pressure p_{ST} (A: magnitudes, B: phases) measured with a FISO pressure sensor in scala tympani, normalized to the stapes velocity v_{stap}. For comparison the range of results obtained by STIEGER ET AL. [2013] with a custom made pressure sensor is given as grey shaded area. Data with an SNR $< 7\,\text{dB}$ were omitted. Lines connecting symbols are for visual guidance only.
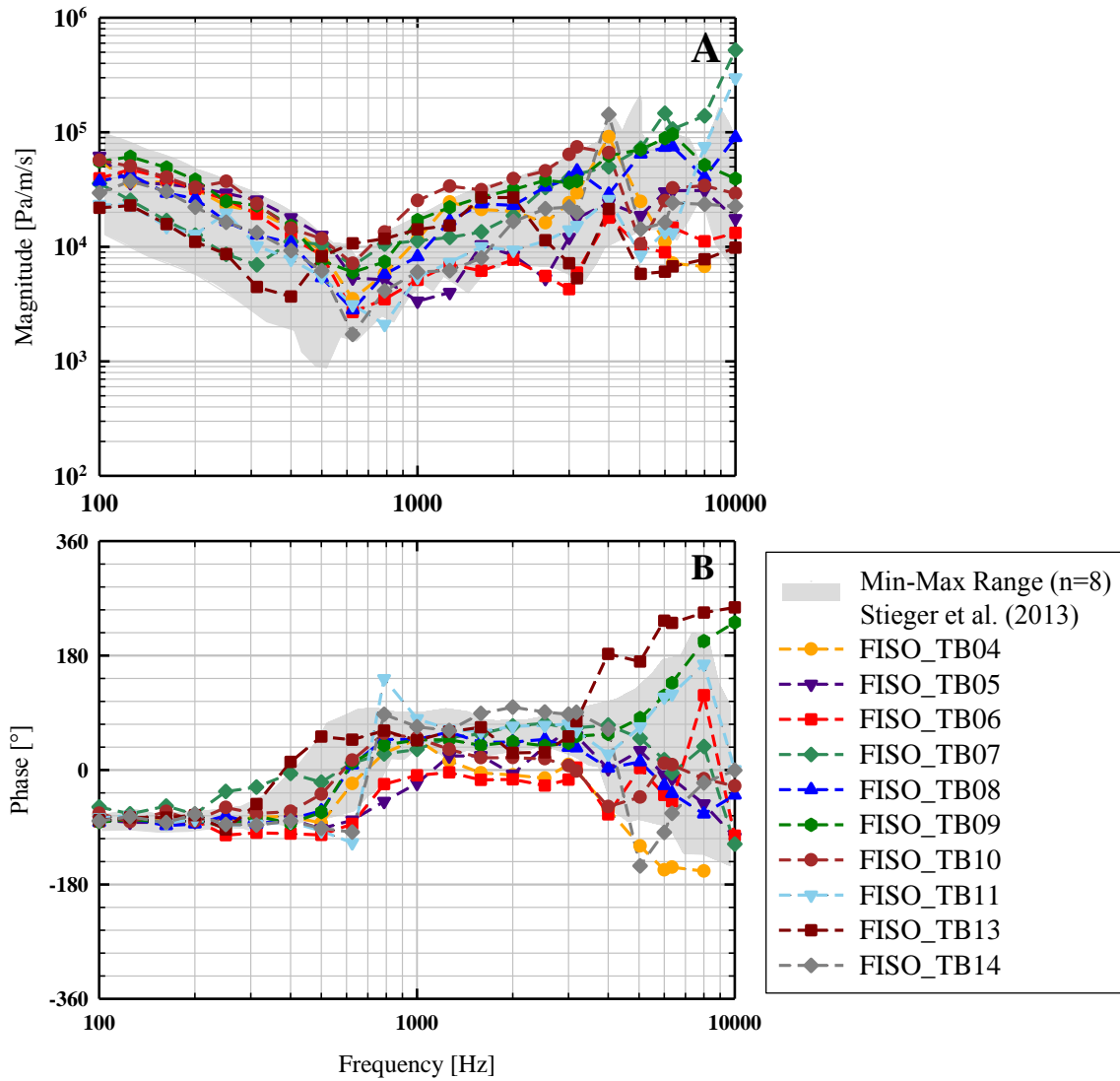
4.2.3   Intracochlear Sound Pressure Differences

Samba: The magnitudes and phases of the complex pressure differences Δp between SV and ST are plotted in Figure 4.12, normalized to the outer ear canal sound pressure p_T. The magnitudes were mainly similar across all TBs with differences $\leq 20\,\mathrm{dB}$ and comparable frequency characteristics. In Samba_TB16 the magnitudes showed a sharp notch at 2.525–3.175 kHz. The phases were also similar in all TBs showing a 1/8–2/3 cycle lead at frequencies below 1 kHz that decreased with increasing frequency to a lag of up to 1 1/3 cycle. Since in Samba_TB05 pressure differences were only measurable at $\leq 0.3125\,\mathrm{kHz}$ with magnitudes 20 dB lower than in the other experiments, it was assumed that the preparation in this TB failed and the TB was not further considered for the analysis. When normalized to the stapes velocity v_stap (Figure 4.13) the magnitudes of Δp had a interindividual variation of up to 21 dB, except in Samba_TB16 where a dip in magnitude at 2.525–3.175 kHz leads to a much larger deviation. The phases were at frequencies $\leq 1\,\mathrm{kHz}$ around $0°$ and varied between -180° and +180° at higher frequencies.

   FISO: The magnitudes and phases of the complex pressure differences Δp between SV and ST are plotted in Figure 4.14 normalized to p_T and in Figure 4.15 normalized to v_stap. In almost all TBs, $\Delta p/p_\mathrm{T}$ and $\Delta p/v_\mathrm{stap}$ magnitudes had the same frequency characteristic and the inter-individual differences were $\leq 20\,\mathrm{dB}$. Δp phases were also very similar across all experiments except in FISO_TB09 where a discrepancy of up to 180° was observed at approx. 0.3 to 3 kHz. $\Delta p/p_\mathrm{T}$ phases showed a 1/8–2/3 cycle lead at frequencies below 1 kHz that decreased with increasing frequency to a lag of up to 1 1/3 cycle. $\Delta p/v_\mathrm{stap}$ phases were around $0°$ at frequencies $\leq 2\,\mathrm{kHz}$ and varied between -180° and +180° at higher frequencies.

4.3   Discussion

4.3.1   Effect of Transducer Insertion on Stapes Vibration Responses

The minor changes in stapes vibration responses to sound (Figures 4.2B & 4.3B) indicate that the opening and re-closure of the cochlea by insertion of the pressure transducers has no pronounced effect on cochlear mechanics. This confirms the assumption that the inserted sensor membrane being much stiffer, has a much higher acoustic impedance than the round window membrane and does not lead to major changes in natural cochlea acoustics.

4.3.2   Sealing Techniques

No correlation between the sealing material used (dental impression material in Samba_TB05–07, silicone rubber plug in Samba_TB16, 18, 19, silicone tube and alginate in all FISO_TBs) and the magnitude of p_SV, p_SV and Δp (Figures 4.4–4.15) was detectable. Since the silicone rubber plug and the silicone tube were easier to use than alginate alone and they were reusable in several experiments when once applied to the transducer, both techniques appeared to be more advantageous. The silicone tube had the additional advantage of
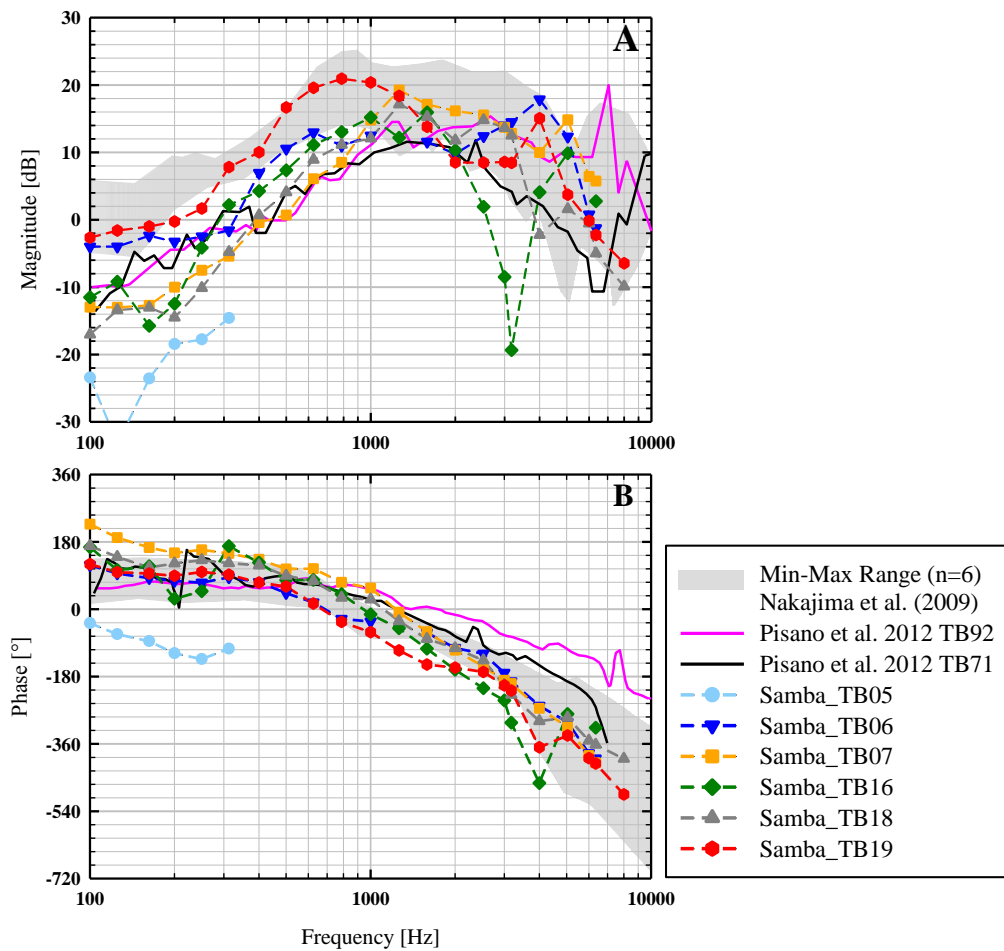
Figure 4.12. Pressure differences Δp measured with the Samba system, normalized to the ear canal sound pressure level p_T. For comparison the range of results ([NAKAJIMA ET AL., 2009], grey shaded area) and two exemplary measurements ([PISANO ET AL., 2012], solid lines) obtained with a custom made pressure sensor are given. Data with an SNR < 7 dB were omitted. Lines connecting symbols are for visual guidance only. Modified from GROSSÖHMICHEN ET AL. [2016b] (CC BY 4.0).

Figure 4.13. Pressure differences Δp measured with the Samba system, normalized to the stapes velocity v_{stap}. For comparison the range of results obtained with a custom made pressure sensor by STIEGER ET AL. [2013] are given. Data with an SNR < 7 dB were omitted. Lines connecting symbols are for visual guidance only. Modified from GROSSÖHMICHEN ET AL. [2016b] (CC BY 4.0).
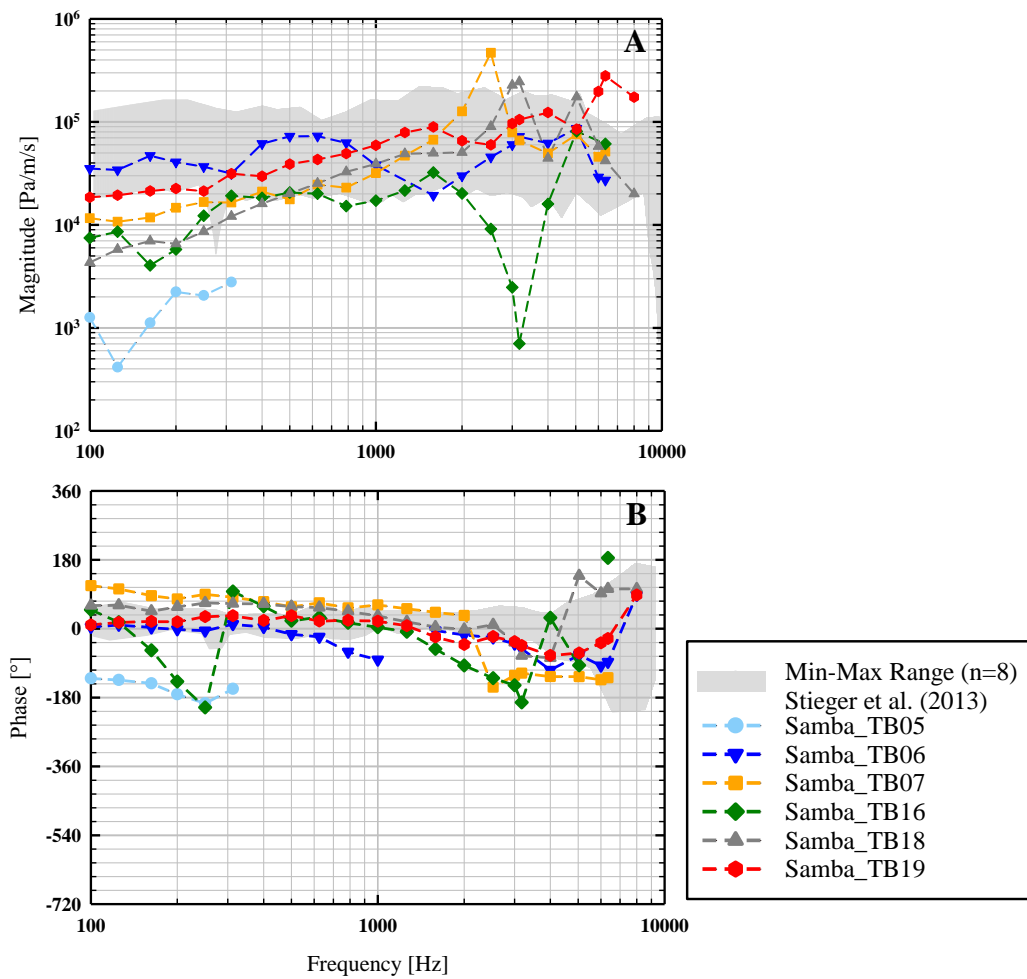
a smaller diameter than the rubber plug allowing a better visual access to the cochleostomy during transducer insertion.

4.3.3 Comparison to Previous Work with Custom-made Pressure Sensors

To assess the results obtained here with off-the-shelf pressure transducer systems, magnitudes and phases of p_{SV}/p_T, p_{SV}/p_T, p_{SV}/v_{stap}, p_{SV}/v_{stap}, $\Delta p/v_{stap}$ and $\Delta p/p_T$ were compared to results obtained in earlier studies [NAKAJIMA ET AL., 2009; PISANO ET AL., 2012; STIEGER ET AL., 2013] with custom-made sensors developed by OLSON [1998] (Figure 4.4–4.15). Results from these studies were used for comparison because this sensor type has proven to provide reliable results in the past.

In consideration of nonlinear effects on the normalized intracochlear pressure magnitudes, the range of acoustical stimulation levels has to be taken into account. In the current study sounds were presented at 105–130 dB SPL (Samba) and 80–120 dB SPL (FISO), whereas in STIEGER ET AL. [2013] stimulation levels between 50–115 dB SPL and in NAKAJIMA ET AL. [2009] levels between 70–130 dB SPL were used. In PISANO ET AL. [2012] no information about the stimulation level was provided, but it was referred to NAKAJIMA ET AL. [2009]. It is known that the vibration response of the stapes in human cadaveric TBs is linear with the level of acoustic stimulation up to 124 dB SPL at 0.4–6 kHz [GOODE ET AL., 1994] and up to 130 dB SPL at 0.1–4 kHz [VOSS ET AL., 2000]. Therefore it can be assumed that the normalized intracochlear pressures and pressure differences measured by NAKAJIMA ET AL. [2009]; PISANO ET AL. [2012]; STIEGER ET AL. [2013] and in the present study are not subject to significant middle ear non-linearities although the stimulation levels were higher in the present experiments. This assumption is supported by the result of a control measurement performed in one Samba experiment where the tympanic membrane was stimulated acoustically first with sound pressure levels of 110–130 dB SPL and second with levels of 90–120 dB SPL. When normalized to p_T the magnitudes of p_{SV} and p_{ST} were similar within 3 dB except at 3.175 kHz where a decrease in p_{ST} by 12 dB was found for the lower simulation level.

Samba: The obtained p_{SV}/p_T and p_{SV}/v_{stap} magnitudes were mostly within the minimum-maximum range of STIEGER ET AL. [2013] and NAKAJIMA ET AL. [2009] (Figures 4.4A & 4.6A). At frequencies ≥ 2 kHz the here obtained p_{SV}/p_T and p_{SV}/v_{stap} magnitudes (Figures 4.5A & 4.7A) were also mostly comparable to these studies but differed up to approx. 20 dB at lower frequencies. Therefore the measured p_{SV} magnitudes partially did not match the characteristic patterns from STIEGER ET AL. [2013] and NAKAJIMA ET AL. [2009], e.g. the dip in p_{SV}/v_{stap} magnitudes around 0.6 kHz. One possible reason for this could be an imperfect sealing between the samba pressure transducer in SV and the surrounding bone.

In the experiments Samba_TB06, Samba_TB07 and Samba_TB16, the magnitudes of p_{SV} and p_{SV} dropped at frequencies ≥ 8 kHz below 7 dB SNR so that these data points were not used for analysis and omitted in all figures. In these measurements the acoustic stimulation level at the tympanic membrane dropped down to 70–90 dB SPL and was therefore below the theoretical resolution limit of the Samba system at ≥ 7 kHz of 95 dB SPL input at the

tympanic membrane (see section 2.5).

The phases of p_{SV}/p_T (Figure 4.4B) and p_{SV}/p_T (Figure 4.5B) were mostly within the range of NAKAJIMA ET AL. [2009]. Only at frequencies $> 4\,\text{kHz}$ the p_{SV}/p_T phases obtained here differed significantly showing an up 360°longer delay. One possible reason for this could be a different unwrapping procedure. p_{SV}/v_{stap} and p_{SV}/v_{stap} phases (Figures 4.6B & 4.7B) were comparable to STIEGER ET AL. [2013] only at frequencies $\leq 1\,\text{kHz}$ and $0.5\,\text{kHz}$, respectively. A 180°shift in p_{SV}/v_{stap} phases around approx. $0.6\,\text{kHz}$ determined by STIEGER ET AL. [2013] was not observable here. One potential reason for this low similarity to STIEGER ET AL. [2013] could be that in their study the vibration response of the stapes was measured at the posterior crus whereas in the Samba experiments performed here it was measured at the SFP leading to a different impact of rocking motions.

When normalized to p_T (Figure 4.12A), the magnitude of the ICPD Δp had a similar frequency characteristic as in NAKAJIMA ET AL. [2009] and covered the same minimum-maximum range at frequencies $\geq 1\,\text{kHz}$. At lower frequencies the here obtained results were up to $16\,\text{dB}$ less. As mentioned before a possible reason for this discrepancy at low frequencies might have been an imperfect sealing between pressure transducer and bone in the present experiments. However, the $\Delta p/p_T$ magnitudes obtained here with the Samba sensors were comparable in the entire frequency range to two exemplary measurements of a later study [PISANO ET AL., 2012] performed by the same researchers (Figure 4.12A). This variance demonstrates that more reference data of ICPD measurements is needed for a reliable database. All phases of $\Delta p/p_T$ obtained here were similar to NAKAJIMA ET AL. [2009]. When normalized to stapes velocity v_{stap}, almost all magnitudes of Δp were within the minimum-maximum range of STIEGER ET AL. [2013], except at frequencies $< 0.3\,\text{kHz}$ where the magnitudes in the Samba experiments were maximally $15\,\text{dB}$ less (Figure 4.13A). Almost all $\Delta p/v_{stap}$ phases obtained here were within the range of STIEGER ET AL. [2013]. Only Samba_TB07 and Samba_TB16 showed at approx. $0.25\,\text{kHz}$ (Samba_TB16) and $3\,\text{kHz}$ (Samba_TB07 and Samba_TB16) a difference of 1/2 cycle lag.

Between 2.525 and $3.175\,\text{kHz}$ where the magnitudes of $\Delta p/p_T$ (Figure 4.12A) and $\Delta p/v_{stap}$ (Figure 4.13A) decreased extraordinarily in Samba_TB16, the absolute values of p_{SV} and p_{SV} were close in magnitude and phase in this experiment. Usually this might be an indication for placement of both pressure transducers accidentally into the same scala. However, in this experiment the differential intracochlear pressure at all other frequencies was normal and a failure of preparation could be excluded based on the visual inspection during dissection. Hence, no explanation was found for this decrease in pressure difference in Samba_TB16.

FISO: When normalized to ear canal sound pressure p_T and stapes velocity v_{stap}, the magnitudes and phases of p_{SV} and p_{SV} measured with the FISO system were mostly consistent with the results from STIEGER ET AL. [2013] and NAKAJIMA ET AL. [2009] (Figure 4.8 – 4.11) and showed similar frequency characteristics. Only in FISO_TB09 p_{SV}/p_T and p_{SV}/v_{stap} magnitudes and phases differed significantly at frequencies $< 1\,\text{kHz}$ (Figures 4.8 & 4.10). When normalized to p_T, most p_{SV} magnitudes (Figure 4.8A) were within the minimum-maximum range of NAKAJIMA ET AL. [2009], except for frequencies between 0.3 and $0.5\,\text{kHz}$. At all investigated frequencies, p_{SV}/v_{stap} magnitudes were largely inside the range reported by STIEGER ET AL. (Figure 4.10A). All p_{SV} magnitudes were at all frequen-

cies consistent with both aforementioned studies (Figure 4.9A and Figure 4.11A). In the entire investigated frequency range, almost all phases of p_{SV} and p_{SV} were inside the ranges of NAKAJIMA ET AL. [2009] and STIEGER ET AL. [2013] (Figure 4.8–4.11B). The characteristic pattern of p_{SV}/v_{stap} magnitudes and phases including a dip in magnitude and a $180°$ phase shift around approx. $0.6\,\text{kHz}$ reported by STIEGER ET AL. [2013] was also found here.

When normalized to stapes velocity v_{stap}, all magnitudes and phases of Δp were mostly within the minimum-maximum ranges reported by STIEGER ET AL. [2013] (Figure 4.15), except experiment FISO_TB09 showing an extraordinary lead in phase of up to $180°$ between 0.3 and $3\,\text{kHz}$. Most $\Delta p/p_T$ magnitudes (Figure 4.14A) were consistent to NAKA-JIMA ET AL. [2009] at frequencies above $4\,\text{kHz}$ and below $0.2\,\text{kHz}$. From 1 to $4\,\text{kHz}$ around half of the magnitudes were approx. $10\,\text{dB}$ less than in NAKAJIMA ET AL. [2009], whereas at 0.2 to $1\,\text{kHz}$ most magnitudes were up to $10\,\text{dB}$ outside this range. However, in this frequency range $\Delta p/p_T$ magnitudes were comparable to two exemplary measurements of a later study [PISANO ET AL., 2012] performed by the same researchers. All $\Delta p/p_T$ phases were inside the range of NAKAJIMA ET AL. [2009], except in experiment FISO_TB09 where an extraordinary lead in phase of up to $180°$ was present between 0.3 and $3\,\text{kHz}$ (Figure 4.14B).

4.3.4 Comparison between both Pressure Measurement Systems

Both, the Samba Preclin pressure measurement system and the FISO pressure measurement system were easy to handle and worked reliably. The FISO transducer has a 26% smaller diameter than the Samba transducer and therefore it required less space in the middle ear cavity and a smaller cochleostomy. The pressure sensitive and fragile front membrane of the FISO pressure transducer is protected by a polyimide tubing filled with gel whereas the tip of the Samba transducer is unprotected. One could assume that the Samba transducer is therefore much more fragile. However, in the present studies both transducer types showed a strong robustness as only one Samba transducer and none of the FISO transducers was destroyed. Although the SPL input and the number of averages was higher in the Samba experiments (Samba: 105–130 dB SPL, 1000 averages; FISO: 80–120 dB SPL, mostly 30 averages), signals recorded with the FISO system had higher SNRs of 20 to 60 dB compared to the Samba system with SNRs of 7 to 60 dB. Moreover intracochlear sound pressures were measurable with the FISO system in both scalae over the entire frequency range of 0.1–10 kHz whereas measurements with the Samba system were successful only at 0.1–8 kHz. Most important, however, is that the results obtained with the FISO system matched the results from NAKAJIMA ET AL. [2009] and STIEGER ET AL. [2013] much better than the results obtained with the Samba system. In summary it can be said that with both tested systems ICPDs are measurable in human cochlear TBs but the FISO system is even better suited for this purpose.

4.4 Summary and Conclusion

Using the Samba system, pressures in both scalae could be obtained at frequencies of 0.1–8 kHz. At 10 kHz pressures were measurable in one single experiment in SV only. Normalized p_{SV} magnitudes and phases were in good accordance with results obtained in earlier
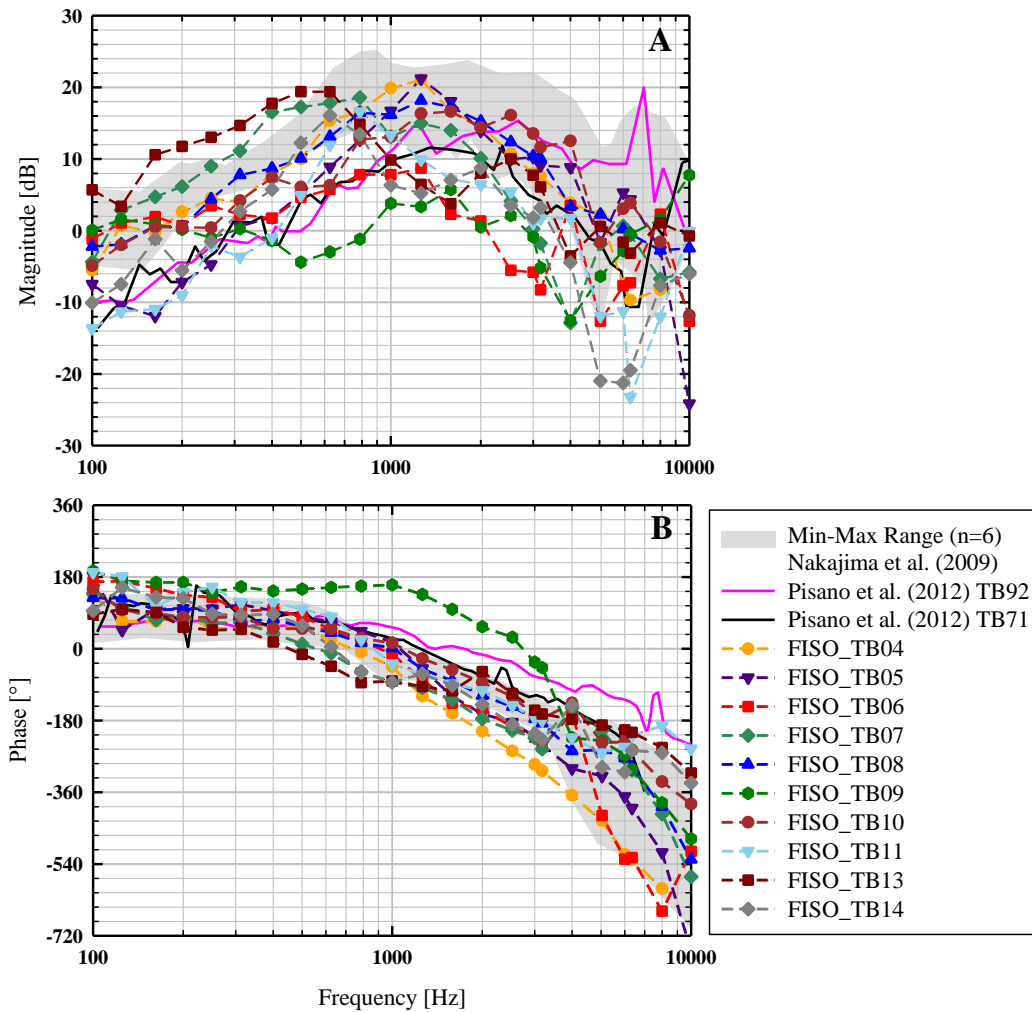
Figure 4.14. Pressure differences Δp measured with the FISO system, normalized to the ear canal sound pressure level p_T. For comparison the range of results ([NAKAJIMA ET AL., 2009], grey shaded area) and two exemplary measurements ([PISANO ET AL., 2012], solid lines) obtained with a custom made pressure sensor are given. Data with an SNR < 7 dB were omitted. Lines connecting symbols are for visual guidance only. Modified from GROSSÖHMICHEN ET AL. [2017] (CC BY 4.0).
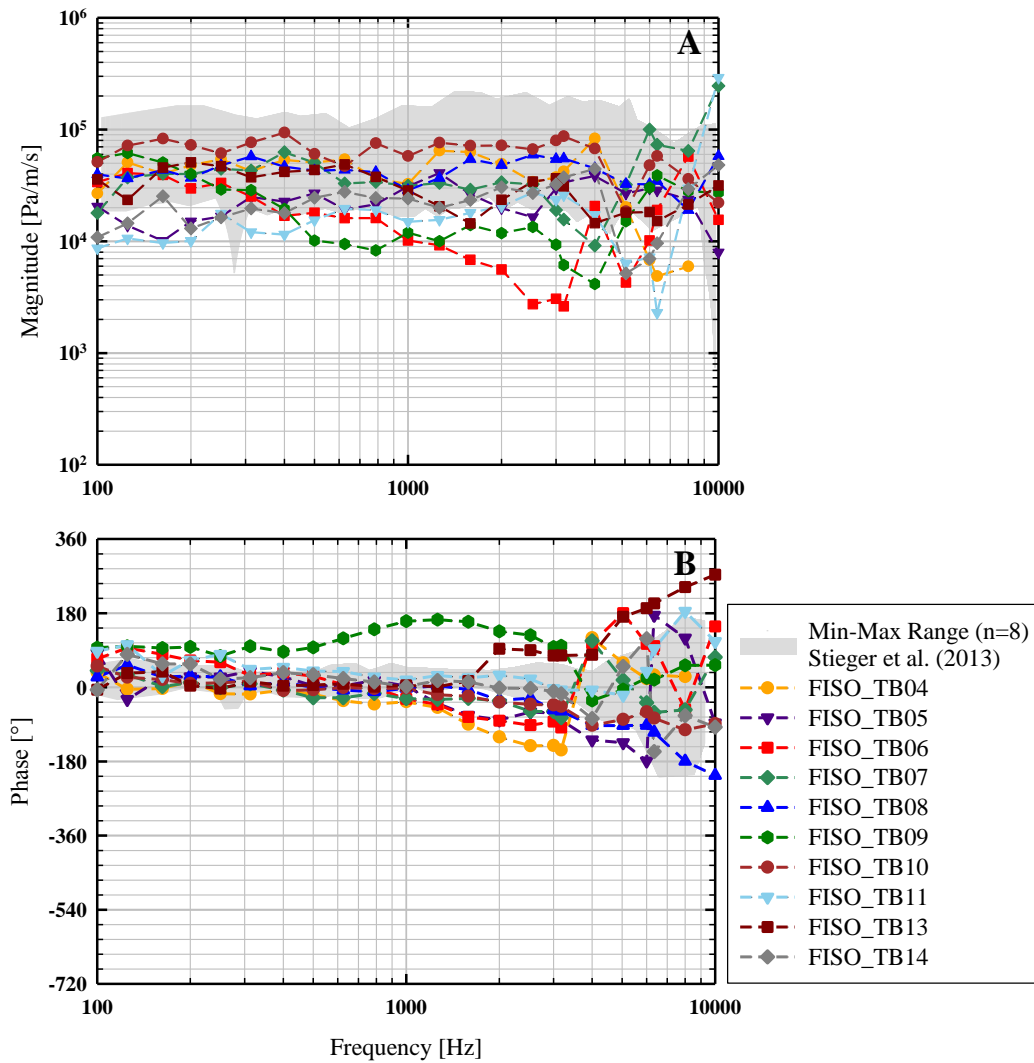
Figure 4.15. Pressure differences Δp measured with the FISO system, normalized to the stapes velocity v_{stap}. For comparison the range of results obtained with a custom made pressure sensor by STIEGER ET AL. [2013] are given. Data with an SNR $< 7\,\text{dB}$ were omitted. Lines connecting symbols are for visual guidance only.

studies with custom-made sensors, whereas normalized p_{SV} magnitudes and phases differed significantly from these studies. However, ICPDs obtained with the Samba systems were at frequencies of 1–8 kHz comparable to these studies, but differed up to 16 dB at lower frequencies. Using the FISO Veloce system, sound pressures could be obtained in both scalae over the entire investigated frequency range of 0.1–10 kHz. Magnitudes and phases of the normalized sound pressures in SV and ST and of the intracochlear pressure differences were mostly comparable with results from the reference studies. Based on these findings, both off-the-shelf pressure measurement systems the Samba Preclin system and the FISO Veloce system, are usable for ICPD measurements in human cadaveric TBs with sufficient SNR. However, the FISO Veloce system is preferable because it covers frequencies up to 10 kHz with higher SNRs and the transducer insertion requires less space. Additionally it could be shown that the insertion of the pressure transducers had only a minor effect of ≤ 5 dB at 0.1–3 kHz and ≤ 7 dB at 3–10 kHz on the stapes vibration response to sound (middle ear transfer function H_{TV}).

Chapter 5

Validating Output Level Predictions from Measurements in Human Cadaveric Ears[1]

As already mentioned before, ICPD measured in a human cadaveric TB has never been used to quantify output levels of an AMEI or DACI in forward direction. Furthermore it has never been proven that output levels predicted from stapes vibration measurements in TBs according to ASTM F2504–05 actually match the real outputs in patients. Therefore the aim of the experiments in this chapter was twofold. First, to test if the procedure predicting clinical equivalent actuator output of an AMEI from cadaver experiments according to ASTM F2504–05 is valid. Second, to validate that ICPD can be used to predict the output level of an AMEI from cadaver studies. For this purpose, AMEI equivalent actuator output levels (eq. dB SPL) in cadaveric ears determined from stapes vibration amplitudes and from ICPD amplitudes were directly compared to equivalent actuator output levels obtained for the same actuator type and stimulation mode from clinical data.

5.1   Materials and Methods

The equivalent sound pressure level (eq. SPL) produced by an AMEI actuator (T2 transducer, Cochlear™ Ltd.) stimulating the incus body was quantified in human cadaveric TBs using both stapes motion and ICPD as a reference. This stimulation mode was chosen because it is within the scope of ASTM F2504-05 [ASTM, 2005] and stapes vibration measurement should provide valid output level predictions in this application (see section 1.4.5). For validation purposes, results from cadaveric ears were compared with T2 actuator output levels for the same actuator type and stimulation mode from clinical data.

The actuator stimulations were performed after the acoustic stimulation (step (5)) in the TBs of the "FISO experiments" described in the previous chapter (section 4.1.4). The experimental setup, the methods of LDV and ICPD measurement and the signal generation and acquisition were therefore, of course, mainly identical to the previous chapter and are not re-

---

[1]Parts of this chapter have been published in GROSSÖHMICHEN ET AL. [2017].
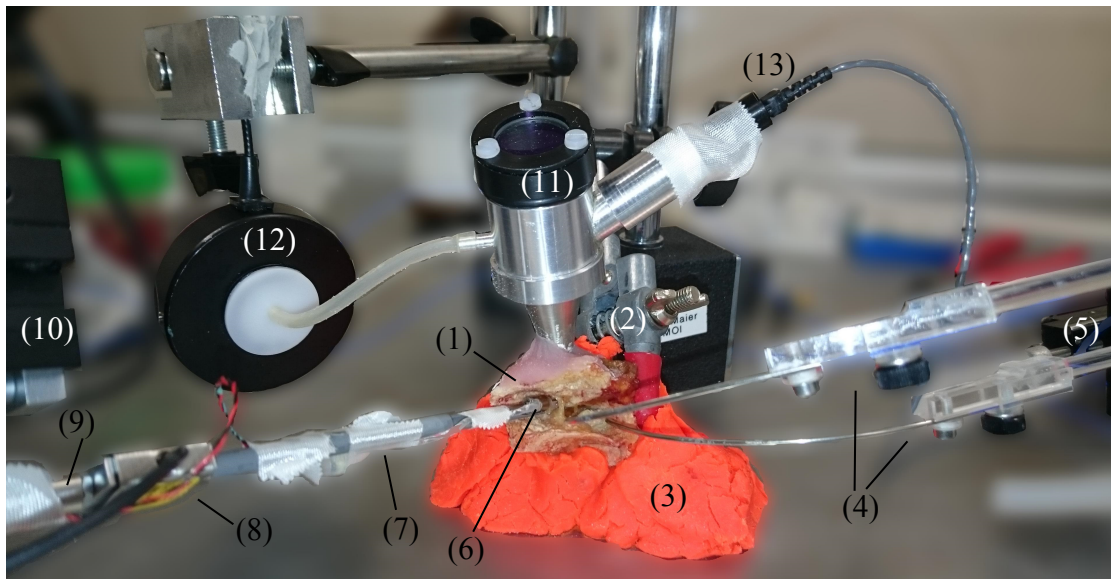
Figure 5.1. Setup for the ICPD and LDV measurements during actuator stimulation. The TB (1) is hold by a clamp (2) and embedded in modeling compound (3) (Play-Doh, HASBRO, Germany) to dampen unwanted vibrations of the TB. Each pressure sensor is mounted to a custom made holder (4) attached to a 3-axis micromanipulator (5) (MM3-3, World Precision Instruments, Germany, only partially visible). The T2 actuator (6) is glued to a rod (7) mounted to the LSB200 force sensor (8). The force sensor is screwed on a rod (9) attached to a 3-axis micromanipulator (10) (M3301, World Precision Instruments, Germany, only partially visible). The sound application setup (11) for the acoustic stimulation comprising a DT48 loudspeaker (12) and a ER-7C microphone (13) is cemented in the ear canal.

peated here. Furthermore the stapes vibration and the ICPDs measured in response to sound in the previous chapter served in the present chapter as references to determine the actuator output levels.

5.1.1   Experimental Setup

A T2 actuator (Cochlear™ Ltd.) as used in the Cochlear™ MET® system or in the Cochlear™ Carina® system was mounted to the actuator stimulation setup with force measurement described in section 2.3. This assembly was positioned on the vibration isolated table (LW3048B, Newport) where the micromanipulators with the pressure sensors and the TB preparation were already placed as described in the previous chapter.

5.1.2   Actuator Stimulation

After completing the acoustic stimulation (step (5) in section 4.1.4) a hole of approx. 0.6 mm diameter was made in the incus for attachment of the actuator using a surgical laser (Iridis, Quantel Medical, France). The actuator stimulation was performed at several contact positions of the actuator. To define a zero position, the T2 actuator was advanced towards the laser hole until the tip of the actuator almost touched the incus and the recording of the force sensor was zeroed. From this position, the actuator was advanced in steps of 20 μm towards
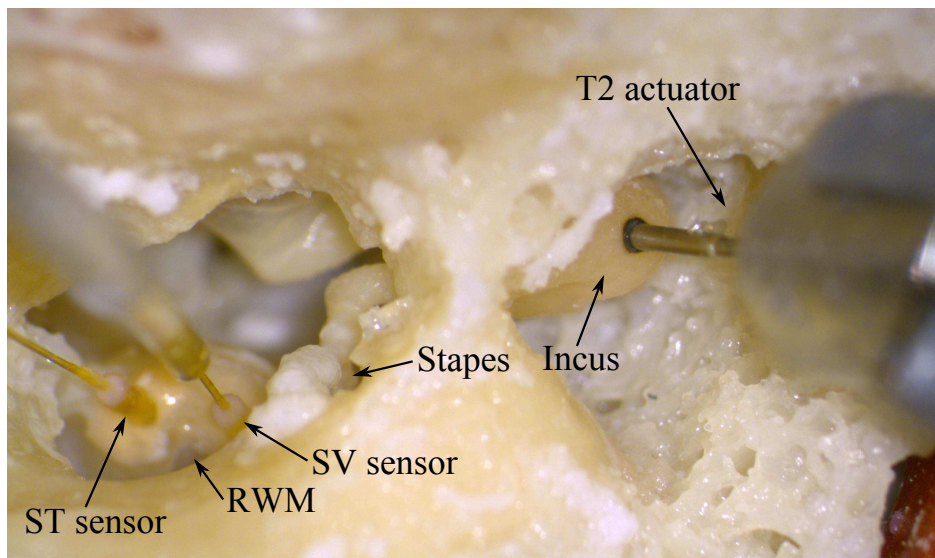
Figure 5.2. Temporal bone preparation for the incus stimulation. The tip of the T2 actuator was attached to the incus body and the FISO FOP-M260 transducers were inserted in scala vestibuli (SV) and scala tympani (ST) next to the round window membrane (RWM). Taken from GROSSÖHMICHEN ET AL. [2017] (CC BY 4.0).

the incus body (Figure 5.2). At each position, the displayed force level was recorded and actuator stimulation and measurements were performed as follows. The actuator was electrically driven with the same sequence of sine wave signals previously used for the acoustic stimulation (see section 4.1.4), having amplitudes of approx. -8 dB re 1 V_{rms} at each stimulation frequency. Sound pressures p_{SV} and p_{ST} and vibration of the stapes were measured sequentially as described in the previous chapter (section 4.1.4). Again amplitude and phase of the input signal had minor differences during both measurements (maximum difference: 0.07 dB, 0.54°) and measurement results were re-normalized to the same input.

From each experiment a set of measurement data at different positions and force levels was available. For the analysis, the measurement data from two specific forces / positions were selected (see section 5.1.3 for details): (1) The position where the contact force between actuator and incus was closest to 4 mN and (2) the position where the actuator was advanced additional 60 µm from position 1 (hereinafter referred to as positions "4 mN" and "4 mN + 60 µm"). On average, the contact force was 3.6 ± 2.6 mN in position "4 mN" and 40.0 ± 11.0 mN in position "4 mN + 60 µm" (mean ± standard deviation, N = 10). After completing all measurements, the pressure transducers were removed and the correct positioning of the cochleostomies in SV and ST and the integrity of the basilar membrane were confirmed visually by dissection of the TB.

5.1.3 Choosing the Contact Force and Position of the Actuator in TB Experiments

Actuator positions "4 mN" and "4 mN + 60 µm" were chosen for analysis based on bench tests using the Carina® transducer loading assistant (transducer loading assistant (TLA),
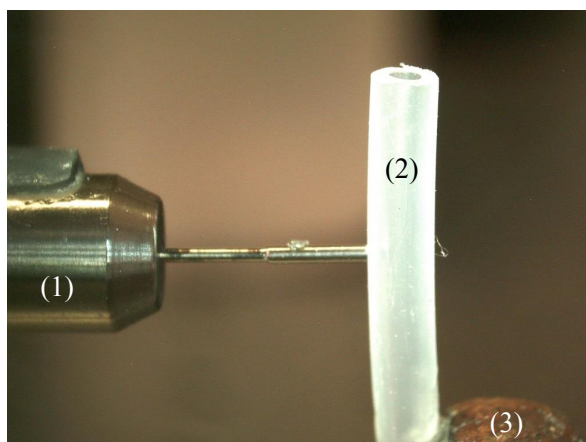
Figure 5.3. Setup for the bench test. The tip of a T2 actuator (1) was moved towards a flexible plastic element (2) mounted to a holder (3).

Cochlear™ Ltd.). Intraoperatively, the TLA is used to guide adjustment of the T2 actuator to the incus body by measuring its electrical impedance at the resonance frequency while the actuator is advanced [COCHLEAR, 2014]. According to the surgical manual [COCHLEAR, 2014] a decrease in impedance of $\geq 50\,\Omega$ indicates initial contact and then the actuator shall be advanced $62.5\,\mu m$ (1/4 turn of the micro-adjustment) to the final position. In the bench test the actuator was mounted to the force sensor and micromanipulator as in the TB experiments and moved towards a flexible plastic element in steps of $20\,\mu m$ (Figure 5.3) while the TLA screen was observed. In six tests the drop in impedance (initial contact) occurred between 1 and 7 mN ($3.4 \pm 2.6\,mN$, mean $\pm$ standard deviation). Therefore that position where the contact force was closest to 4 mN was selected from from the data set of each TB experiment. To mimic the assumed final position of the loading procedure with the TLA (1/4 turn of the micro-adjustment after indication of the TLA), from each TB experiment also that position was selected where the actuator was moved $60\,\mu m$ towards the incus from the "4 mN" position.

5.1.4 Signal Generation and Acquisition

As during acoustic stimulation (previous chapter), signals were generated and acquired with the custom built LabVIEW™ program controlling two 24 bit, 4-channel data acquisition modules (NI USB-4431, National Instruments, Germany) and the electric input signals to the actuator buffered by a power amplifier (SA1, Tucker-Davis Technologies, USA). Electric output signals from LDV and FISO pressure measurement system were acquired as averaged complex spectra using 800 FFT lines between 0 and 10 kHz with 12.5 Hz resolution. During measurement the SNR of the intracochlear pressure and vibratory responses at each stimulation frequency was calculated in LabVIEW™ as described in section 2.7. Measurements were averaged until an SNR of ≥ 12 dB was reached, but minimally 30 times and maximally 1000 times. In a great majority of measurements an SNR of 20 to 60 dB was already reached with 30 averages and averaging more than 30 times was necessary in a few cases only. Responses with SNR < 12 dB (after 1000 averages) were not considered for

analysis.

5.1.5 Equivalent Sound Pressure Level Calculation

Equivalent SPLs were calculated from stapes motion according to ASTM F2504–05 as described in section 3.1.5 for an hypothetical electrical actuator input of $E_{\max} = 1\,\mathrm{V_{rms}}$. Equivalent SPLs were calculated from ICPD in a similar way. First, the equivalent ear canal sound pressure transfer function H_{ET} was calculated by comparing the sound-induced ICPD (Δp_{U}) with the ICPD (Δp_{A}) generated by the actuator:

$$H_{\mathrm{ET}} = \frac{\Delta p_{\mathrm{A}}}{E} \cdot \frac{p_{\mathrm{T}}}{\Delta p_{\mathrm{U}}}, \tag{5.1}$$

with E being the actuator input voltage and p_{T} the ear canal sound pressure at the tympanic membrane during acoustic stimulation. With an hypothetical electrical actuator input of $E_{\max} = 1\,\mathrm{V_{rms}}$, the maximum eq. ear canal SPL $L_{E\max}$ was then calculated as

$$L_{E\max} = 20\log_{10}\left(E_{\max} \cdot H_{\mathrm{ET}} \big/ \left(2 \cdot 10^{-5}\,\mathrm{Pa}\right)\right). \tag{5.2}$$

To make the results comparable to clinically obtained data all equivalent ear canal SPLs [eq. dB $\mathrm{SPL_{TM}}$] calculated from stapes vibration and from ICPD were converted to eq. free field SPLs L_{FF} [eq. dB $\mathrm{SPL_{FF}}$] by

$$L_{\mathrm{FF}} = L_{E\max} - T_{\mathrm{D}}, \tag{5.3}$$

with T_{D} [dB] being a frequency-specific sound pressure transformation value given in tables I to III in SHAW & VAILLANCOURT [1985]. At frequencies where no transformation value T_{D} was given, T_{D} was estimated by a linear interpolation between the given transformation values at the adjacent frequency above and below.

5.1.6 Clinical Data Collection

In clinical routine at the department of Otorhinolaryngology of the Hannover Medical School, bone conduction (BC) thresholds were measured in 24 recipients of a MET® middle ear implant system coupled to the incus at audiometric frequencies between 0.25 and 6 kHz using conventional equipment. "Direct thresholds" for stimulation via the Cochlear™ MET® middle ear implant system were measured in the same patients using the Cochlear™ Button® audio processor as a signal generator, via the Cochlear™ Carina® fitting Softwars. Using the fitting software psychophysical pure tone thresholds can be determined that are displayed in units of "dB MET", which can be converted to Volts electrical input [JENKINS ET AL., 2007]. It was assumed that the loudness perception at BC threshold and at direct threshold is the same. If a recipient has b dB HL BC threshold and a dB MET direct threshold at the same frequency, b was converted to b' [dB $\mathrm{SPL_{FF}}$] using ANSI S3.6-2004 [ANSI, 2004] Table 9, and a to a' [dB V] using information from JENKINS ET AL. [2007]. Actuator output L_{E} [eq. dB $\mathrm{SPL_{FF}}$] at $1\,\mathrm{V_{rms}}$ input voltage was then calculated as:

$$L_{\mathrm{E}} = b' - a'. \tag{5.4}$$

In rare cases where the BC threshold was not measurable at a particular frequency and no indication for an air-bone-gap[2] was visible in preoperative results (air-bone-gap $\leq$ 10 dB), the postoperative corresponding BC threshold was estimated from the measured air conduction threshold.

5.2 Results

As described in the method section, experimentally determined actuator output [eq. dB SPL$_{FF}$] presented here is the free field sound pressure level needed to produce a stapes vibration amplitude or ICPD amplitude equal to that produced by the actuator stimulation. All clinically and experimentally determined actuator output levels presented here were normalized to a hypothetical actuator input voltage of 1 V$_{rms}$. Actuator output levels determined experimentally are shown for an actuator position with a coupling force of approx. 4 mN ("4 mN static coupling force") and for a position where the actuator was moved additional 60 µm towards the incus ("4 mN + 60 µm"). The former corresponds to a static force level found experimentally for the trigger point of the suggested loading procedure with the TLA and the latter corresponds to the assumed final position of the loading procedure with the TLA as detailed in section 5.1.3.

5.2.1 Actuator Output in Cadaveric Ears Calculated from Stapes Motion

4 mN static coupling force: Based on stapes vibration amplitude, the actuator produced in the individual TBs eq. SPLs between 82 and 135 eq. dB SPL$_{FF}$ (Figure 5.4A). The results were normally distributed (Shapiro-Wilk test) at all frequencies except at 3.175 kHz (p = 0.030). The median output level was in the range of 100 to 122 eq. dB SPL$_{FF}$.

   4 mN + 60 µm: Actuator SPL output in individual TBs, calculated from stapes vibration amplitude, was mostly in the range of 95 to 140 eq. dB SPL$_{FF}$ (Figure 5.4B) with the exception of TB13 where it was 75 to 90 eq. dB SPL$_{FF}$ between 4 and 8 kHz. Actuator output level was normally distributed (Shapiro-Wilk test) at all frequencies except at 3.175 kHz (p = 0.008), 5.0375 kHz (p = 0.012), 6 kHz (p = 0.006) and 6.35 kHz (p = 0.015). The median output level was between 105 and 125 eq. dB SPL$_{FF}$.

5.2.2 Actuator Output in Cadaveric Ears Calculated from ICPD

4 mN static coupling force: At frequencies $\leq$ 2 kHz, the actuator output calculated from ICPD in the individual TBs was mostly in the range of 100 to 133 eq. dB SPL$_{FF}$ (Figure 5.5A). Only at some frequencies in TB5, TB07 and TB09, the output was lower. Above 2 kHz the individual results showed an increased inter-individual variability with outputs from 78 to 131 eq. dB SPL$_{FF}$. Responses in TB04 at 10 kHz and in TB09 at 0.125 and

---

[2]"The difference between the thresholds for hearing when the stimuli are delivered by air conduction and by bone conduction." [STEDMAN, 2005].

Figure 5.4. T2 actuator output (eq. dB SPL_FF) in TBs, calculated from stapes vibration amplitudes. Colored small symbols represent results from individual TBs, black large circles medians, and error bars 25 % and 75 % percentiles. A: Results obtained at approx. 4 mN static coupling force. B: Results obtained when the actuator was advanced 60 μm from position A. Lines connecting symbols are for visual guidance only. Modified from GROSSÖHMICHEN ET AL. [2017] (CC BY 4.0).

0.1625 kHz had an SNR $<$ 12 dB and were excluded from analysis. The results were normally distributed (Shapiro-Wilk test) at all frequencies except 0.1 kHz ($p = 0.017$) and 3 kHz ($p = 0.023$). The median output levels were in the range of 88 to 116 eq. dB SPL$_{FF}$.

4 mN + 60 μm: Based on ICPD, actuator output in individual TBs was 86 to 133 eq. dB SPL$_{FF}$ over the entire frequency range (Figure 5.5B). Responses in TB04 at 10 kHz, in TB09 at 0.1 to 0.1625 kHz and in TB13 at 8 kHz had an SNR $<$ 12 dB and were excluded from analysis. Outputs were normally distributed (Shapiro-Wilk test) at all frequencies except at 0.2 kHz ($p = 0.011$) and 0.12625 kHz ($p = 0.044$). The median output levels were in the range of 102 to 122 eq. dB SPL$_{FF}$.

5.2.3 Actuator Output determined from Clinical Data

Actuator output levels in individual patients were between 90 and 135 eq. dB SPL$_{FF}$ at 0.25 to 2 kHz and mainly between 80 and 120 eq. dB SPL$_{FF}$ at 3 to kHz (Figure 5.6). The median eq. SPLs were in the range of 90 to 120 eq. dB SPL$_{FF}$. The results were normally distributed (Shapiro-Wilk test) at all frequencies. Data points are missing at frequencies where the direct or bone conduction threshold was not or could not be measured.

5.2.4 Actuator Output in Cadaveric Ears: Stapes Vibration vs. ICPD

4 mN static coupling force: Median eq. SPLs calculated from stapes motion and ICPD were in good accordance with differences of $<$ 4 dB at frequencies below 2 kHz (except 7 dB at 0.125 kHz) and of 4 to 11 dB at higher frequencies (Figure 5.7A). The difference between the actuator outputs calculated from stapes motion and ICPD was statistically not significant (Wilcoxon Signed Rank Test), except at 0.625 kHz ($p = 0.049$), 0.7875 kHz ($p = 0.049$), 2.525 kHz ($p = 0.037$), 3 kHz ($p = 0.027$), 3.175 kHz ($p = 0.014$), 4 kHz ($p = 0.037$), 5.0375 kHz ($p = 0.049$), 6 kHz ($p = 0.006$) and 8 kHz ($p = 0.049$).

4 mN + 60 μm: Median eq. SPLs calculated from stapes motion and from ICPD were similar with differences of $<$ 4 dB at frequencies below 2 kHz and of 4 to 13 dB at higher frequencies (Figure 5.7B). At most frequencies the differences were statistically not significant (Wilcoxon Signed Rank Test), except at 2 kHz ($p = 0.027$), 3.175 kHz ($p = 0.049$) and 8 kHz ($p = 0.027$).

5.2.5 Actuator Output in Cadaveric Ears vs. Clinical Data

Actuator outputs measured in TBs and in patients were statistically compared at audiometric frequencies 0.25, 0.5, 1, 1.5, 2, 3, 4 and 6 kHz. For this purpose the actuator output levels in TBs at 1.5 kHz were estimated by a linear interpolation between the measured outputs levels at 1.2625 and 1.5875 kHz.

4 mN static coupling force: The median actuator outputs calculated from stapes vibration amplitudes in TBs were similar to the output in patients with differences of 1 to 6 dB at 0.25 to 2 kHz and of 8 to 9 dB at higher frequencies. The differences were statistically not significant (Mann-Whitney Rank Sum Test), except at 2 kHz ($p = 0.047$) and 4 kHz ($p = 0.027$). Median actuator output levels obtained in cadaveric TBs from ICPD and in patients

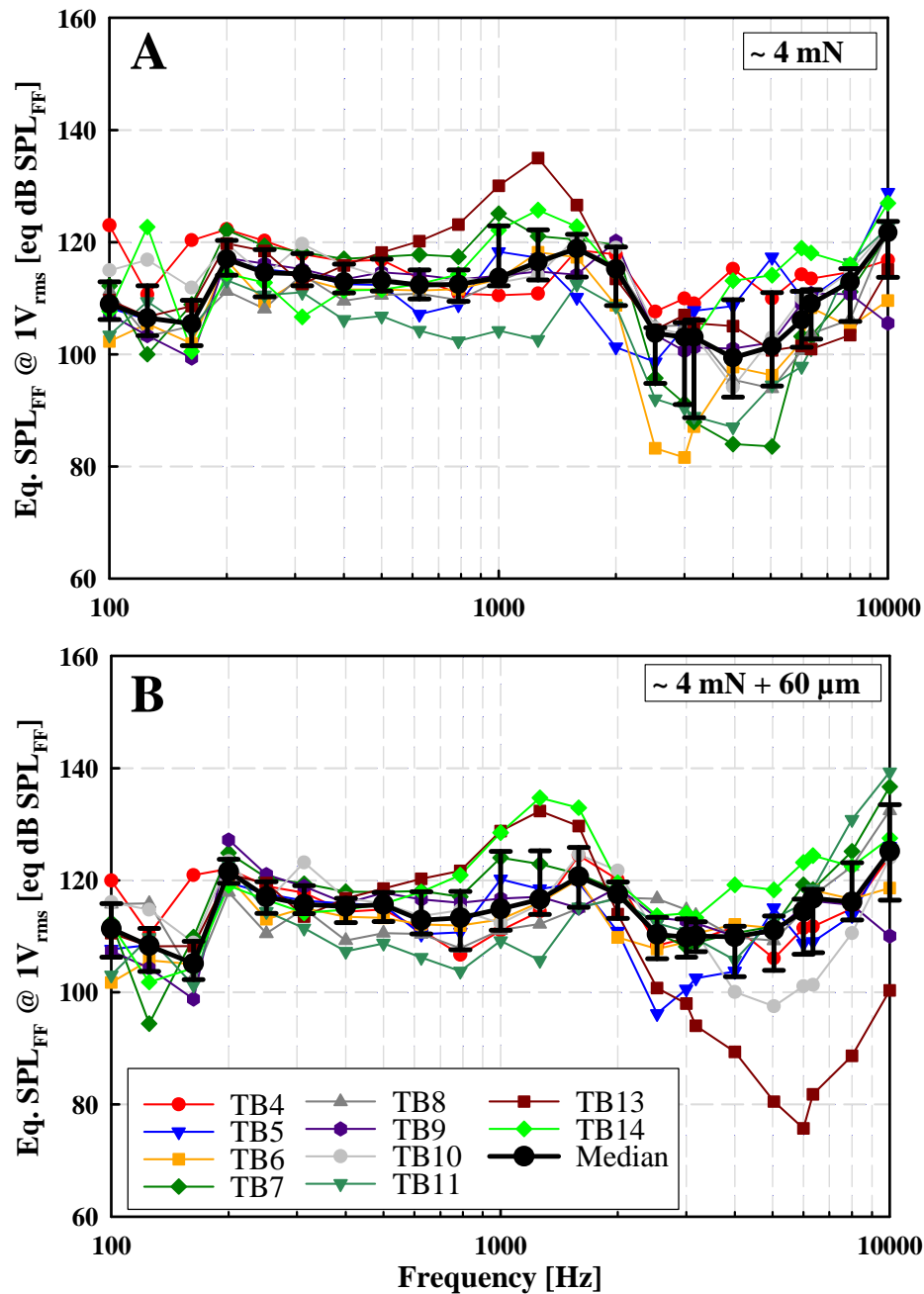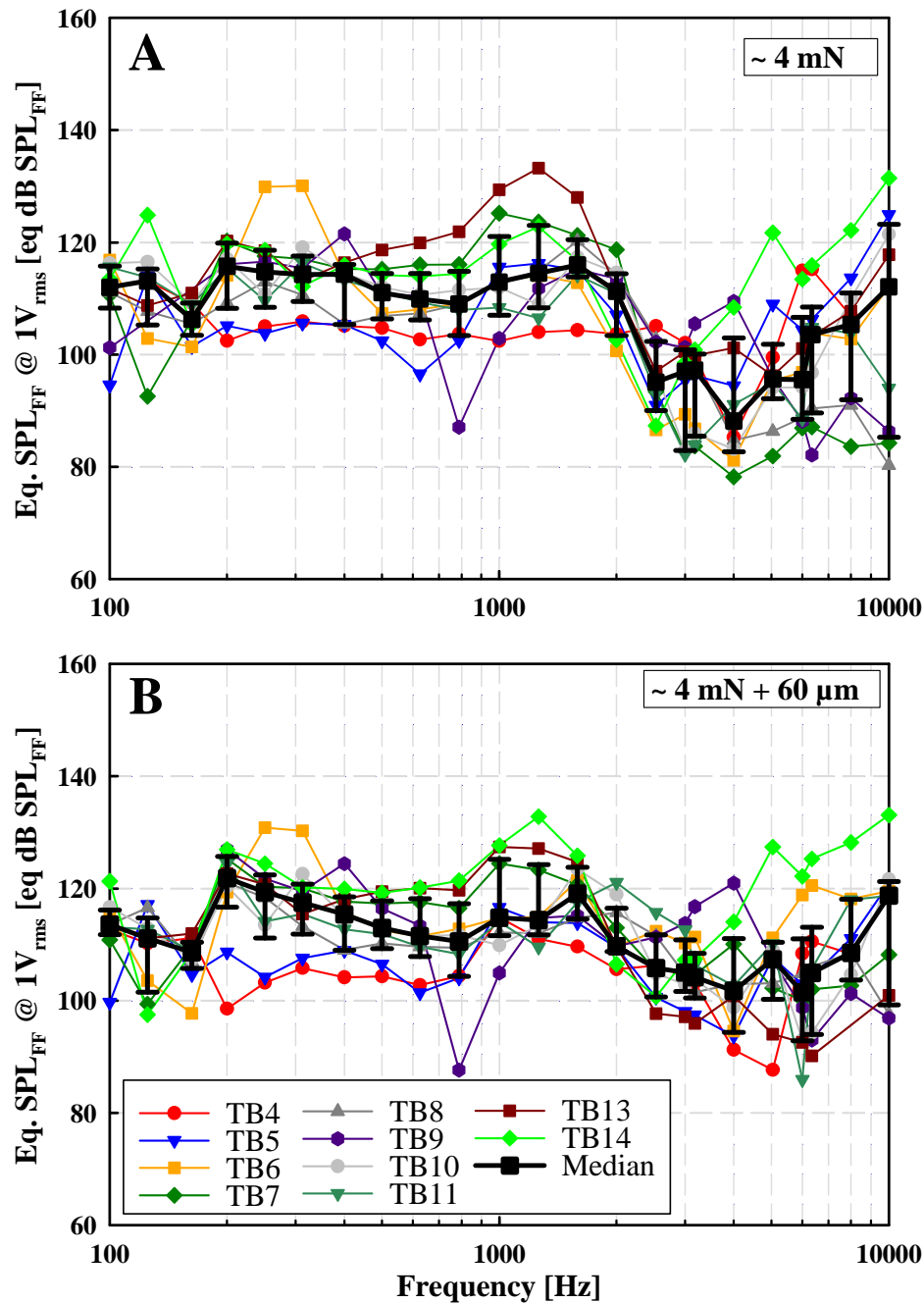**Figure 5.5.** T2 actuator output (eq. dB SPL$_{FF}$) in TBs, calculated from ICPD. Colored small symbols represent results from individual TBs, black large squares medians, and error bars 25 % and 75 % percentiles. A: Results obtained at approx. 4 mN static coupling force. B: Results obtained when the actuator was advanced 60 μm from position A. Data points having SNR < 12 dB was omitted (A: TB04 at 10 kHz and TB09 at 0.1 and 0.1625 kHz; B: TB04 at 10 kHz, TB09 at 0.1–0.1625 kHz and TB13 at 8 kHz). Lines connecting symbols are for visual guidance only. Modified from GROSSÖHMICHEN ET AL. [2017] (CC BY 4.0).

Figure 5.6. Actuator output (eq. dB SPL$_{FF}$) in patients calculated from direct and bone conduction thresholds. Colored small symbols depict results from individual patients, black large triangles median and the grey shaded area 25% and 75% percentiles. Number of patients contributing data: N = 5 at 0.25 kHz, N = 20 at 0.5 kHz, N = 23 at 1 kHz, N = 24 at 1.5 kHz, N = 24 at 2 kHz, N = 16 at 3 kHz, N = 22 at 4 kHz and N = 20 at 6 kHz. Lines connecting symbols are for visual guidance only. Modified from GROSSÖHMICHEN ET AL. [2017] (CC BY 4.0).
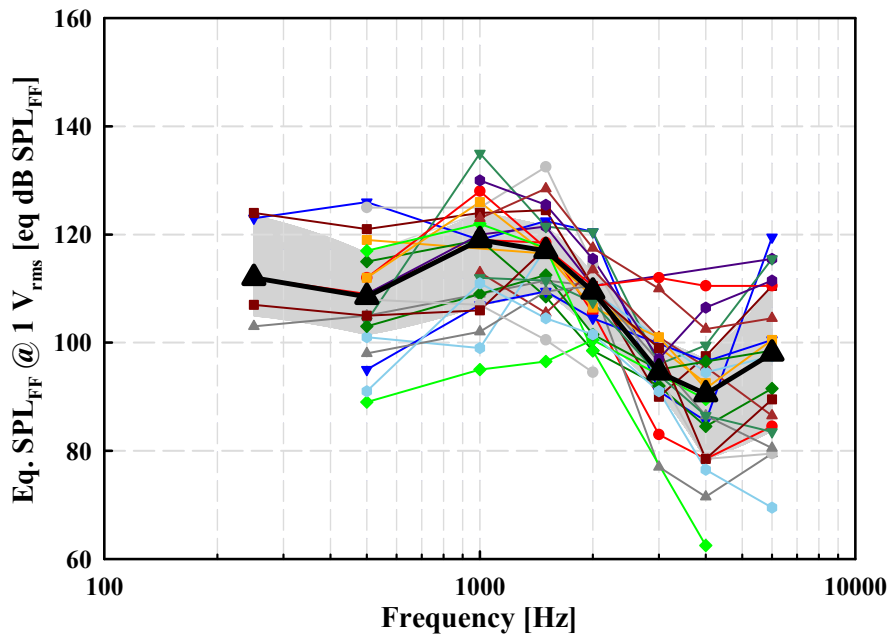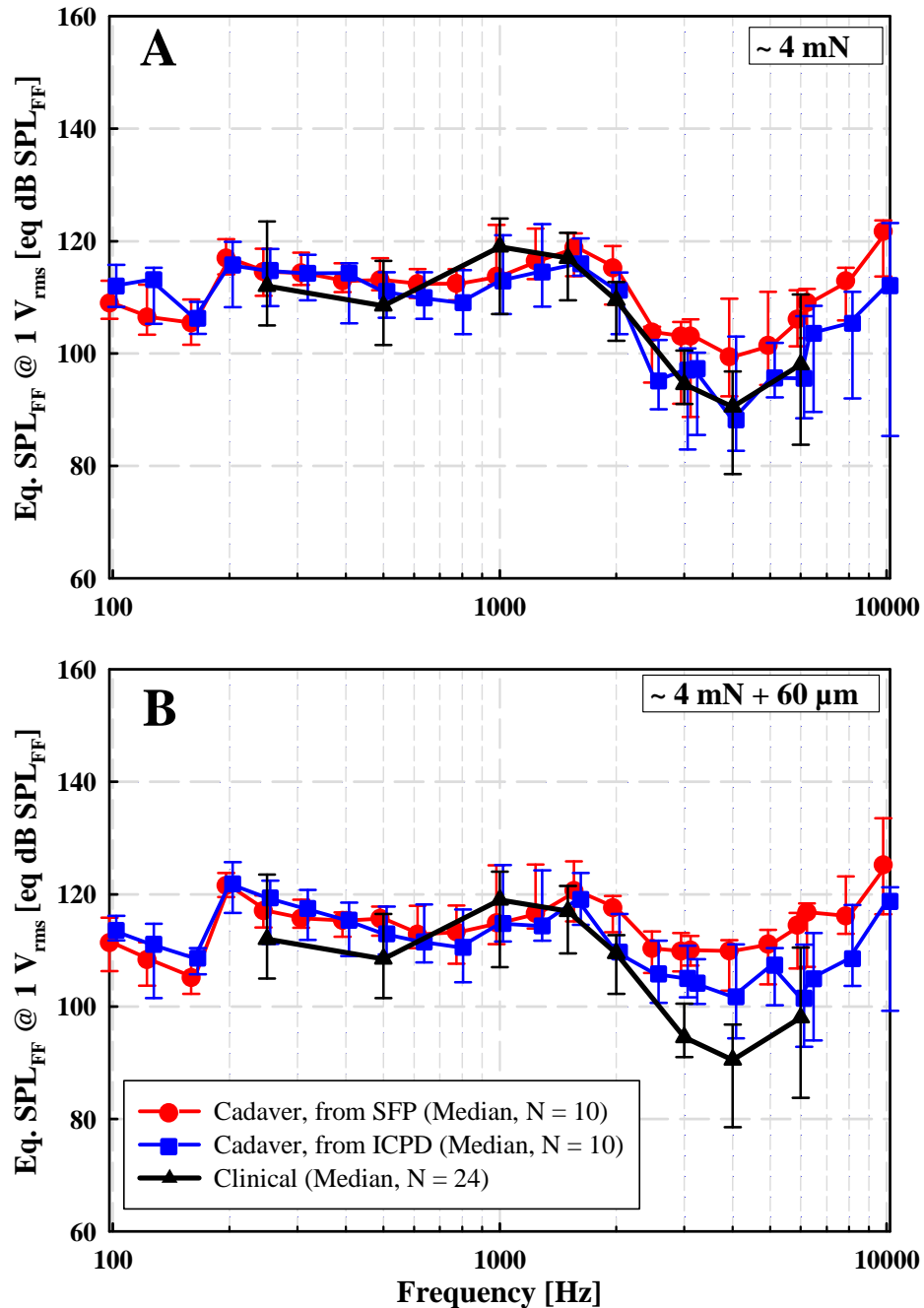
Figure 5.7. Comparison of median actuator output levels (eq. dB SPL_{FF}) in cadaveric TBs, calculated from ICPD (blue), stapes motion (red) and based on clinically measured psychoacoustic thresholds (black). Error bars represent 25% and 75% percentiles. Blue and red symbols and error bars are shifted by $\pm 2\%$ along the frequency-axis for clarity. Lines connecting symbols are for visual guidance only. A: Cadaver results obtained at approx. 4 mN static coupling force. B: Cadaver results obtained when the actuator was advanced 60 μm from position A. Modified from GROSSÖHMICHEN ET AL. [2017] (CC BY 4.0).

were very similar over the entire frequency range with statistically non-significant (Mann-Whitney Rank Sum Test) differences of 6 dB at 1 kHz and of < 3 dB at all other frequencies (Figure 5.7A).

4 mN + 60 µm: Median actuator output levels obtained in TBs and clinical results had similar frequency dependency (Figure 5.7B). The differences between the median eq. dB SPL_{FF} calculated from stapes vibration amplitudes in TBs and from clinical data were 3 to 8 dB at 0.25 to 2 kHz and 15 to 19 dB at 3 to 6 kHz. Differences were statistically not significant (Mann-Whitney Rank Sum Test) at 0.25 to 1.5 kHz but statistically significant at higher frequencies ($p = 0.002$ at 2 kHz, $p < 0.001$ at 3 and 4 kHz, $p = 0.021$ at 6 kHz). The differences between the median eq. dB SPL_{FF} calculated from ICPD in TBs and from clinical data were ≤ 7 dB and statistically not significant (Mann-Whitney Rank Sum Test) at 0.25 to 2 kHz and at 6 kHz. At 3 and 4 kHz the differences were 11 dB and statistically significant ($p = 0.002$ at 3 kHz, $p = 0.005$ at 4 kHz, Mann-Whitney Rank Sum Test).

5.3   Discussion

5.3.1   AMEI Output Levels calculated from Stapes Motion

AMEI output levels calculated from stapes motion were comparable to literature. Using the "classic" reference stapes vibration amplitude, the output of a T2 actuator in incus body stimulation had also been determined in earlier cadaver studies by TRINGALI ET AL. [2011] and DEVÈZE ET AL. [2013]. Output levels in these studies were given as eq. SPLs at the tympanic membrane [eq. dB SPL_{TM}] and have been converted according to equation (5.3) to eq. free field SPLs [eq. dB SPL_{FF}] for direct comparison with the present results (Figure 5.8). At most frequencies the median output obtained in the present study at actuator position "4 mN + 60 µm" was similar to the mean results of Tringali et al. and Devèze et al. However, in the publication by Tringali et al. (5 TBs) the T2 actuator output seems to be overestimated in the mid-frequency range. It may have contributed that two out of five TBs in Tringali et al. had middle ear transfer functions H_{TV} outside the modified acceptance range [ROSOWSKI ET AL., 2007] of ASTM standard F2504-05 at 0.25–4 kHz (see section 1.4.2). The output in Devèze et al. (6 TBs) was similar to the data presented here except for frequencies ± 0.6 kHz although coupling forces were not specified in their study.

5.3.2   AMEI Output Levels Calculated from ICPD

This is the first study quantifying the eq. SPL output of mechanical AMEI stimulation of the ossicular chain in human cadaveric TBs from ICPD measurements. In existing studies [NAKAJIMA ET AL., 2010; STIEGER ET AL., 2013] with a Floating Mass Transducer (Vibrant MED-EL Hearing Technology GmbH) ICPDs were measured during mechanical stimulation of the RW in TBs, but not converted into eq. SPLs.

In the here presented study AMEI output levels calculated from ICPD were similar to output levels calculated from stapes vibration according to the "gold standard method" ASTM F2504–05. Deviations at higher frequencies could be due to the complex nature of stapes motion. As incus stimulation is within the scope of ASTM F2504–05, eq. SPL calculated

from stapes motion and from ICPD should be similar. Here, the median actuator output level calculated from stapes motion and from ICPD were almost identical below 2 kHz, independent from the force / position of the actuator ("4 mN" or "4 mN + 60 μm") and thus from the level of contact force (approx. 4 mN or approx. 40 mN). However, at higher frequencies the actuator output level determined from stapes motion was up to 13 dB higher. This discrepancy may be explained by the fact that the complex nature of stapes motion at higher frequencies (rocking motions) are more likely to affect stapes vibration measured at a single location than ICPD that integrate pressure fields at a more remote location in the cochlea. In both live and cadaveric human ears the stapes motion is primarily piston-like below 1 kHz, but above this frequency rocking motions become more dominant with frequency [HATO ET AL., 2003; HUBER ET AL., 2001]. Based on numerical simulations, rocking motion does not produce net volume displacement of the perilymph and has negligible effects on cochlear excitation [EDOM ET AL., 2013]. Thus, rocking motion components measured at a single point with a 1-D single-point LDV may be misinterpreted as piston-like motions and contribute to the measured vibration amplitude. Of course, this would have no effect on the eq. SPL calculation if the complex motion pattern of the stapes were identical in the acoustic reference stimulation and the mechanical stimulation. However, in the present study the eq. SPLs estimated from stapes motion differed up to 13 dB from the eq. SPLs estimated from ICPD and obtained from clinical data above 2 kHz. Therefore it is assumed that the pattern of the complex stapes motion at high frequencies changed when the T2 actuator vibrated the incus body in a direction different to the direction of incus motion during acoustic stimulation. Under this assumption, the use of stapes vibration amplitudes measured with a 1-D single-point LDV as reference could lead to a slight overestimation of the real stimulation output as it is visible in the results (Figure 5.7). In contrast, ICPD considered as the input to the cochlea[NAKAJIMA ET AL., 2009] is a result of the net volume displacement of the stapes footplate and should not be affected by stapes rocking motions. This assumption is confirmed by the present study as the eq. SPL estimates from ICPD and clinical data were almost identical at all frequencies from 0.1 to 10 kHz (Figure 5.7A).

5.3.3   Predicted AMEI Output Levels vs. Clinical Data

Independent from the reference (stapes motion or ICPD), all estimated eq. SPL were close to the clinical data at actuator position "4 mN" but above 2 kHz the prediction from ICPD was even more accurate. It can therefore be concluded that in incus stimulation, both measurements of ICPD and of stapes movement can be used to predict the achievable loudness levels of AMEIs, but ICPD as reference provides even more accurate results because it is not affected by altered stapes motion patterns at higher frequencies as discussed above.

   The discrepancy between AMEI output levels estimated from cadaver experiments and clinical data could be due to unexpectedly low coupling forces in patients. At the assumed final position (60 μm from the initial contact of 4 mN) for the loading procedure with the TLA, the median actuator output (eq. dB SPL_{FF}) determined in our TB experiments from ICPD was similar to the output obtained from clinical data at frequencies ≤ 2 kHz but up to 11 dB higher at frequencies above. At the detection limit of the TLA (static coupling force of approx. 4 mN), however, output levels from cadaver and clinical data were very similar over
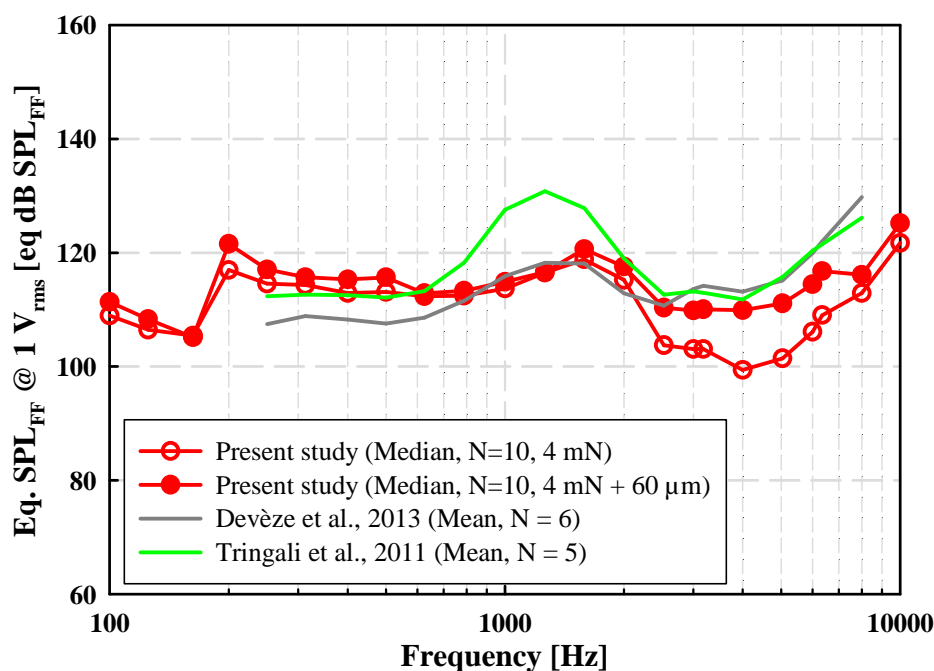
Figure 5.8. Comparison of the T2 actuator output (eq. dB SPL_{FF}) in TBs, calculated from stapes vibration amplitudes, between the present study, TRINGALI ET AL. [2011] and DEVÈZE ET AL. [2013]. Output levels in Devèze et al. and Tringali et al. were given as eq. ear canal SPLs [eq. dB SPL_{TM}] for nominally $1 \, V_{rms}$ actuator input voltage and have been converted to eq. free field SPLs [eq. dB SPL_{FF}] using tables I to III in SHAW & VAILLANCOURT [1985] to make them comparable to outputs from the present study. Lines connecting symbols are for visual guidance only. Modified from GROSSÖHMICHEN ET AL. [2017] (CC BY 4.0).

the entire frequency range. These results suggest that the post-operative coupling force in our patients was also approx. 4 mN. One potential reason for the presumably smaller force level in the patients may be that at the Hannover Medical School the final contact position of the T2 actuator during surgery is determined not by using the TLA but by measuring the stapes vibration response with an LDV during actuator stimulation. Based on personal experience this method is more sensitive than using the TLA, because proper stapes vibration responses are measurable with the LDV already before the TLA procedure indicates initial. Another reason might be a long-term relaxation of the ossicular chain in patients leading to a shift of the incus and a decreasing contact force. Long-term effects such as tissue growth around the actuator that may occur in patients could not be simulated in the TB experiments. At least, an attenuating effect of surrounding tissue on the mechanical output of the AMEI actuator is unlikely [GROSSÖHMICHEN ET AL., 2016a].

5.4   Summary and Conclusion

Clinical output level of an AMEI stimulating the incus could be successfully estimated as eq. dB SPL by measuring ICPD in human cadaveric ears. At 4 mN coupling force, these estimates were up to 3 kHz very close (maximal difference of 6 dB) to estimates from stapes

velocity and to audiometric data from patients treated with the same AMEI type and stimulation mode. Above 3 kHz, the stapes velocity estimates deviated up to 11 dB from ICPD estimates and up to 9 dB from clinical data, whereas the estimates from ICPD and clinical data were almost identical for all frequencies from 0.1 to 10 kHz. These results demonstrate for the first time that both ICPD and stapes motion can be used as a valid measure to predict the clinically achievable loudness of AMEIs in cadaver studies. However, ICPD measurement provided results matching the output from clinical data even better and has the advantage of being applicable to stimulation scenarios where the stapes footplate is not possible as reference.

Chapter 6

Summary and Conclusion

Today, AMEIs and DACIs are good treatment options if a provision with a conventional hearing aid is not possible or not sufficient [PIRLICH ET AL., 2017]. To improve the treatment with AMEIs and DACIs and to develop new devices their clinical output level [eq dB SPL] must be predicted with high precision before clinical data are available. In this thesis two different methods to quantify the output level of AMEIs and DACIs in preclinical cadaver studies have been developed, investigated, tested, assessed and compared, namely vibration measurements according to ASTM F2504–05 and ICPD measurement.

Measuring stapes vibration responses with a single-point LDV is a commonly used method to investigate and compare stimulation efficiencies of AMEIs in human cadaveric TBs. This measurement technique has the great advantage of being non-invasive and contact-free so that the delicate structures of the middle ear and inner ear remain unaffected. Since ready to use single-point LDV systems are commercially available this measurement technique is generally accessible. The only necessary preparations are the creation of a direct visual access and the placement of a reflector or glass bead to obtain sufficient reflectance at the measurement site. For this reason and because single-point LDVs can be integrated in common surgical microscopes, LDV measurements are easy and fast to conduct. To predict the clinical output level [eq dB SPL] of an AMEI stimulating the ossicles from such LDV measurements ASTM standard F2504–05 describes a procedure using stapes vibration amplitudes in human TBs as reference. This practice is well established and has become the current "gold standard" for experimental AMEI evaluations. More than ten years after the publication of ASTM standard F2504–05 the present work demonstrates for the first time that the predicted output levels of an AMEI stimulating the ossicles match the actual clinical output levels within 1 to 6 dB at 0.1 to 2 kHz and within 8 to 9 dB at 3 to 10 kHz. Furthermore the procedure of ASTM standard F2504–05 could be successfully modified to estimate the output levels of actuator stimulations where stapes motions are not measurable by using measured vibration amplitudes of the RW as reference. Using this modified method it could be demonstrated that the actuator of the Codacs DACI system can also be used for RW stimulation, stapes stimulation and oval window stimulation. However, the presented results showed also that in stimulation modes other than ossicular chain stimulation, the accuracy of output levels determined from vibration measurements is limited and these values should be used only for rough estimates, especially at frequencies > 1 kHz.

In contrast to stapes motion, ICPD - considered as the direct input to the cochlea partition

- is a result of the perilymph net volume displacement and thus independent of the kind of stimulation. Therefore ICPD measurement is a good candidate for a method to quantify the output level of AMEIs and DACIs in all common stimulation modes in human cadaveric TBs. In the present thesis it could demonstrate that ICPDs are measurable in human cadaveric TBs with commercially available fiber-optical pressure measurement systems which are intended for other applications. Additionally it could be shown that the insertion of the pressure transducers had a minor effect of mostly ≤ 5 dB on the stapes vibration response to sound (middle ear transfer function H_{TV}). In the present work, ICPDs were used for the first time to quantify the output levels of an AMEI stimulation in human cadaveric TBs. A direct comparison with clinical data demonstrated that the eq. SPL outputs predicted from ICPD for an AMEI stimulating the incus are almost identical with the real stimulation outputs in patients. The match between clinical data and predicted output levels was even better than for stapes motion measurement according to ASTM F2504–05. However, in comparison with LDV measurement the preparation needed for ICPD measurement is more complex so that this method is more time consuming and requires more training. Another disadvantage is that the TB may not be moved once the pressure transducers are inserted and sealed in the cochlea to avoid damages and dislocations of the transducers. Furthermore the pressure transducers limit the available space in the middle ear cavity, but according to the author's experience the remaining space is still sufficient for placing an AMEI actuator.

In summary, both ICPD and stapes motion can be used as a valid measure to predict the clinical output level of mechanical actuator stimulation as eq. SPL in cadaver studies. LDV measurement as the faster and easier to conduct method should be preferred to predict the output level of AMEI stimulations at the ossicular chain. In other stimulation modes such as reverse RW stimulation and direct perilymph stimulation, LDV measurements should be used only for initial assessments. ICPD measurement should be used to predict the clinical output level of stimulations at the ossicular chain even more precisely and is preferable in all other stimulation modes. The findings of the present thesis may contribute to establish ICPD measurement as a strong tool beside LDV measurements and to increase the practical value of actuator output level prediction based on cadaver studies. Therefore the here presented results make an important contribution to improve the efficiency of current and future AMEIs and DACIs and to optimize the treatment of hearing losses.

Bibliography

AIBARA R., WELSH J.T., PURIA S. & GOODE R.L. Human middle-ear sound transfer function and cochlear input impedance. *Hearing Research*, 152 (2001) (1-2): 100–109.

ANSI. S3.6-2004 Specification for Audiometers (2004).

ASAI M., HUBER A.M. & GOODE R.L. Analysis of the best site on the stapes footplate for ossicular chain reconstruction. *Acta Oto-Laryngologica*, 119 (1999) (3): 356–61.

ASTM. F 2504 – 05 Standard Practice for Describing System Output of Implantable Middle Ear Hearing Devices (2005).

VON BÉKÉSY G. *Experiments in Hearing*. McGraw-Hill Book Company, New York, 1960.

BERNHARD H., STIEGER C. & PERRIARD Y. Design of a semi-implantable hearing device for direct acoustic cochlear stimulation. *IEEE transactions on bio-medical engineering*, 58 (2011) (2): 420–428.

BEUTNER D. & HÜTTENBRINK K.B. [Passive and active middle ear implants]. *Laryngo-Rhino-Otol*, 88 Suppl 1 (2009): S32–47.

BITTENCOURT A., BURKE P., JARDIM I., BRITO R. ET AL. Implantable and Semi-Implantable Hearing Aids: A Review of History, Indications, and Surgery. *International Archives of Otorhinolaryngology*, 18 (2014) (03): 303–310.

BÖHNKE F., BRETAN T., LEHNER S. & STRENGER T. Simulations and measurements of human middle ear vibrations using multi-body systems and laser-doppler vibrometry with the floating mass transducer. *Materials*, 6 (2013) (10): 4675–4688.

BORNITZ M., HARDTKE H.J. & ZAHNERT T. Evaluation of implantable actuators by means of a middle ear simulation model. *Hearing research*, 263 (2010) (1-2): 145–51.

BORNITZ M., ZAHNERT T., HARDTKE H. & HÜTTENBRINK K. Identification of parameters for the middle ear model. *Audiology & Neurootology*, 4 (1999) (3-4): 163–9.

BURGEAT M., BURGEAT-MENGUY C. & LEHMANN R. Étude de la transmission des pressions acoustiques du milieu aérien aux liquides cochléaires au moyen de sondes microphoniques. *Acta Acustica united with Acustica*, 13 (1963) (6): 377–382.

BURGEAT M., LEHMANN R. & BURGEAT-MENGUY C. [TRANSMISSION OF ACOUSTIC PRESSURES IN THE SCALAE COCHLEAE]. *Comptes rendus hebdomadaires des seances de l'Academie des sciences*, 258 (1964): 5976–8.

BUSCH S., KRUCK S., SPICKERS D., LEUWER R. ET AL. First clinical experiences with a direct acoustic cochlear stimulator in comparison to preoperative fitted conventional hearing aids. *Otology & Neurotology*, 34 (2013) (9): 1711–8.

CASTELLINI P., REVEL G.M. & TOMASINI E.P. Laser Doppler Vibrometry. In RIGHINI G., TAJANI A. & CUTOLO A., eds., *An Introduction to Optoelectronic Sensors*. World Scientific Publishing Co. Pte. Ltd., 2009.

CHATZIMICHALIS M., SIM J.H. & HUBER A.M. Assessment of a direct acoustic cochlear stimulator. *Audiology & neuro-otology*, 17 (2012) (5): 299–308.

CHEN F., ZHA D., FRIDBERGER A., ZHENG J. ET AL. A differentially amplified motion in the ear for near-threshold sound detection. *Nature neuroscience*, 14 (2011) (6): 770–4.

CHEN Y., GUAN X., ZHANG T. & GAN R.Z. Measurement of Basilar Membrane Motion During Round Window Stimulation in Guinea Pigs. *Journal of the Association for Research in Otolaryngology*, 15 (2014) (6): 933–943.

CHIEN W., ROSOWSKI J.J., RAVICZ M.E., RAUCH S.D. ET AL. Measurements of stapes velocity in live human ears. *Hearing research*, 249 (2009) (1-2): 54–61.

CHITTKA L. & BROCKMANN A. Perception space - The final frontier. *PLoS Biology*, 3 (2005) (4): 0564–0568.

CLARK G. *Cochlear Implants*. Modern Acoustics and Signal Processing. Springer-Verlag, New York, 2003.

COCHLEAR. MET Counseling Cards. Cochlear Boulder LLC. (2014).

COLLETTI V., SOLI S.D. & CARNER M. Treatment of mixed hearing losses via implantation of a vibratory transducer on the round window. *International Journal of Audiology*, 45 (2006) (10): 600–608.

DANCER A. & FRANKE R. Intracochlear sound pressure measurements in guinea pigs. *Hearing research*, 2 (1980) (3-4): 191–205.

DEUTSCHE GESELLSCHAFT FÜR HALS-NASEN-OHREN-HEILKUNDE K.U.H.C.E.V. Cochlea-Implantat Versorgung und zentral-auditorische Implantate. Technical report, Deutsche Gesellschaft fuer Hals-Nasen-Ohrenheilkunde und Kopf und Hals-Chirurgie e.V. (2012).

DEVÈZE A., KOKA K., TRINGALI S., JENKINS H.A. ET AL. Active middle ear implant application in case of stapes fixation: a temporal bone study. *Otology & neurotology*, 31 (2010) (7): 1027–34.

DEVÈZE A., KOKA K., TRINGALI S., JENKINS H.A. ET AL. Techniques to improve the efficiency of a middle ear implant: effect of different methods of coupling to the ossicular chain. *Otology & Neurotology*, 34 (2013) (1): 158–66.

EDOM E., OBRIST D., HENNIGER R., KLEISER L. ET AL. The effect of rocking stapes motions on the cochlear fluid flow and on the basilar membrane motion. *The Journal of the Acoustical Society of America*, 134 (2013) (5): 3749–58.

FISO. Veloce 50 User Guide (2012).

FISO. FOP-M260 Datasheet (2015).

FRANKE R. & DANCER A. Cochlear mechanisms at low frequencies in the guinea pig. *Archives of oto-rhino-laryngology*, 234 (1982) (2): 213–8.

GOODE R.L., BALL G. & NISHIHARA S. Measurement of umbo vibration in human subjects–method and possible clinical applications. *The American journal of otology*, 14 (1993) (3): 247–51.

GOODE R.L., KILLION M., NAKAMURA K. & NISHIHARA S. New knowledge about the function of the human middle ear: development of an improved analog model. (1994).

GROSSÖHMICHEN M., SALCHER R., KREIPE H.H., LENARZ T. ET AL. The Codacs™ Direct Acoustic Cochlear Implant Actuator: Exploring Alternative Stimulation Sites and Their Stimulation Efficiency. *PLOS ONE*, 10 (2015) (3): e0119 601.

GROSSÖHMICHEN M., SALCHER R., LENARZ T. & MAIER H. The Effect of Simulated Mastoid Obliteration on the Mechanical Output of Electromagnetic Transducers. *Otology & Neurotology*, 37 (2016a) (7): 919–925.

GROSSÖHMICHEN M., SALCHER R., LENARZ T. & MAIER H. Measurement of Intra-cochlear Pressure Differences in Human Temporal Bones Using an Off-the-Shelf Pressure Sensor. In WRIGGERS P. & LENARZ T., eds., *Biomedical Technology*, pages 335–348. Springer, Cham, 2018.

GROSSÖHMICHEN M., SALCHER R., PÜSCHEL K., LENARZ T. ET AL. Differential Intra-cochlear Sound Pressure Measurements in Human Temporal Bones with an Off-the-Shelf Sensor. *BioMed Research International*, 2016 (2016b) (Article ID 6059479): 1–10.

GROSSÖHMICHEN M., WALDMANN B., SALCHER R., PRENZLER N. ET AL. Validation of methods for prediction of clinical output levels of active middle ear implants from measurements in human cadaveric ears. *Scientific Reports*, 7 (2017) (15877).

GULYA A.J., MINOR L.B. & POE D.S. *Glasscock-Shambaugh's Surgery of the Ear*. PMPH-USA Limited, 2010, 6 edition.

HATO N., STENFELT S. & GOODE R.L. Three-Dimensional Stapes Footplate Motion in Human Temporal Bones. *Audiology and Neuro-Otology*, 8 (2003) (3): 140–152.

HÄUSLER R., STIEGER C., BERNHARD H. & KOMPIS M. A novel implantable hearing system with direct acoustic cochlear stimulation. *Audiology & Neurotology*, 13 (2008) (4): 247–56.

HELMHOLTZ H. Die Mechanik der Gehörknöchelchen und des Trommelfells. *Pflüger, Archiv für die Gesammte Physiologie des Menschen und der Thiere*, 1 (1868) (1): 1–60.

HUBER A., LINDER T., FERRAZZINI M., SCHMID S. ET AL. Intraoperative assessment of stapes movement. *Annals of Otology, Rhinology and Laryngology*, 110 (2001) (1): 31–35.

HÜTTENBRINK K.B. & HUDDE H. [Studies of sound condition in the reconstructed middle ear with a hydrophone. Initial results]. *HNO*, 42 (1994) (1): 49–57.

JAVEL E., GRANT I.L. & KROLL K. In vivo characterization of piezoelectric transducers for implantable hearing AIDS. *Otology & Neurotology*, 24 (2003) (5): 784–95.

JENKINS H.A., ATKINS J.S., HORLBECK D., HOFFER M.E. ET AL. U.S. Phase I preliminary results of use of the Otologics MET Fully-Implantable Ossicular Stimulator. *Otolaryngology–head and neck surgery*, 137 (2007) (2): 206–12.

JOHANSMANN M., SIEGMUND G. & PINEDA M. Targeting the limits of laser Doppler vibrometry. In *Proceedings of the IDEMA 2005*, pages 1–12. 2005.

KASIC J.F. & FREDRICKSON J.M. The Otologics MET ossicular stimulator. *Otolaryngologic clinics of North America*, 34 (2001) (2): 501–13.

KOKA K., HOLLAND N.J., LUPO J.E., JENKINS H.A. ET AL. Electrocochleographic and mechanical assessment of round window stimulation with an active middle ear prosthesis. *Hearing Research*, 263 (2010) (1-2): 128–137.

KOMPIS M. *Audiologie*. Verlag Hans Huber, Bern, 2013, 3rd edition.

KRINGLEBOTN M. The equality of volume displacements in the inner ear windows. *The Journal of the Acoustical Society of America*, 98 (1995) (1): 192.

KUHN J.J. Middle Ear Implantable Hearing Devices: Present and Future. In RUCKENSTEIN M.J., ed., *Cochlear Implants and Other Implantable Hearing Devices*. Plural Publishing Inc., San Diego, 2012, 1st edition.

KUROKAWA H. & GOODE R.L. Sound pressure gain produced by the human middle ear. *Otolaryngology–head and neck surgery*, 113 (1995) (4): 349–55.

KWACZ M., MROWKA M. & WYSOCKI J. Round window membrane motion before and after stapedotomy surgery - an experimental study. *Acta of bioengineering and biomechanics / Wrocław University of Technology*, 13 (2011) (3): 27–33.

LAUXMANN M. *Nichtlineare Modellierung des Mittelohrs und seiner angrenzenden Strukturen*. Dissertation, Universität Stuttgart (2012).

LAUXMANN M., EIBER A., HAAG F. & IHRLE S. Nonlinear stiffness characteristics of the annular ligament. *The Journal of the Acoustical Society of America*, 136 (2014) (4): 1756–1767.

LEE H.Y., RAPHAEL P.D., PARK J., ELLERBEE A.K. ET AL. Noninvasive in vivo imaging reveals differences between tectorial membrane and basilar membrane traveling waves in the mouse cochlea. *Proceedings of the National Academy of Sciences*, 112 (2015) (10): 3128–3133.

LENARZ T. & BOENNINGHAUS H.G. *Hals-Nasen-Ohren-Heilkunde*. Springer-Lehrbuch. Springer Berlin Heidelberg, Berlin, Heidelberg, 2012, 14th edition.

LENARZ T., VERHAERT N., DESLOOVERE C., DESMET J. ET AL. A comparative study on speech in noise understanding with a direct acoustic cochlear implant in subjects with severe to profound mixed hearing loss. *Audiology and Neurotology*, 19 (2014) (3): 164–174.

LENARZ T., ZWARTENKOT J.W., STIEGER C., SCHWAB B. ET AL. Multicenter study with a direct acoustic cochlear implant. *Otology & neurotology*, 34 (2013) (7): 1215–25.

LIU H., RAO Z., HUANG X., CHENG G. ET AL. An Incus-Body Driving Type Piezoelectric Middle Ear Implant Design and Evaluation in 3D Computational Model and Temporal Bone. *The Scientific World Journal*, 2014 (2014): 1–8.

LODWIG A., HUDDE H. & HÜTTENBRINK K. Akustische und mechanische Messungen an Felsenbeinpräparaten. In *Fortschritte der Akustik - DAGA 93*, pages 764–767. Bad Honnef, 1993.

LUPO J.E., KOKA K., HOLLAND N.J., JENKINS H.A. ET AL. Prospective Electrophysiologic Findings of Round Window Stimulation in a Model of Experimentally Induced Stapes Fixation. *Otology & Neurotology*, 30 (2009) (8): 1215–1224.

LUPO J.E., KOKA K., JENKINS H.A. & TOLLIN D.J. Vibromechanical assessment of active middle ear implant stimulation in simulated middle ear effusion: a temporal bone study. *Otology & Neurotology*, 35 (2014) (3): 470–5.

LYNCH T.J., NEDZELNITSKY V. & PEAKE W.T. Input impedance of the cochlea in cat. *The Journal of the Acoustical Society of America*, 72 (1982) (1): 108–130.

MAIER H., SALCHER R., SCHWAB B. & LENARZ T. The effect of static force on round window stimulation with the direct acoustic cochlea stimulator. *Hearing Research*, 301 (2013) (0): 115–124.

MARTIN C., DEVEZE A., RICHARD C., LEFEBVRE P.P. ET AL. European Results With Totally Implantable Carina Placed on the Round Window. *Otology & Neurotology*, 30 (2009) (8): 1196–1203.

MLYNSKI R., DALHOFF E., HEYD A., WILDENSTEIN D. ET AL. Reinforced active middle ear implant fixation in incus vibroplasty. *Ear and hearing*, 36 (2015a) (1): 72–81.

MLYNSKI R., DALHOFF E., HEYD A., WILDENSTEIN D. ET AL. Standardized Active Middle-Ear Implant Coupling to the Short Incus Process. *Otology & Neurotology*, 36 (2015b) (8): 1390–1398.

NAKAJIMA H.H., DONG W., OLSON E.S., MERCHANT S.N. ET AL. Differential intracochlear sound pressure measurements in normal human temporal bones. *Journal of the Association for Research in Otolaryngology : JARO*, 10 (2009) (1): 23–36.

NAKAJIMA H.H., DONG W., OLSON E.S., ROSOWSKI J.J. ET AL. Evaluation of round window stimulation using the floating mass transducer by intracochlear sound pressure measurements in human temporal bones. *Otology & Neurotology*, 31 (2010) (3): 506–11.

NEDZELNITSKY V. Measurements of Sound Pressure in the Cochleae of Anesthetized Cats. In ZWICKER E. & TERHARDT E., eds., *Facts and Models in Hearing: Proceedings of the Symposium on Psychophysical Models and Physiological Facts in Hearing, held at Tutzing, Oberbayern, Federal Republic of Germany, April 22–26, 1974*, pages 45–53. Springer Berlin Heidelberg, Berlin, Heidelberg, 1974.

NEDZELNITSKY V. Sound pressures in the basal turn of the cat cochlea. *The Journal of the Acoustical Society of America*, 68 (1980) (6): 1676.

NUTTALL A.L., DOLAN D.F. & AVINASH G. Laser Doppler velocimetry of basilar membrane vibration. *Hearing Research*, 51 (1991) (2): 203–213.

NUTTALL A.L. & FRIDBERGER A. Instrumentation for studies of cochlear mechanics: from von Békésy forward. *Hearing research*, 293 (2012) (1-2): 3–11.

OLSON E.S. Observing middle and inner ear mechanics with novel intracochlear pressure sensors. *The Journal of the Acoustical Society of America*, 103 (1998) (6): 3445.

OLSON E.S., DUIFHUIS H. & STEELE C.R. Von Békésy and cochlear mechanics (2012).

OLSON E.S. & NAKAJIMA H.H. A family of fiber-optic based pressure sensors for intracochlear measurements. In *SPIE Photonics West; 7–12 February 2015*, volume 9303, page 93031O. San Francisco, California, United States, 2015.

PENNINGS R.J.E., HO A., BROWN J., VAN WIJHE R.G. ET AL. Analysis of Vibrant Soundbridge placement against the round window membrane in a human cadaveric temporal bone model. *Otology & Neurotology*, 31 (2010) (6): 998–1003.

PICKLES J.O. *An Introduction to the Physiology of Hearing*. BRILL, 2013.

PINET É. Fabry-Pérot Fiber-Optic Sensors for Physical Parameters Measurement in Challenging Conditions. *Journal of Sensors*, 2009 (2009): 1–9.

PIRLICH M., DIETZ A., MEURET S. & HOFER M. Implantierbare Knochenleitungs- und aktive Mittelohrhörsysteme. *Laryngo-Rhino-Otologie*, 96 (2017) (02): 120–129.

PISANO D.V., NIESTEN M.E.F., MERCHANT S.N. & NAKAJIMA H.H. The Effect of Superior Semicircular Canal Dehiscence on Intracochlear Sound Pressures. *Audiology and Neurotology*, 17 (2012) (5): 338–348.

POEGGEL S., TOSI D., DURAIBABU D., LEEN G. ET AL. Optical Fibre Pressure Sensors in Medical Applications. *Sensors*, 15 (2015) (12): 17 115–17 148.

POLYTEC. Möglichkeiten der Vibrometrie. (2003).

POLYTEC. CLV-3D Compact 3-D Laser Vibrometer For Simultaneous 3-D Measurement of Dynamics (2005).

POPELKA G.R., MOORE B.C.J., FAY R.R. & POPPER A.N., eds. *Hearing Aids*, volume 56 of *Springer Handbook of Auditory Research*. Springer International Publishing, Cham, 2016.

PURIA S., FAY R.R. & POPPER A.N., eds. *The Middle Ear*, volume 46 of *Springer Handbook of Auditory Research*. Springer New York, New York, NY, 2013.

PURIA S., PEAKE W.T. & ROSOWSKI J.J. Sound-pressure measurements in the cochlear vestibule of human-cadaver ears. *The Journal of the Acoustical Society of America*, 101 (1997) (5 Pt 1): 2754–70.

REINFELDT S., HÅKANSSON B., TAGHAVI H. & EEG-OLOFSSON M. New developments in bone-conduction hearing implants: a review. *Medical devices (Auckland, N.Z.)*, 8 (2015): 79–93.

ROSOWSKI J.J., CHIEN W., RAVICZ M.E. & MERCHANT S.N. Testing a method for quantifying the output of implantable middle ear hearing devices. *Audiology and Neurotology*, 12 (2007) (4): 265–276.

ROSOWSKI J.J., DAVIS P.J., MERCHANT S.N., DONAHUE K.M. ET AL. Cadaver middle ears as models for living ears: comparisons of middle ear input immittance. *The Annals of otology, rhinology, and laryngology*, 99 (1990) (5 Pt 1): 403–12.

SAMBA SENSORS AB. Samba Preclin Datasheet (2007).

SAMBA SENSORS AB. Samba 201/202 User Manual (2011).

SCHMIDT R.F., LANG F. & HECKMANN M., eds. *Physiologie des Menschen*. Springer-Lehrbuch. Springer Berlin Heidelberg, Berlin, Heidelberg, 2011.

SCHRAVEN S.P., HIRT B., GOLL E., HEYD A. ET AL. Conditions for highly efficient and reproducible round-window stimulation in humans. *Audiology & Neuro-otology*, 17 (2012) (2): 133–8.

SCHWAB B., SALCHER R.B., MAIER H. & KONTORINIS G. Oval Window Membrane Vibroplasty for Direct Acoustic Cochlear Stimulation. *Otology & Neurotology*, 33 (2012) (5): 804–809.

SHAW E.A. & VAILLANCOURT M.M. Transformation of sound-pressure level from the free field to the eardrum presented in numerical form. *The Journal of the Acoustical Society of America*, 78 (1985) (3): 1120–3.

SHAW E.A.G. Transformation of sound pressure level from the free field to the eardrum in the horizontal plane. *The Journal of the Acoustical Society of America*, 56 (1974) (6): 1848–1861.

SHERWOOD L. *Fundamentals of Human Physiology*. Brooks/Cole, Belmont, 2012, 4th edition.

SILVESTRI S. & SCHENA E. Optical-Fiber Measurement Systems for Medical Applications. In PREDEEP P., ed., *Optoelectronics - Devices and Applications*, page 642. InTech, 2011.

SIM J.H., CHATZIMICHALIS M., LAUXMANN M., RÖÖSLI C. ET AL. Complex stapes motions in human ears. *JARO - Journal of the Association for Research in Otolaryngology*, 11 (2010) (3): 329–341.

SONDERGAARD S., KARASON S., HANSON A., NILSSON K. ET AL. Direct measurement of intratracheal pressure in pediatric respiratory monitoring. *Pediatric research*, 51 (2002) (3): 339–45.

STEDMAN. *Stedman's Medical Dictionary*. LWW, Baltimore, 2005, 28th edition.

STENFELT S., HATO N. & GOODE R.L. Fluid volume displacement at the oval and round windows with air and bone conduction stimulation. *The Journal of the Acoustical Society of America*, 115 (2004a) (2): 797.

STENFELT S., HATO N. & GOODE R.L. Round window membrane motion with air conduction and bone conduction stimulation. *Hearing research*, 198 (2004b) (1-2): 10–24.

STIEGER C., BERNHARD H., WAECKERLIN D., KOMPIS M. ET AL. Human temporal bones versus mechanical model to evaluate three middle ear transducers. *The Journal of Rehabilitation Research and Development*, 44 (2007) (3): 407.

STIEGER C., ROSOWSKI J.J. & NAKAJIMA H.H. Comparison of forward (ear-canal) and reverse (round-window) sound stimulation of the cochlea. *Hearing research*, 301 (2013): 105–14.

TISCH M. Implantierbare Hörsysteme Implantable Hearing Devices. *Laryngo-Rhino-Otologie*, (2017): S84–S102.

TORBATIAN Z., GARLAND P., ADAMSON R., SAVAGE J. ET AL. Listening to the Cochlea With High-Frequency Ultrasound. *Ultrasound in Medicine & Biology*, 38 (2012) (12): 2208–2217.

TRINGALI S., KOKA K., DEVEZE A., FERBER A.T. ET AL. Intraoperative adjustments to optimize active middle ear implant performance. *Acta Oto-Laryngologica*, 131 (2011) (1): 27–35.

TRINGALI S., KOKA K., DEVEZE A., HOLLAND N.J. ET AL. Round window membrane implantation with an active middle ear implant: a study of the effects on the performance of round window exposure and transducer tip diameter in human cadaveric temporal bones. *Audiology & Neuro-otology*, 15 (2010) (5): 291–302.

VOSS S.E., ROSOWSKI J.J., MERCHANT S.N. & PEAKE W.T. Acoustic responses of the human middle ear. *Hearing research*, 150 (2000) (1-2): 43–69.

WORLD HEALTH ORGANIZATION. Grades of hearing impairment. http://www.who.int/pbd/deafness/hearing_impairment_grades/en/index.html (2016).

ZAHNERT T. Laser in der Ohrforschung. *Laryngo-Rhino-Otologie*, 82 (2003): 157–180.

ZWARTENKOT J.W., MULDER J.J.S., SNIK A.F.M., CREMERS C. ET AL. Active Middle Ear Implantation: Long-term Medical and Technical Follow-up, Implant Survival, and Complications. *Otology and Neurotology*, (2016): 513–519.

Wissenschaftlicher Werdegang

Martin Großöhmichen

Berufliche Tätigkeiten

Seit 08.2017	Forschungsingenieur Advanced Bionics GmbH, Hannover
11.2012 – 07.2017	Wissenschaftlicher Mitarbeiter HNO-Klinik der Medizinischen Hochschule Hannover, Hannover

Studium

04.2011 – 11.2012	Biomedizintechnik, Leibniz Universität Hannover Abschluss: Master of Science
10.2007 – 03.2011	Maschinenbau, Universität Kassel Abschluss: Diplom-Ingenieur
10.2005 – 09.2007	Wirtschaftsingenieurwesen, Universität Kassel Abschluss: Vordiplom
1997 – 2004	Gymnasium Martino-Katharineum, Braunschweig Abitur

Publikationen (Peer-reviewed Journale und Buchbeiträge)

GROSSÖHMICHEN M., SALCHER R., LENARZ T. & MAIER H. Measurement of Intracochlear Pressure Differences in Human Temporal Bones Using an Off-the-Shelf Pressure Sensor. In WRIGGERS P. & LENARZ T., eds., *Biomedical Technology*, pages 335–348. Springer, Cham, 2018

GROSSÖHMICHEN M., WALDMANN B., SALCHER R., PRENZLER N. ET AL. Validation of methods for prediction of clinical output levels of active middle ear implants from measurements in human cadaveric ears. *Scientific Reports*, 7 (2017) (15877)

GROSSÖHMICHEN M., SALCHER R., PÜSCHEL K., LENARZ T. ET AL. Differential Intracochlear Sound Pressure Measurements in Human Temporal Bones with an Off-the-Shelf Sensor. *BioMed Research International*, 2016 (2016b) (Article ID 6059479): 1–10

GROSSÖHMICHEN M., SALCHER R., LENARZ T. & MAIER H. The Effect of Simulated Mastoid Obliteration on the Mechanical Output of Electromagnetic Transducers. *Otology & Neurotology*, 37 (2016a) (7): 919–925

GROSSÖHMICHEN M., SALCHER R., KREIPE H.H., LENARZ T. ET AL. The Codacs™ Direct Acoustic Cochlear Implant Actuator: Exploring Alternative Stimulation Sites and Their Stimulation Efficiency. *PLOS ONE*, 10 (2015) (3): e0119 601

Danksagung

An dieser Stelle möchte ich mich bei all denjenigen bedanken, die mich während meiner Forschungsarbeit und dem Verfassen der vorliegenden Arbeit unterstützt und begleitet haben.

Herrn Prof. Peter Wriggers danke ich für sein Interesse an meiner Forschungstätigkeit und die Begutachtung meiner Arbeit. Mein besonderer Dank gilt Herrn Prof. Hannes Maier für die großartige Möglichkeit in diesem spannenden Forschungsgebiet zu arbeiten, für die Betreuung und fachliche Unterstützung in den letzten Jahren, sowie für seine offene Art des persönlichen Umgangs und den mir gewährten Freiraum beim Arbeiten. Herrn Prof. Bernd-Arno Behrens danke ich für die freundliche Übernahme des Prüfungsvorsitzes. Herrn Dr. Bernd Waldmann möchte ich meinen Dank aussprechen für die wertvollen fachlichen Diskussionen und persönlichen Ratschläge. Der Firma Cochlear danke ich für die Unterstützung meiner Arbeit, die es mir unter anderem ermöglicht hat, an zahlreichen Kongressen teilzunehmen. Danken möchte ich außerdem Herrn Dr. Rolf Salcher und Herrn Dr. Nils Prenzler für das unermüdliche Präparieren der Felsenbeine.

Für eine tolle und spaßige Zeit, auch außerhalb der Arbeit, danke ich meinen ehemaligen Kollegen, insbesondere Mohammad Ghoncheh, Mathias Müller, Alexander Rettenmaier, Sarah Vormelcher, Heike Janssen, Jakob Lexow, Samuel John, Franziska Lexow und Wouter van Drunen.

Ein besonders großer Dank geht an meine Eltern für die lebenslange Unterstützung in jeglicher Hinsicht.

Zu guter Letzt möchte ich mich vor allem bei meiner Frau Linda bedanken für die liebevolle Unterstützung und die enorme Geduld während der Fertigstellung meiner Arbeit.